

THE UCSD HIRES/KECK I DAMPED Ly α ABUNDANCE DATABASE: I. THE DATA

JASON X. PROCHASKA^{1,2}, ARTHUR M. WOLFE^{1,3}, DAVID TYTLER^{1,3}, SCOTT BURLES^{1,4}, JEFF COOKE^{1,3}, ERIC GAWISER^{1,3}, DAVID KIRKMAN^{1,3}, JOHN M. O'MEARA^{1,3}, & LISA STORRIE-LOMBARDI^{1,5}

Accepted to the Astrophysical Journal Supplements: June 8, 2001

ABSTRACT

We present new chemical abundance measurements of 16 damped Ly α systems at $z > 1.5$ and update our previous abundance analyses. The entire database presented here was derived from HIRES observations on the Keck I telescope, reduced with the same software package, and analysed with identical techniques. Altogether, we present a large, homogeneous database of chemical abundance measurements for protogalaxies in the early universe, ideal for studying a number of important aspects of galaxy formation. In addition, we have established an online directory for this database and will continuously update the results.

Subject headings: galaxies: abundances — galaxies: chemical evolution — quasars : absorption lines — nucleosynthesis

1. INTRODUCTION

Since their discovery nearly twenty years ago (Wolfe et al. 1986), the damped Ly α systems have provided an extraordinary means for probing the properties of high redshift galaxies. For example, Wolfe and his collaborators have led a number of observing programs to trace the universal neutral baryonic content, a study made possible by the fact that the damped Ly α systems are the dominant neutral gas reservoirs at every epoch (e.g. Wolfe et al. 1995; Lanzetta et al. 1995; Storrie-Lombardi et al. 1996; Storrie-Lombardi and Wolfe 2000). Through accurate metallicity measurements, damped Ly α studies also provide an examination of the chemical enrichment history of the universe (Pettini et al. 1994, 1997; Prochaska & Wolfe 2000; Prochaska, Gawiser, & Wolfe 2001, hereafter PGW01). In addition, the advent of high resolution echelle spectrographs on 10m class telescopes have enabled researchers to trace the relative chemical abundances of these systems, measurements which provide direct insight into processes of nucleosynthesis and dust depletion in the early universe (Lu et al. 1996, hereafter L96; Prochaska & Wolfe 1999, hereafter PW99; Pettini et al. 2000).

In this paper, we build on previous observations of the chemical abundances of damped Ly α systems. In particular, we introduce new measurements of over 15 damped Ly α systems and revise the measurements of our previously analysed systems (PW99). The principle goal of this paper is to provide the community with a uniform, homogeneous database of $z > 1.5$ damped Ly α abundances. To this end, we have created a web site⁶ where we will

continuously update our observations and possibly include measurements from throughout the community. Our new observations include spectra with wavelength coverage extending blueward of Ly α where elements like Ar, P, S, N, and O can be examined. In the second paper in this series (Paper II; Prochaska & Wolfe 2001a), we address the implications of the complete data set on chemical evolution, dust depletion, dust obscuration, and nucleosynthesis. In companion papers, we address the N/O abundance of the damped Ly α systems, examine the kinematic characteristics of the full sample (Prochaska & Wolfe 2001b), infer the star formation rate of the damped systems (Wolfe, Prochaska, & Gawiser 2001), and investigate the observational evidence for photoionization in these systems.

2. OBSERVATIONS AND ANALYSIS

All of the observations presented in this paper were acquired with the High Resolution Echelle Spectrograph (HIRES; Vogt et al. 1994) on the Keck I 10m telescope. The HIRES spectrograph is mounted at the Nasmyth focus of Keck I and is equipped with an image rotator, two collimators (red and blue sensitive), and a Tektronix 2048 \times 2048 CCD. For each observation, we implemented either a 1.1'' or 0.8'' slit which provides a resolution of FWHM \approx 8.4 and 6.3 km/s respectively. The HIRES spectrograph affords \approx 2500 \AA of wavelength coverage per setting with continuous coverage below $\lambda \approx$ 5100 \AA . Table 1 summarizes all of the new observations; refer to PW99 for previous observations.

All of the data were reduced with the MAKEE package as tailored for HIRES observations by T. Barlow⁷. This package flat-fields the exposures, optimally extracts the spectra from the 2-D images traced by a standard star or pinhole image, removes cosmic rays, and wavelength calibrates the spectra by cross-correlating each object's Th-Ar calibrations with a large database of calibrated HIRES data. We then continuum fit each spectrum with an in-house routine similar to the IRAF task CONTINUUM. For quasars with multiple exposures, the individual spectra were coadded (weighting by S/N and rejecting bad pixels) to produce a single 1-D spectrum with 2 km/s pixels.

¹ Visiting Astronomer, W.M. Keck Telescope. The Keck Observatory is a joint facility of the University of California and the California Institute of Technology.

² The Observatories of the Carnegie Institute of Washington, 813 Santa Barbara St., Pasadena, CA 91101

³ Department of Physics, and Center for Astrophysics and Space Sciences, University of California, San Diego, C-0424, La Jolla, CA 92093-0424

⁴ Experimental Astrophysics Department, Fermi National Accelerator Laboratory, MS 127, P.O. Box 500, 500 Wilson Rd., Batavia, IL 60637-1433

⁵ SIRTf Science Center, California Institute of Technology, MS 100-22, Pasadena, CA 91125

⁶ <http://kingpin.ucsd.edu/~hiresdla>

⁷ <http://spider.ipac.caltech.edu/staff/tab/makee>

TABLE 1
JOURNAL OF NEW OBSERVATIONS

QSO	Alt. name	z_{em}	Wavelength (\AA)	Date	Exposure (s)	Resolution (km/s)	SNR (pix $^{-1}$)
J0255+00	...	4.02	5100–8160	F99,F00	20200	6.3	15
Q0336–01	...	3.22	3940–6390	F99	5400	8.2	10
Q0347–38	...	3.23	3600–5900	F98	4500	8.2	6
HS0741+4741		3.20	3600–5900	F98,S00	10800	8.2	25
			5050–7470	F00	5400	6.3	30
Q0951–04	BRI0951–0450	4.37	5720–8150	F99	7200	8.2	10
BRI 0952–0115	...	4.43	5700–8150	S99	28800	8.2	15
PSS0957+33	...	4.25	6440–8760	F00	7200	6.3	15
BRI 1108–0747	...	3.92	5950–8340	F98,F99	12600	8.2	20
Q1210+17		2.54	3760–6170	S00	7200	8.2	20
Q1223+17		2.92	4780–7160	S98	19600	8.2	30
			3560–5900	S98	5000	8.2	7
BRI1346–0322		3.99	4280–6600	S00	7200	8.2	4
PSS1443+27		4.41	6070–8500	S99	25200	8.2	20
			6790–9180	S00	11000	8.2	15
Q1759+75	GB1759+7539	3.05	3500–5800	S00	22200	8.2	30
Q1946+7658		2.99	3470–5055	F98	47970	8.2	50
Q2344+12		4.30	3400–4985	F98	4000	8.2	12
Q2348–01		3.01	5060–7480	F99,F00	16200	8.2	15

3. IONIC COLUMN DENSITIES

In this section, we present ionic column density measurements for all of the new systems as well as a number of transitions excluded in PW99. All of the ionic column densities were derived with the apparent optical depth method (AODM; Savage and Sembach 1991). This technique corrects for hidden saturation by comparing the apparent column density, N_a , for multiple transitions from a single ion. This technique also gives an efficient means of calculating total column densities for each ion. The analysis involves calculating $N_a(v)$ for each pixel from the optical depth equation

$$N_a(v) = \frac{m_e c \tau_a(v)}{\pi e^2 f \lambda}, \quad (1)$$

where $\tau_a(v) = \ln[I_i(v)/I_a(v)]$, f is the oscillator strength, λ is the rest wavelength, and I_i and I_a are the incident and measured intensity. By summing over the velocity profile of a given transition one calculates the total column density,

$$N_T = \sum N_a(v) \Delta v, \quad (2)$$

and a 1σ error on the column density through standard error propagation

$$\sigma^2(N_T) = \sum \left(\frac{m_e c}{\pi e^2 f \lambda} \right)^2 \frac{\sigma^2(I_a(v))}{I_a^2(v)} \Delta v^2. \quad (3)$$

In previous papers (Wolfe et al. 1994; Prochaska & Wolfe 1996, 1997), we showed that the damped Ly α profiles are not contaminated by hidden saturation. Furthermore, we demonstrated the total column densities derived with the AODM agree very well with line-profile fitting, which should give a more accurate measure of the ionic column densities when hidden saturation is negligible. As the AODM is easier to apply to a large data set, we have chosen to use this technique to measure the ionic column densities for the damped Ly α sample.

Tables 3–40 present the results of the abundance measurements including an estimate of the 1σ error. For those transitions where the profile saturates, i.e. $I_a/I_i < 0.05$ in at least one pixel, the column densities are listed as lower limits. The values reported as upper limits are 3σ limits except in the cases where we set an upper limit due to significant line blending. We have ignored continuum error in our analysis which may dominate the measurements of very weak transitions especially those blueward of Ly α emission. We estimate a systematic error of $\approx 10\%$ in most cases. The 3σ statistical limits are conservative, however, and are likely to account for the continuum error in all but the noisiest and/or crowded absorption regions. In the following subsections, we comment briefly on each damped Ly α system, plot the metal-line profiles, and tab-

TABLE 2
ATOMIC DATA

Transition	λ	f	Ref
HI-19 914	914.0390	0.00019700	1
HI-18 914	914.2860	0.00023000	1
HI-17 914	914.5760	0.00027000	1
HI-16 914	914.9190	0.00032100	1
HI-15 915	915.3290	0.00038600	1
NII 915	915.6120	0.14490000	1
HI-14 915	915.8240	0.00046900	1
HI-13 916	916.4290	0.00057700	1
PIII 917	917.1180	0.40490000	1
HI-12 917	917.1806	0.00072260	1
HI-11 918	918.1294	0.00092100	1

References. — Key to References – 1: Morton (1991); 2: Howk et al. (2000); 3: Lawler et al. (1999); 4: Verner et al. (1994); 5: Lawler et al. (2000); 6: Verner et al. (1994); 7: Fedchak, Wiese, & Lawler (2000); 8: Bergeson et al. (1996); 9: Bergeson & Lawler (1993); 10: Wiese, Fedchak, & Mullman, & Lawler (1994); 11: Bergeson & Lawler (1993); 12: Wiese, Fedchak, & Mullman, & Lawler (1994); 13: Verner (1996); 14: Raassen & Uylings (1998); 15: Verner (1996); 16: Raassen & Uylings (1998).

Note. — The complete version of this table is in the electronic edition of the Journal. The printed edition contains only a sample.

ulate column densities for each profile. We adopt ionic column densities from these measurements by calculating the weighted-mean. In the velocity plots, $v = 0$ is chosen arbitrarily and corresponds to the redshift listed in the figure caption. We indicate regions of blending, primarily through blends with other metal-line systems or the Ly α forest, by plotting with dotted lines. For those systems previously analysed in PW99, we report only upon the changes made since publication. For completeness, when we include the measurement of a new transition (e.g. Ni II 1317) we report other measurements of the same ion and the new adopted ionic column density.

Throughout the paper, we adopt the wavelengths and oscillator strengths presented in Table 2. When possible, we have adopted laboratory values for the oscillator strengths. Since PW99 there have been several new measurements of f -values which impact the abundances of the damped Ly α systems, including new Ni II and Ti II oscillator strengths which have significantly revised the abundances of these elements. Most importantly, however, is the adoption of new oscillator strengths for the majority of Fe II transitions and in particular the Fe II λ 1608, 1611 transitions. In this paper, we adopt $f(1608) = 0.0580$ from the laboratory measurement of Bergeson et al. (1996) and $f(1611) = 0.00136$ from Raassen & Uylings (1998). In general, these values revise the abundance of Fe⁺ downward by ≈ 0.1 dex. Finally, we adopt solar meteoritic abundances from Grevesse et al. (1996).

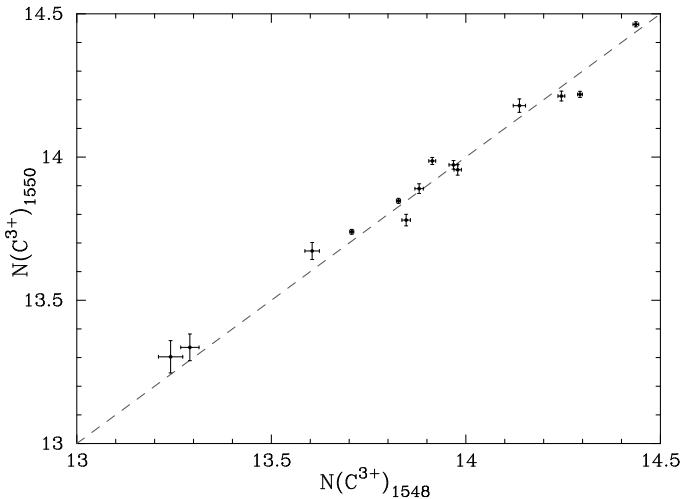


FIG. 1.— A comparison of C³⁺ column densities measured independently from C IV 1548 and 1550 in the same system using the apparent optical depth method (AODM). The dashed line traces the line of equality. The good agreement between the two values over a large range in $N(\text{C}^{3+})$ indicates the AODM is an accurate method for measuring column densities in unblended transitions.

To assess the accuracy of our measurements and the reliability of the error analysis, one can compare the column density measurements from two transitions for the same ion with very accurately known relative oscillator strengths. The majority of our damped Ly α systems exhibit absorption from the high-ion C³⁺ (Wolfe & Prochaska 2000) which exhibits a pair of resonance absorption lines at

$\lambda \approx 1550 \text{ \AA}$ due to the spin-orbit coupling of the 2p electronic level. Because the physics of spin-orbit coupling is well understood, we have high confidence that the relative oscillator strengths of the $\lambda\lambda$ 1548, 1550 transitions is 2:1. Figure 1 plots the $N(1550)$ value vs. $N(1548)$ for all of the damped Ly α systems where the transitions are unsaturated and unblended. One notes that the agreement in the values is excellent even out to $N(\text{C}^{3+}) \approx 14.5$ where saturation could affect the stronger C IV 1548 transition. In short, Figure 1 demonstrates that the AODM provides a reasonably accurate measure of the column densities and 1σ errors for our analysis.

We now comment on the individual systems noting revisions from previous works where applicable. In the figures, we have dotted out identified line blends.

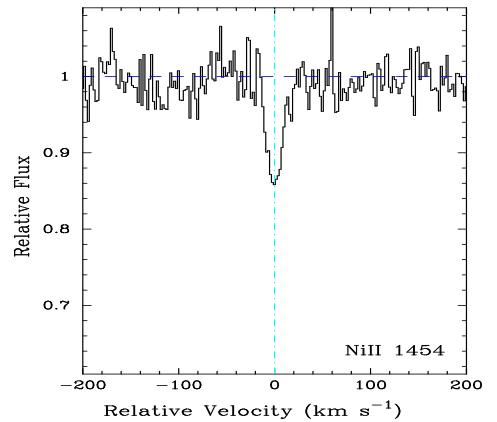


FIG. 2.— Velocity plot of the new metal-line transition for the damped Ly α system at $z = 3.390$ toward Q0000–26. The vertical line at $v = 0$ corresponds to $z = 3.3901$.

TABLE 3
IONIC COLUMN DENSITIES: Q0000-2619, $z = 3.390$

Ion	λ	AODM	N_{adopt}	[X/H]
HI	1215	21.410 ± 0.080		
Ni II	1454	13.365 ± 0.045	13.365 ± 0.045	-2.295 ± 0.092
Ni II	1751	< 13.689		

3.1. Q0000–26, $z = 3.390$

We presented metal abundances for this system in PW99, but missed the Ni II 1454 profile (Figure 2). Furthermore, we have identified a telluric blend with the Ni II 1751 profile which lead to an overestimate of Ni for this system. The Ni II 1454 column density is in excellent agreement with the Ni abundance derived by Molaro et al. (2000) and further clouds the nucleosynthetic interpretation of this system (Molaro et al. 2001). Owing to the higher signal-to-noise of the UVES spectrum, we now adopt the Fe⁺ column density from Molaro et al. (2000) but revise it downward to $N(\text{Fe}^+) = 14.75 \pm 0.03$ due to the new Fe II 1611 oscillator strength. This places the Fe⁺ column density in reasonably good agreement with the $N(\text{Ni}^+)$

measurement and further supports the notion that the α -elements (O, Si) are enhanced in this system. We note in passing that the $N(\text{Fe}^+)$ value derived from our HIRES spectrum of Fe II 1611 still significantly exceeds the UVES measurement for reasons we do not fully appreciate.

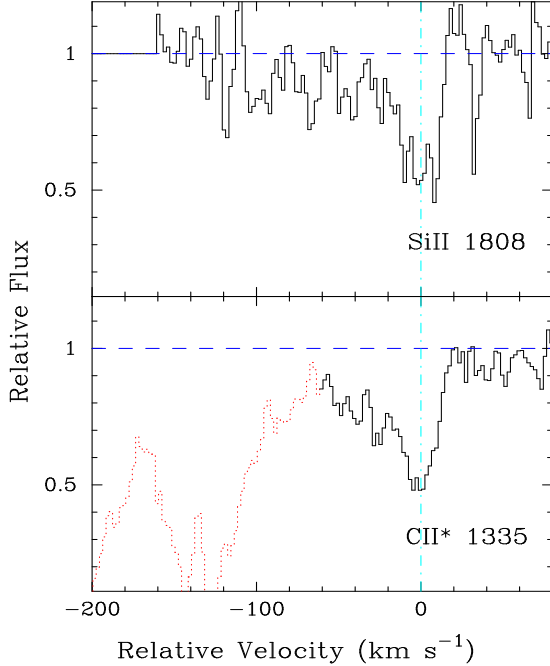


FIG. 3.— Velocity plot of the C II* 1335 profile for the damped Ly α system at $z = 3.439$ toward BR0019–15. The Si II 1808 profile is shown for comparison. The vertical line at $v = 0$ corresponds to $z = 3.4388$.

3.2. BR0019–15, $z = 3.439$

This system was analysed in PW99. Since publication, we have identified the C II* 1335 profile (Figure 3) and revised the Fe II 1608 column density to a lower limit because the profile is mildly saturated. This revision accounts for the large Ni/Fe ratio reported in PW99.

TABLE 4

IONIC COLUMN DENSITIES: BR0019-15, $z = 3.439$

Ion	λ	AODM	N_{adopt}	[X/H]
HI	1215	20.920 ± 0.100		
C II	1335	13.838 ± 0.018		
Fe II	1608	> 14.789	> 14.789	> -1.631
Ni II	1709	13.607 ± 0.105	13.683 ± 0.040	-1.487 ± 0.108
Ni II	1741	13.701 ± 0.043		

3.3. PH957, $z = 2.309$

This system was carefully studied in Wolfe et al. (1994) and subsequently in PW99. We present new limits on $N(\text{Co}^+)$ and $N(\text{Ti}^+)$, the latter which places a tight constraint on the Ti/Fe ratio ($[\text{Ti}/\text{Fe}] < -2.04$ dex). We also present a measurement of $N(\text{Mg}^0)$ from the Mg I 2026

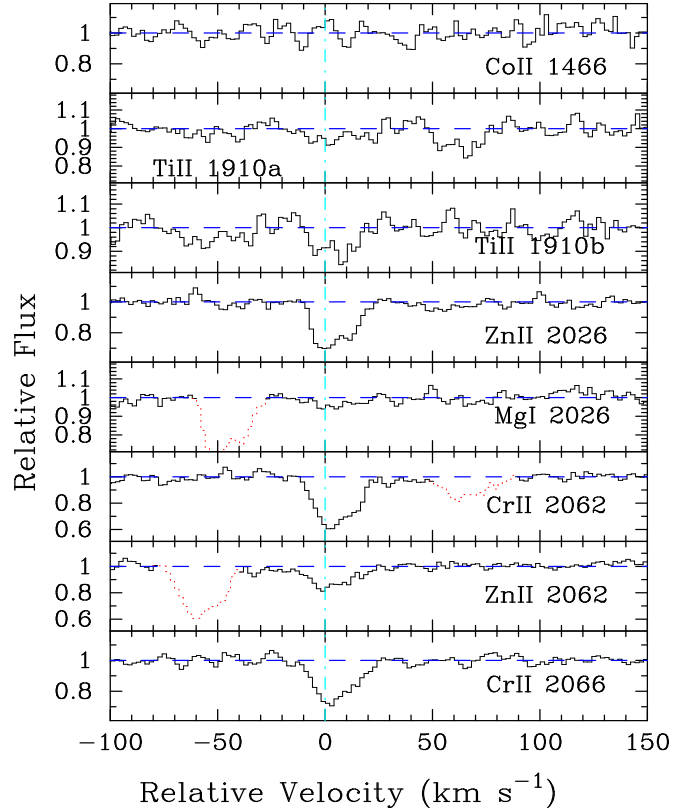


FIG. 4.— Velocity plot of several new metal-line transitions for the damped Ly α system at $z = 2.309$ toward PH 957. The vertical line at $v = 0$ corresponds to $z = 2.309$.

transition. Figure 4 presents the new profiles as well as several Zn II and Cr II transitions which provide clarification with respect to the identification of Mg I 2026. Table 5 lists the new values.

TABLE 5

IONIC COLUMN DENSITIES: PH957, $z = 2.309$

Ion	λ	AODM	N_{adopt}	[X/H]
HI	1215	21.400 ± 0.050		
Mg I	2026	12.344 ± 0.126		
Ti II	1910	< 12.207	< 12.207	< -2.133
Co II	1466	< 13.164	< 13.164	< -1.146

3.4. Q0149+33, $z = 2.140$

We have several changes to report on this system since PW99. Figure 5 presents the Ni II 1317 and Ti II 1910 profiles which were overlooked in PW99. We have also revised the Si II 1304 and Si II 1526 column densities to lower limits and base the Si abundance solely on the unsaturated Si II 1808 profile. For Cr, we now include the Cr II 2062 profile in our analysis. Finally, we warn that the Fe II 1608 column density might be considered a lower limit for $N(\text{Fe}^+)$ which would explain its underabundance relative to Cr and Ni. As noted in PW99, this system exhibits a

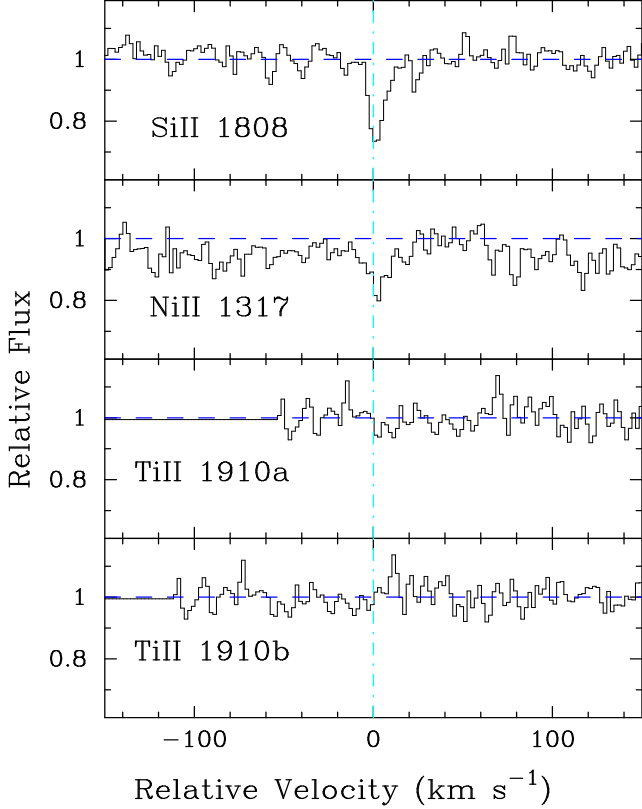


FIG. 5.— Velocity plot of several new metal-line transitions for the damped Ly α system at $z = 2.141$ toward Q0149+33. For comparison, we also plot the Si II 1808 profile. The vertical line at $v = 0$ corresponds to $z = 2.140755$.

super-solar Cr/Zn ratio ($[\text{Cr}/\text{Zn}] +0.22 \pm 0.1$). Because of its low $[\text{Zn}/\text{H}]$ and $N(\text{HI})$ values, this system has special significance in terms of dust depletion (Paper II, § 3).

TABLE 6

IONIC COLUMN DENSITIES: Q0149+33, $z = 2.141$

Ion	λ	AODM	N_{adopt}	$[\text{X}/\text{H}]$
HI	1215	20.500 ± 0.100		
Si II	1304	> 14.432	14.572 ± 0.047	-1.488 ± 0.110
Si II	1526	> 14.339		
Si II	1808	14.572 ± 0.047		
Ti II	1910	< 12.169	< 12.169	< -1.271
Cr II	2056	12.793 ± 0.044	12.720 ± 0.035	-1.450 ± 0.106
Cr II	2062	12.520 ± 0.090		
Cr II	2066	12.841 ± 0.062		
Ni II	1317	13.092 ± 0.071	13.169 ± 0.036	-1.581 ± 0.106
Ni II	1370	13.192 ± 0.103		
Ni II	1703	< 13.885		
Ni II	1709	13.184 ± 0.088		
Ni II	1741	13.250 ± 0.064		
Ni II	1751	13.179 ± 0.090		

3.5. Q0201+36, $z = 2.463$

This system was studied at length in Prochaska & Wolfe (1996) and we now include an upper limit on the Ti II 1910

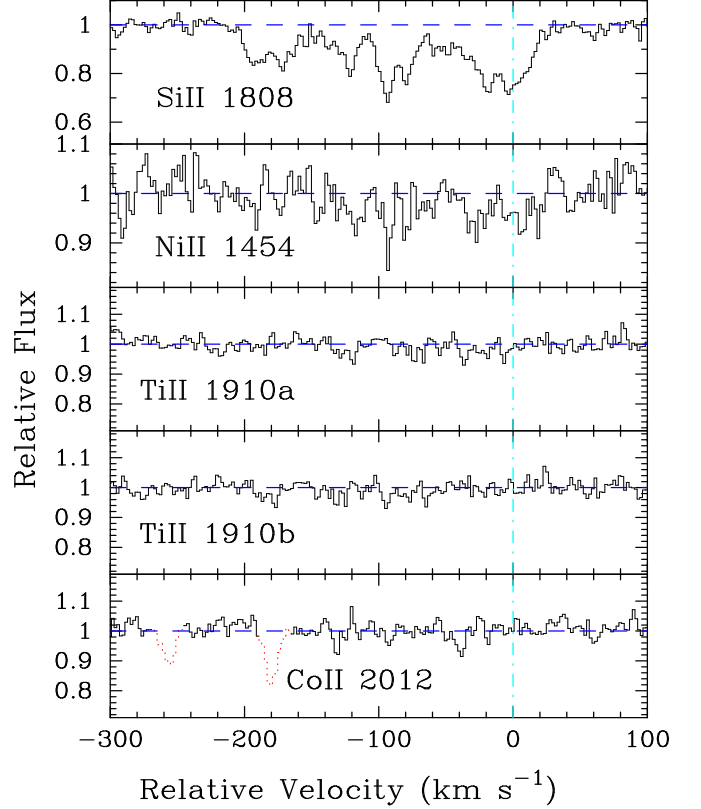


FIG. 6.— Velocity plot of several new metal-line transitions for the damped Ly α system at $z = 2.463$ toward Q0201+36. For comparison, we also plot the Si II 1808 profile. The vertical line at $v = 0$ corresponds to $z = 2.4628$.

transition and a measurement for the Ni II 1454 profile (Figure 6). To provide the best comparison with other objects in the complete sample, we adopt AODM column densities for all of the transitions (Table 7).

TABLE 7

IONIC COLUMN DENSITIES: Q0201+36, $z = 2.463$

Ion	λ	AODM	N_{adopt}	$[\text{X}/\text{H}]$
HI	1215	20.380 ± 0.045		
C IV	1550	14.612 ± 0.005		
Al II	1670	> 14.133	> 14.133	> -0.737
Al III	1862	13.601 ± 0.007		
Si II	1808	15.534 ± 0.010	15.534 ± 0.010	-0.406 ± 0.046
Si IV	1393	> 14.071		
Ti II	1910	< 12.196	< 12.196	< -1.124
Cr II	2056	13.266 ± 0.030	13.248 ± 0.029	-0.802 ± 0.054
Cr II	2066	13.132 ± 0.094		
Fe II	1608	15.010 ± 0.004	15.010 ± 0.004	-0.870 ± 0.045
Co II	2012	< 12.957	< 12.957	< -0.333
Ni II	1454	13.669 ± 0.073	14.022 ± 0.010	-0.608 ± 0.046
Ni II	1709	14.080 ± 0.021		
Ni II	1741	14.021 ± 0.013		
Ni II	1751	13.984 ± 0.021		

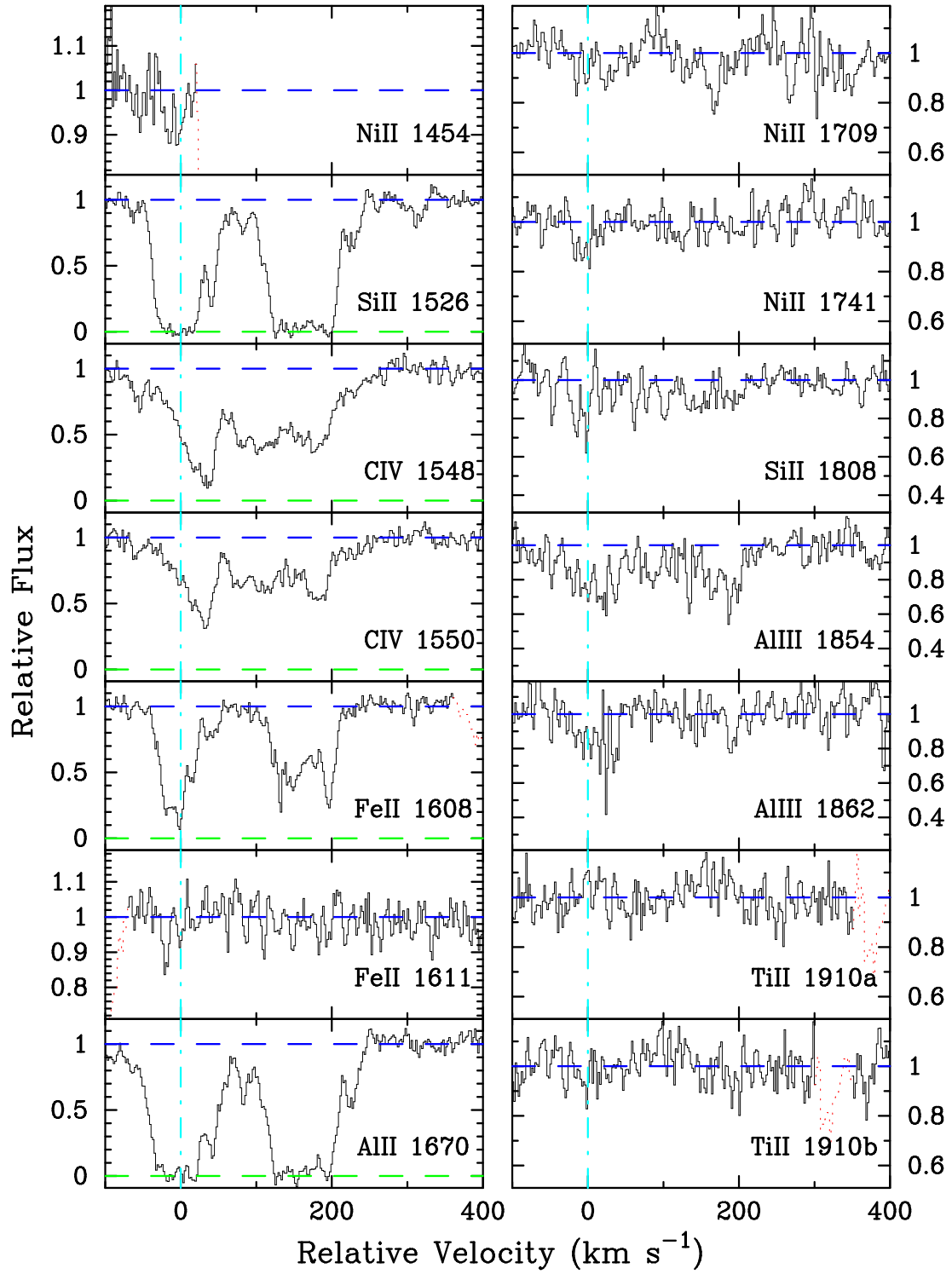


FIG. 7.— Velocity plot of the metal-line transitions for the damped Ly α system at $z = 3.253$ toward J0255+00. The vertical line at $v = 0$ corresponds to $z = 3.252931$.

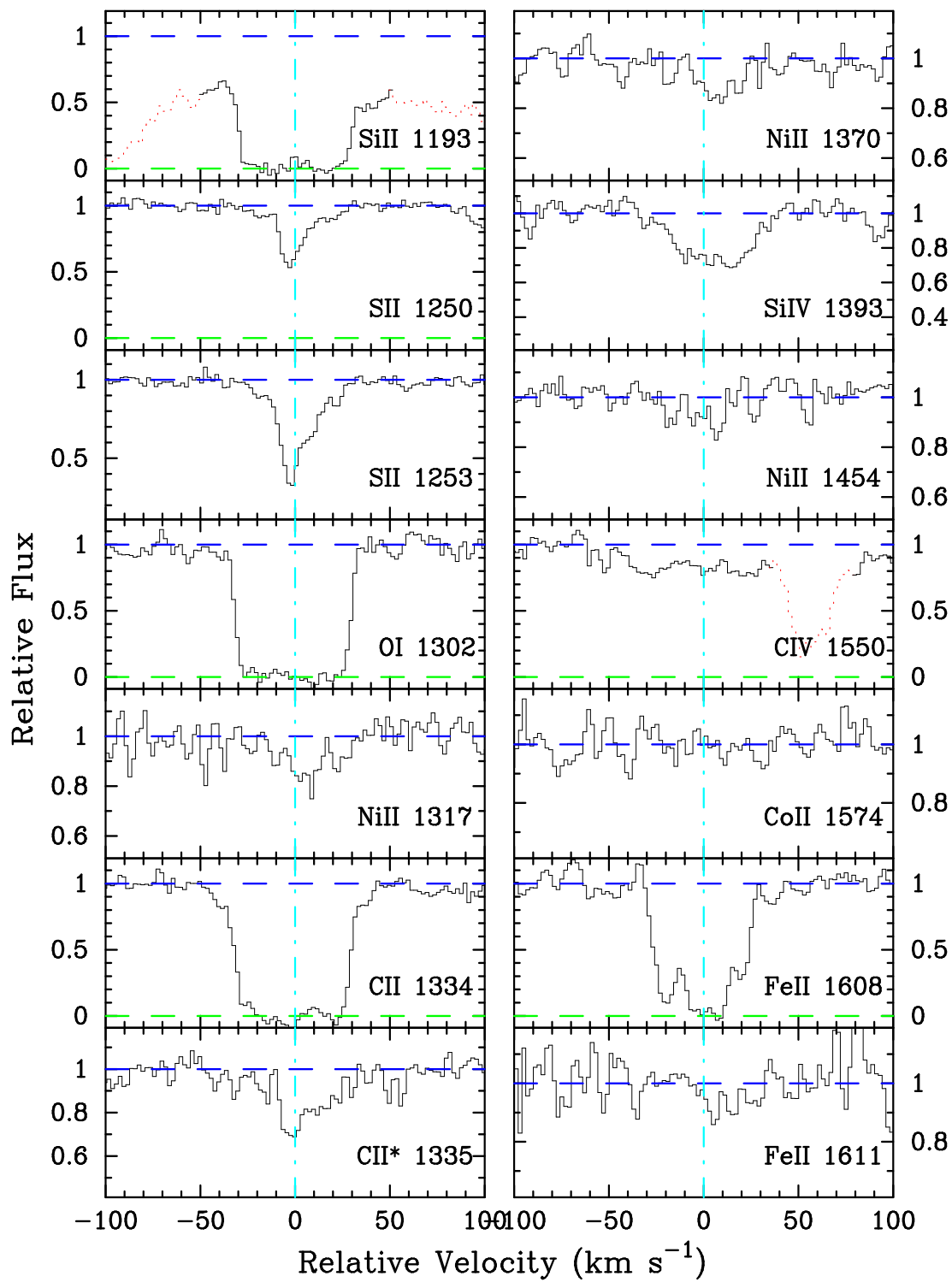


FIG. 8.— Velocity plot of the metal-line transitions for the damped Ly α system at $z = 3.915$ toward J0255+00. The vertical line at $v = 0$ corresponds to $z = 3.914617$.

3.6. J0255+00, $z=3.253$ and $z=3.915$

The two damped Ly α systems observed toward this faint SDSS quasar ($r = 19.1$; Fan et al. 1999) were identified as part of a program designed to survey $z > 3$ damped Ly α systems (Wolfe et al. 2001). We measured the $N(\text{HI})$ column densities of the two systems with an LRIS spectrum and then acquired HIRES observations at wavelengths redward of the Ly α forest. Figures 7 and 8 present the metal-line profiles for the two systems and Tables 8 and 9 list the ionic column densities. For the system at $z = 3.915$, $N(\text{Fe}^+)$ is well constrained by the lower and upper limits from the Fe II 1608 and Fe II 1611 transitions respectively and we have adopted a column density by averaging the two limits: $\log N(\text{Fe}^+) = 14.75 \pm 0.08$ dex.

TABLE 8
IONIC COLUMN DENSITIES: J0255+00, $z = 3.253$

Ion	λ	AODM	N_{adopt}	[X/H]
HI	1215	20.700 ± 0.100		
C IV	1548	14.437 ± 0.007		
C IV	1550	14.463 ± 0.009		
Al II	1670	> 13.879	> 13.879	> -1.311
Al III	1854	13.277 ± 0.025		
Al III	1862	12.977 ± 0.102		
Si II	1526	> 15.119	15.323 ± 0.038	-0.937 ± 0.107
Si II	1808	15.323 ± 0.038		
Ti II	1910	< 12.805	< 12.805	< -0.835
Fe II	1608	14.764 ± 0.010	14.764 ± 0.010	-1.436 ± 0.100
Fe II	1611	< 14.832		
Ni II	1709	13.771 ± 0.075	13.608 ± 0.066	-1.342 ± 0.120
Ni II	1741	13.473 ± 0.114		

TABLE 9
IONIC COLUMN DENSITIES: J0255+00, $z = 3.915$

Ion	λ	AODM	N_{adopt}	[X/H]
HI	1215	21.300 ± 0.050		
C II	1334	> 14.732	> 14.732	> -3.118
C II	1335	13.442 ± 0.040		
O I	1302	> 15.167	> 15.167	> -3.003
Si II	1193	> 14.193	> 14.193	> -2.667
Si IV	1393	12.856 ± 0.028		
S II	1250	14.763 ± 0.021	14.721 ± 0.011	-1.779 ± 0.051
S II	1253	14.707 ± 0.013		
Fe II	1608	> 14.707	14.750 ± 0.088	-2.050 ± 0.101
Fe II	1611	< 14.809		
Co II	1574	< 13.212	< 13.212	< -0.998
Ni II	1317	13.315 ± 0.052	13.271 ± 0.037	-2.279 ± 0.062
Ni II	1370	13.213 ± 0.058		
Ni II	1454	13.387 ± 0.104		

3.7. Q0336-01, $z=3.062$

This LBQS quasar is one of the few damped Ly α systems at $z > 3$ with $N(\text{HI}) > 10^{21} \text{ cm}^{-2}$. Although most of the transitions that we examine lie within the Ly α forest, we have carefully avoided lines which are clearly blended with forest clouds. Unfortunately, we only place a lower limit on $N(\text{Si}^+)$ although we do report a reasonably secure value for $N(\text{S}^+)$. The system also provides an accurate measurement of Ar I and a reasonable estimate of P II. Finally, we note a very large $N(\text{O}^0)$ lower limit derived

from the saturated O I 988 transition. This limit may be influenced by blending in the Ly α forest, but we have no reason to believe this is the case at present.

TABLE 10
IONIC COLUMN DENSITIES: Q0336-01, $z = 3.062$

Ion	λ	AODM	N_{adopt}	[X/H]
HI	1215	21.200 ± 0.100		
C II	1334	> 14.958	> 14.958	> -2.792
C II	1335	14.041 ± 0.025		
C IV	1548	14.138 ± 0.016		
C IV	1550	14.180 ± 0.023		
O I	988	> 16.940	> 16.940	> -1.130
O I	1302	> 15.389		
Si II	1020	> 15.141	> 15.141	> -1.619
Si II	1193	> 14.322		
Si II	1304	> 14.926		
Si IV	1393	13.767 ± 0.015		
Si IV	1402	13.656 ± 0.032		
P II	1152	13.133 ± 0.075	13.133 ± 0.075	-1.597 ± 0.125
S II	1250	15.118 ± 0.022	14.994 ± 0.011	-1.406 ± 0.101
S II	1259	14.970 ± 0.012		
Ar I	1048	> 13.860	14.346 ± 0.065	-1.374 ± 0.119
Ar I	1066	14.346 ± 0.065		
Fe II	1081	14.879 ± 0.055	14.905 ± 0.033	-1.795 ± 0.105
Fe II	1125	14.920 ± 0.046		
Fe II	1142	14.936 ± 0.099		
Fe II	1144	> 14.719		
Ni II	1317	< 13.389	13.469 ± 0.057	-1.981 ± 0.115
Ni II	1370	13.424 ± 0.065		
Ni II	1454	13.880 ± 0.091		

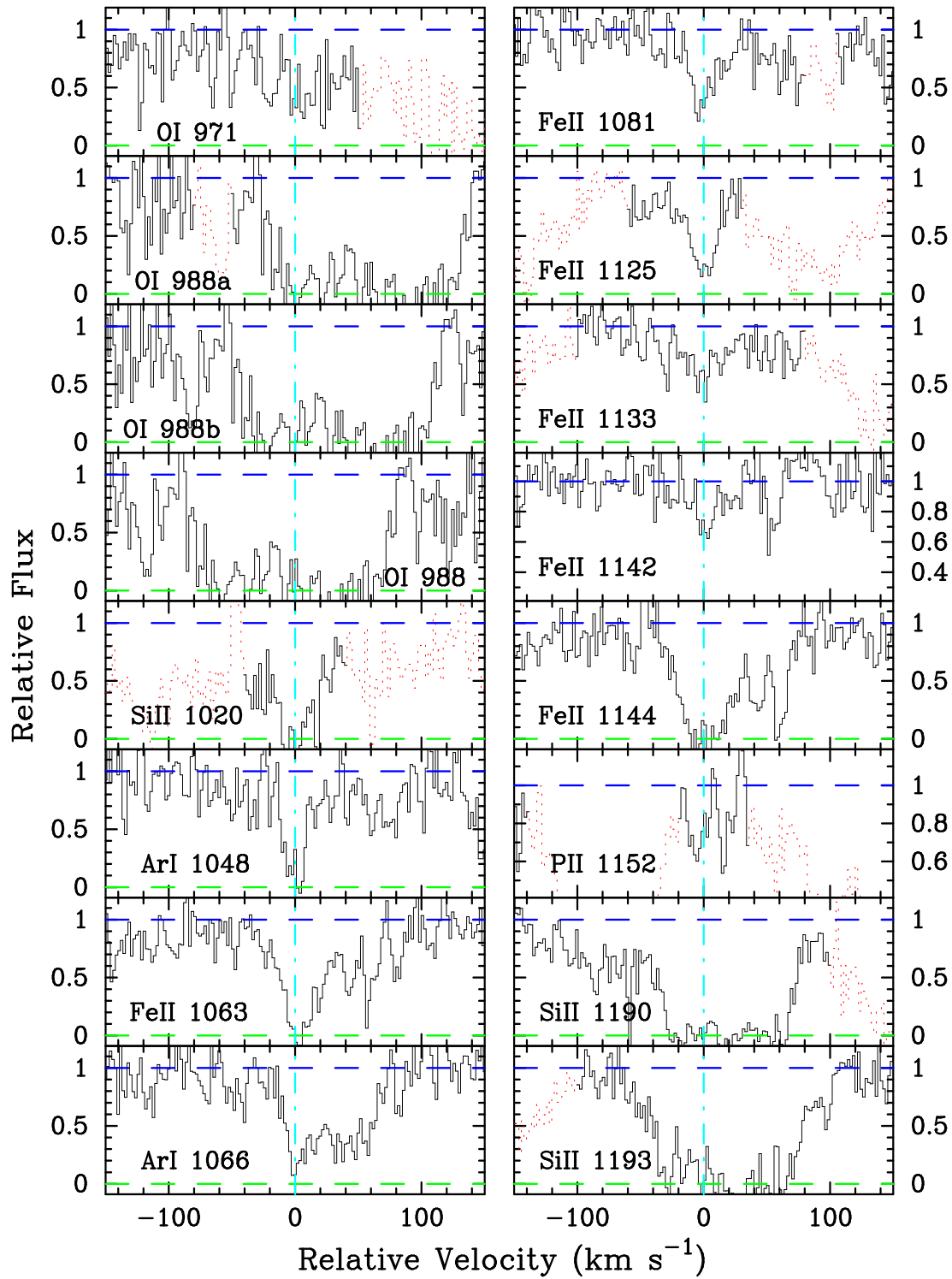
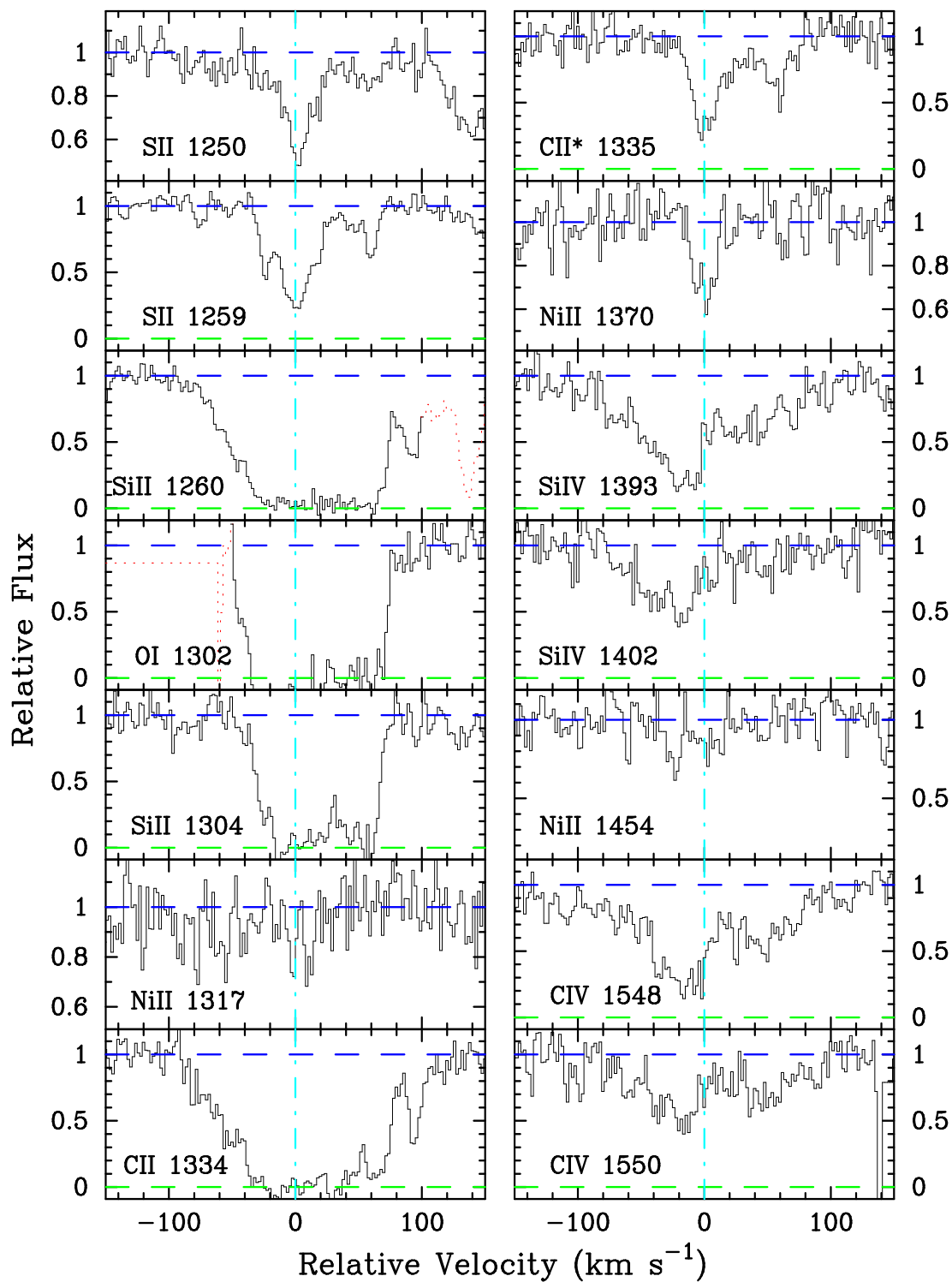


FIG. 9.— Velocity plot of the metal-line transitions for the damped Ly α system at $z = 3.062$ toward Q0336-01. The vertical line at $v = 0$ corresponds to $z = 3.062078$.



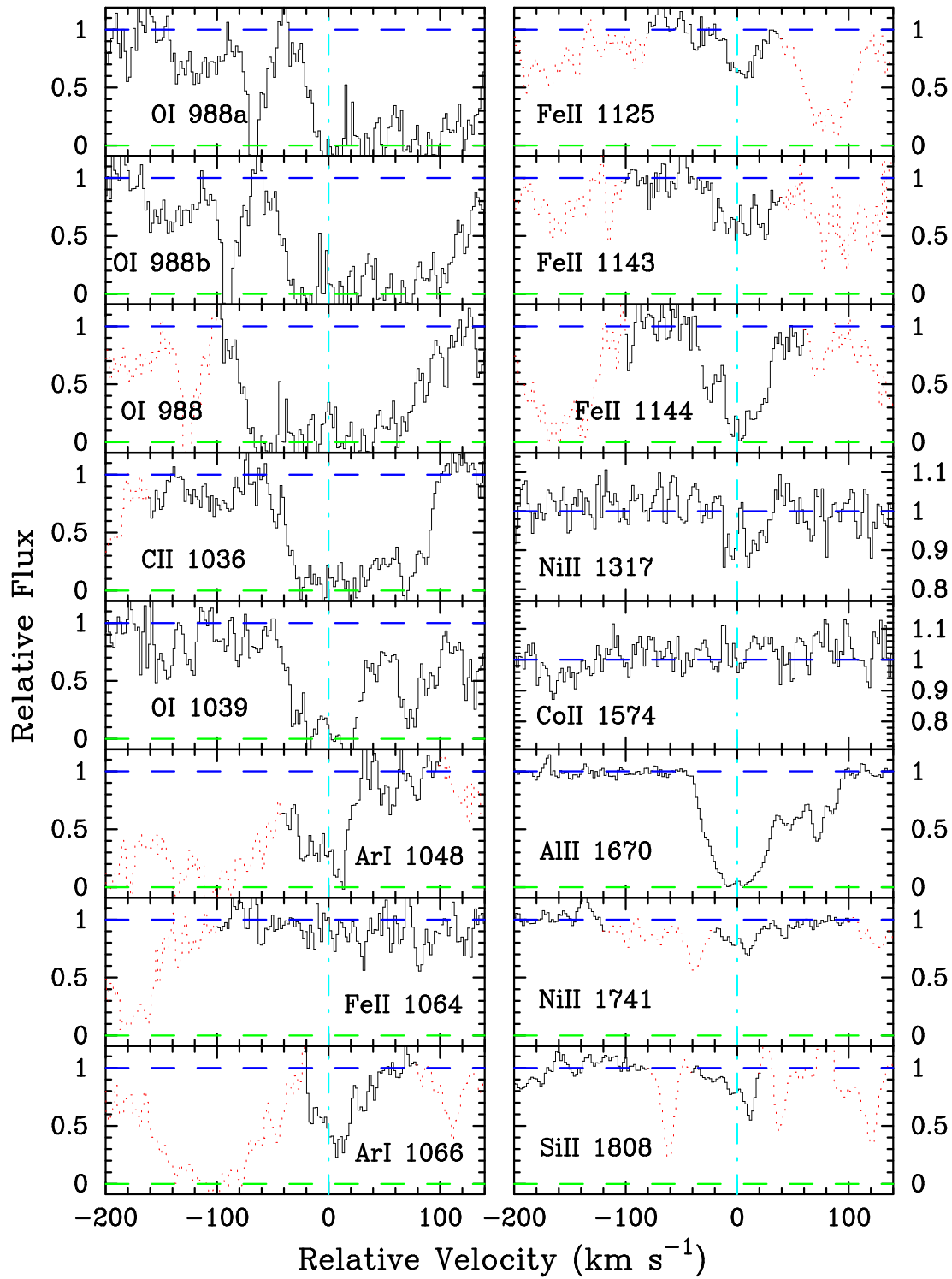


FIG. 10.— Velocity plot of several new metal-line transitions for the damped Ly α system at $z = 3.025$ toward Q0347–38. The vertical line at $v = 0$ corresponds to $z = 3.0247$.

3.8. Q0347–38, $z = 3.025$

Although this system was analysed in PW99, we report a number of measurements and limits based on the original data and new observations taken with a second, blue setup. Table 11 presents the ionic column densities and Figure 10 plots the new profiles. We also reclassify the sulfur abundance as an upper limit because this transition is blended with a Ly α forest cloud.

TABLE 11

IONIC COLUMN DENSITIES: Q0347-38, $z = 3.025$

Ion	λ	AODM	N_{adopt}	[X/H]
HI	1215	20.800 ± 0.100		
C II	1036	> 14.930	> 15.065	> -2.285
C II	1334	> 15.066		
O I	1039	> 15.953	> 15.953	> -1.717
O I	1302	> 15.449		
Al II	1670	> 13.408	> 13.408	> -1.882
Si II	1260	> 14.329	15.017 ± 0.026	-1.343 ± 0.103
Si II	1304	> 14.889		
Si II	1808	15.017 ± 0.026		
S II	1259	< 14.760	< 14.760	< -1.240
Ar I	1048	> 14.063	14.282 ± 0.035	-1.038 ± 0.106
Ar I	1066	14.282 ± 0.035		
Fe II	1063	14.763 ± 0.143	14.503 ± 0.007	-1.797 ± 0.100
Fe II	1125	14.453 ± 0.056		
Fe II	1143	14.712 ± 0.040		
Fe II	1608	14.501 ± 0.007		
Fe II	1611	< 14.447		
Co II	1574	< 13.196	< 13.196	< -0.514
Ni II	1317	13.034 ± 0.093	13.383 ± 0.031	-1.667 ± 0.105
Ni II	1370	13.115 ± 0.099		
Ni II	1741	14.056 ± 0.019		

TABLE 12

IONIC COLUMN DENSITIES: Q0458-02, $z = 2.040$

Ion	λ	AODM	N_{adopt}	[X/H]
HI	1215	21.650 ± 0.090		
C I	1656	< 12.453		
Mg I	2026	13.117 ± 0.031		
Ti II	1910	< 12.495	< 12.495	< -2.095
Co II	2012	< 13.092	< 13.093	< -1.467
Ni II	1317	14.257 ± 0.024	14.181 ± 0.018	-1.719 ± 0.092
Ni II	1370	14.315 ± 0.071		
Ni II	1454	14.187 ± 0.114		
Ni II	1703	13.987 ± 0.090		
Ni II	1709	14.158 ± 0.034		
Ni II	1741	14.195 ± 0.032		
Ni II	1751	14.170 ± 0.033		
Zn II	2026	13.134 ± 0.020	13.134 ± 0.020	-1.186 ± 0.092
Zn II	2062	> 13.031		

3.9. Q0458–02, $z = 2.040$

In reviewing this system, we identified a number of transitions missed in PW99. Figure 11 presents the metal-line profiles and Table 12 shows the column densities. Most of these only yield upper limits on ionic column densities, but given the very large HI column density of this system these limits are valuable. For example, the limit on Ti II 1910 implies $[\text{Ti}/\text{Fe}] < -0.45$ dex which is highly suggestive of dust depletion. As discussed in Paper II, § 2.1.6,

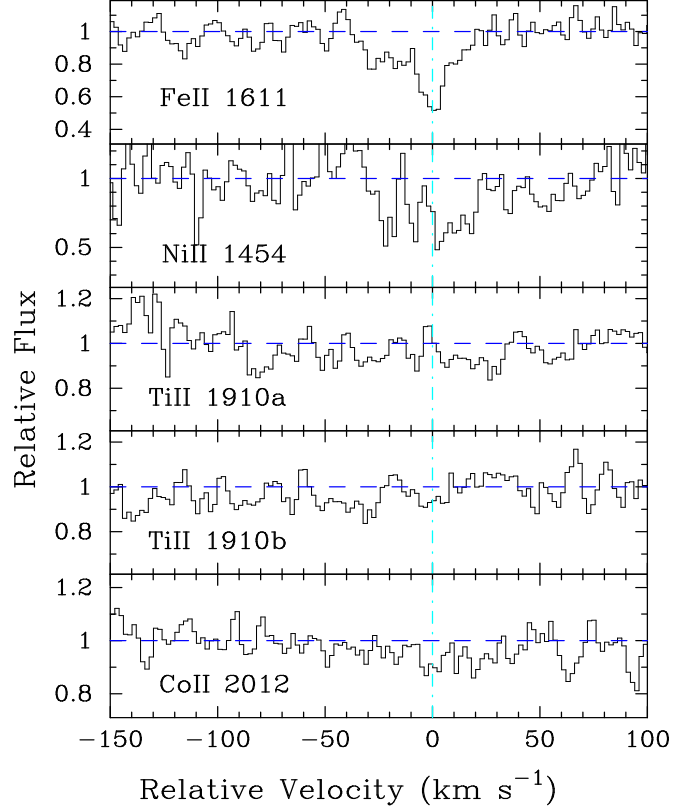


FIG. 11.— Velocity plot of several new metal-line transitions for the damped Ly α system at $z = 2.040$ toward Q0458–02. The vertical line at $v = 0$ corresponds to $z = 2.03955$.

we have revised the measurement of $N(\text{Zn}^+)$ downward by 0.02 dex due to mild blending between the Zn II 2026 and Mg I 2026 profiles.

3.10. HS0741+47, $z = 3.017$

The very bright QSO HS0741+47 is taken from the Hamburg ESO QSO survey (Hagen et al. 1999). Our wavelength coverage of the damped Ly α system spans from 3600–7500Å and we have identified over 20 metal-line profiles. Figure 12 plots the velocity profiles and Table 13 presents all of the measurements. Unfortunately, our observations do not include the Zn II and Cr II transitions, although the $N(\text{Si}^+)$ value indicates it would require very high S/N to obtain a measurement.

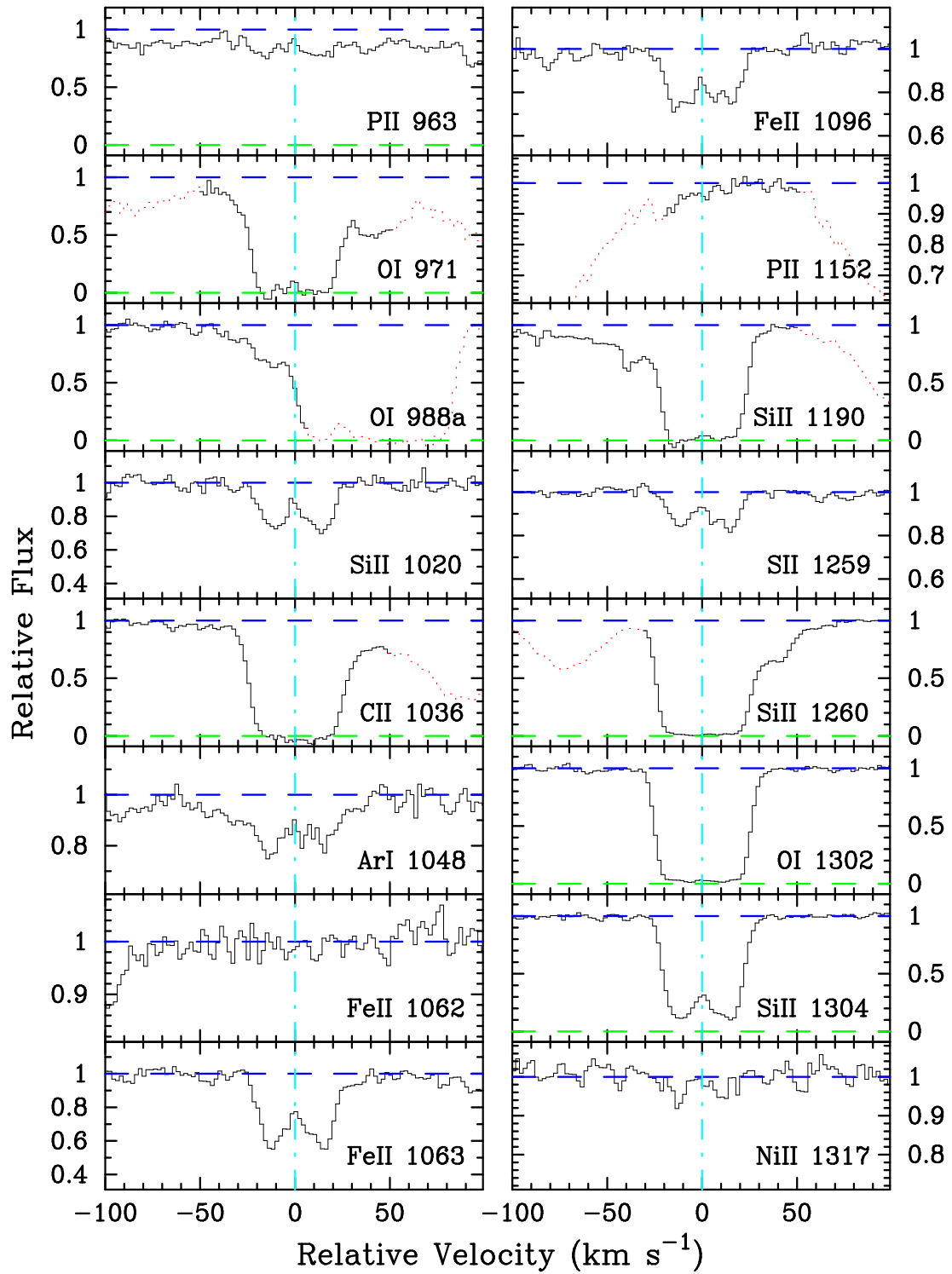
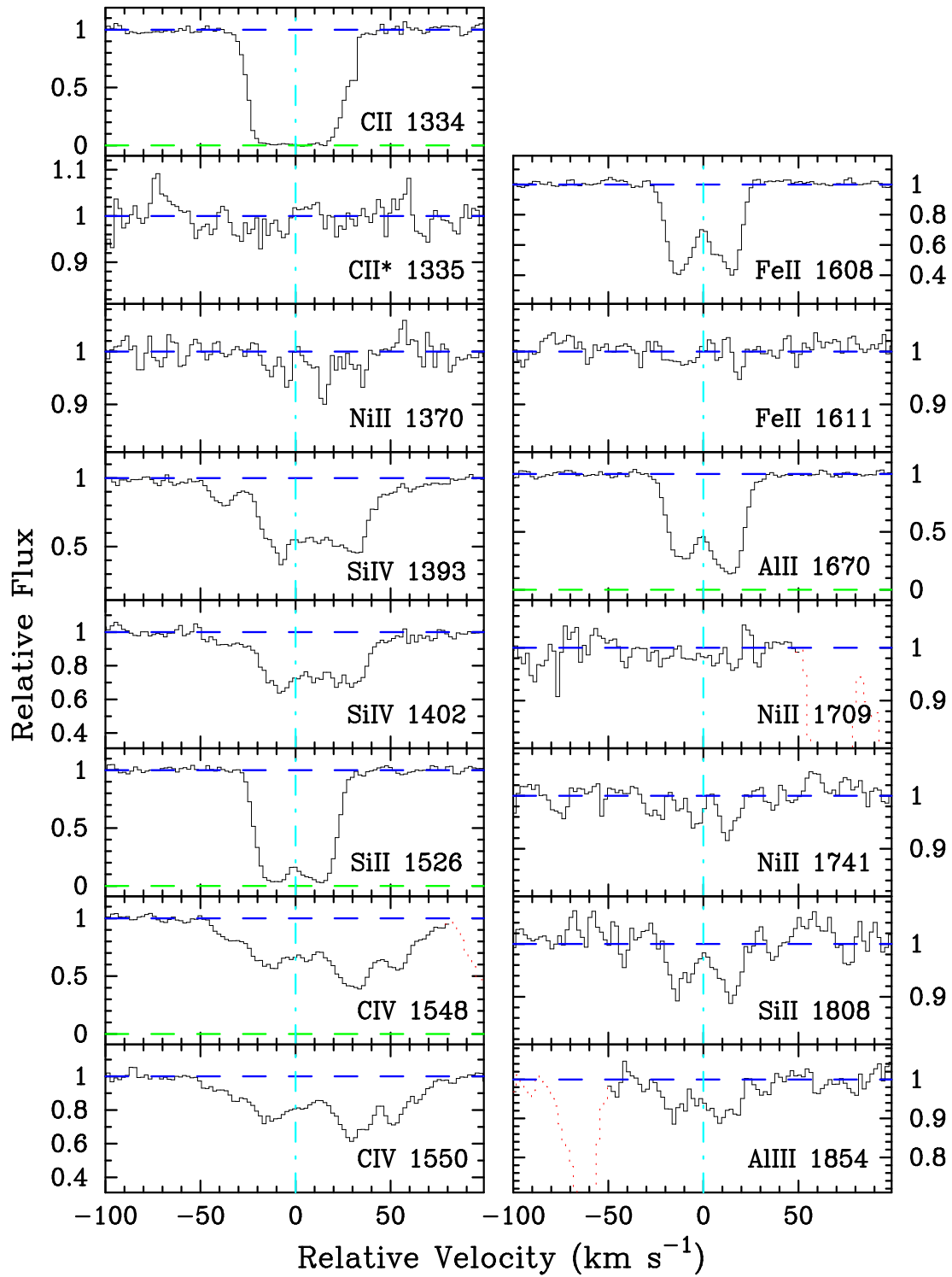


FIG. 12.— Velocity plot of the metal-line transitions for the damped Ly α system at $z = 3.017$ toward HS0741+4741. The vertical line at $v = 0$ corresponds to $z = 3.017399$.



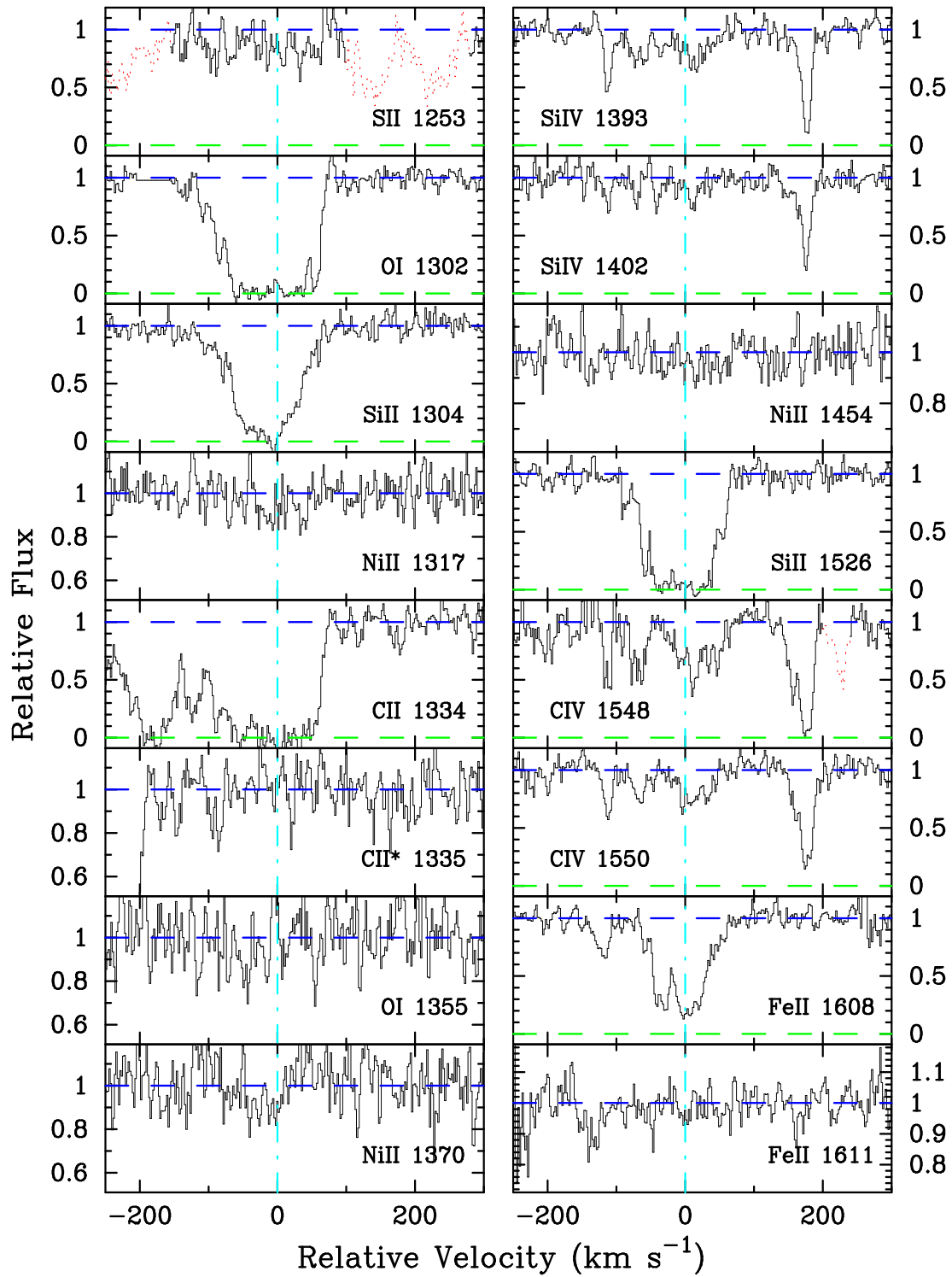


FIG. 13.— Velocity plot of the metal-line transitions for the damped Ly α system at $z = 2.465$ toward Q0836+11. The vertical line at $v = 0$ corresponds to $z = 2.46527$.

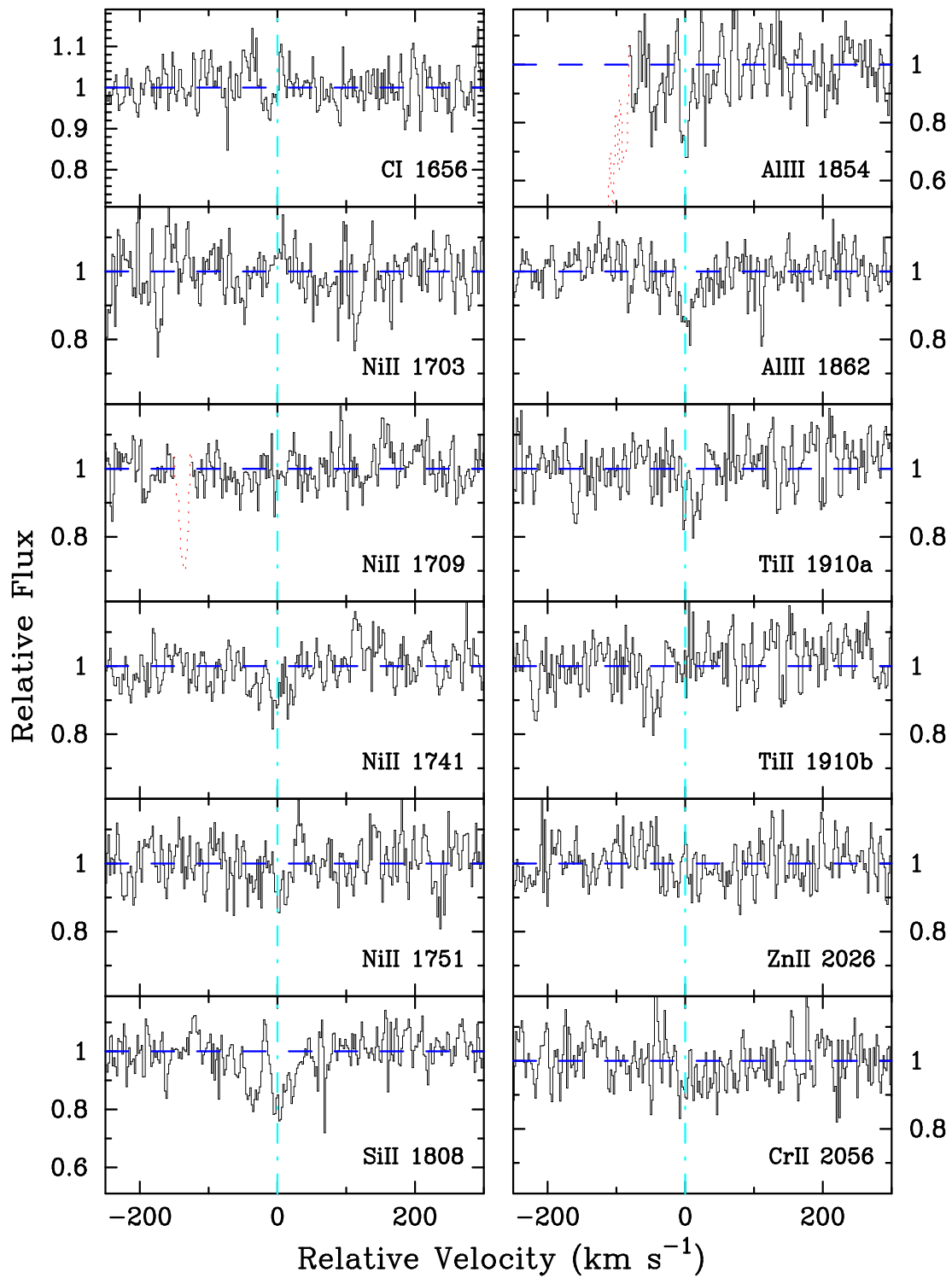


TABLE 13

IONIC COLUMN DENSITIES: HS0741+4741, $z = 3.017$

Ion	λ	AODM	N_{adopt}	[X/H]
HI	1215	20.480 ± 0.100		
C II	1036	> 14.864	> 14.864	> -2.166
C II	1334	> 14.737		
C II	1335	< 12.554		
C IV	1548	13.827 ± 0.005		
C IV	1550	13.847 ± 0.009		
O I	971	> 15.711	> 15.711	> -1.639
O I	1302	> 15.229		
Al II	1670	12.823 ± 0.005	12.824 ± 0.005	-2.146 ± 0.100
Al III	1854	12.161 ± 0.043		
Si II	1020	14.162 ± 0.019	14.354 ± 0.003	-1.686 ± 0.100
Si II	1260	> 13.937		
Si II	1304	14.368 ± 0.003		
Si II	1526	> 14.469		
Si II	1808	14.395 ± 0.051		
Si IV	1393	13.382 ± 0.006		
Si IV	1402	13.376 ± 0.011		
P II	1152	< 12.080	< 12.080	< -1.930
S II	1259	14.000 ± 0.016	14.000 ± 0.016	-1.680 ± 0.101
Ar I	1048	13.166 ± 0.020	13.166 ± 0.020	-1.834 ± 0.102
Fe II	1063	14.075 ± 0.010	14.052 ± 0.005	-1.928 ± 0.100
Fe II	1096	14.068 ± 0.015		
Fe II	1608	14.041 ± 0.006		
Fe II	1611	< 14.082		
Co II	1574	< 12.958	< 12.958	< -0.432
Ni II	1317	12.658 ± 0.110	12.758 ± 0.049	-1.972 ± 0.111
Ni II	1370	12.736 ± 0.081		
Ni II	1454	< 12.833		
Ni II	1709	12.745 ± 0.144		
Ni II	1741	12.943 ± 0.078		

TABLE 14

IONIC COLUMN DENSITIES: Q0836+11, $z = 2.465$

Ion	λ	AODM	N_{adopt}	[X/H]
HI	1215	20.580 ± 0.100		
C II	1334	> 15.026	> 15.026	> -2.104
C II	1335	< 13.121		
C IV	1548	> 14.218		
O I	1302	> 15.485	> 15.485	> -1.965
O I	1355	< 18.186		
Al III	1854	12.459 ± 0.093		
Al III	1862	12.634 ± 0.076		
Si II	1304	> 14.918	14.987 ± 0.045	-1.153 ± 0.110
Si II	1526	> 14.850		
Si II	1808	14.987 ± 0.045		
Si IV	1393	13.557 ± 0.024		
Si IV	1402	13.592 ± 0.043		
S II	1253	< 14.660	< 14.660	< -1.120
Ti II	1910	< 12.537	< 12.538	< -0.982
Cr II	2056	< 12.898	< 12.898	< -1.352
Cr II	2066	< 13.230		
Fe II	1608	14.677 ± 0.011	14.677 ± 0.011	-1.403 ± 0.101
Fe II	1611	< 14.784		
Co II	1466	< 13.383	< 13.383	< -0.107
Co II	1574	< 13.442		
Ni II	1317	13.364 ± 0.105	13.388 ± 0.065	-1.442 ± 0.119
Ni II	1370	< 13.339		
Ni II	1454	< 13.365		
Ni II	1703	< 14.058		
Ni II	1709	< 13.275		
Ni II	1741	13.406 ± 0.083		
Ni II	1751	< 13.393		
Zn II	2026	< 12.119	< 12.119	< -1.131

3.11. Q0836+11, $z = 2.465$

This damped Ly α system is drawn from the LBQS survey (Wolfe et al. 1995) and we adopt the $N(\text{HI})$ value obtained from their analysis. Our observations cover a large number of transitions, many of which only provide upper limits owing to the relatively poor S/N (Figure 13, Table 14). In passing, we note that some of the Ni II upper limits are in contradiction with our adopted $N(\text{Ni}^+)$ value. This might reflect an error in the relative f -values but more likely reflects the large error in the adopted value.

TABLE 15

IONIC COLUMN DENSITIES: Q0841+12, $z = 2.375$

Ion	λ	AODM	N_{adopt}	[X/H]
HI	1215	20.950 ± 0.087		
Co II	1466	< 13.047	< 12.990	< -0.870
Co II	1941	< 12.990		
Ni II	1454	13.415 ± 0.075	13.523 ± 0.030	-1.677 ± 0.092
Ni II	1741	13.560 ± 0.040		
Ni II	1751	13.547 ± 0.055		

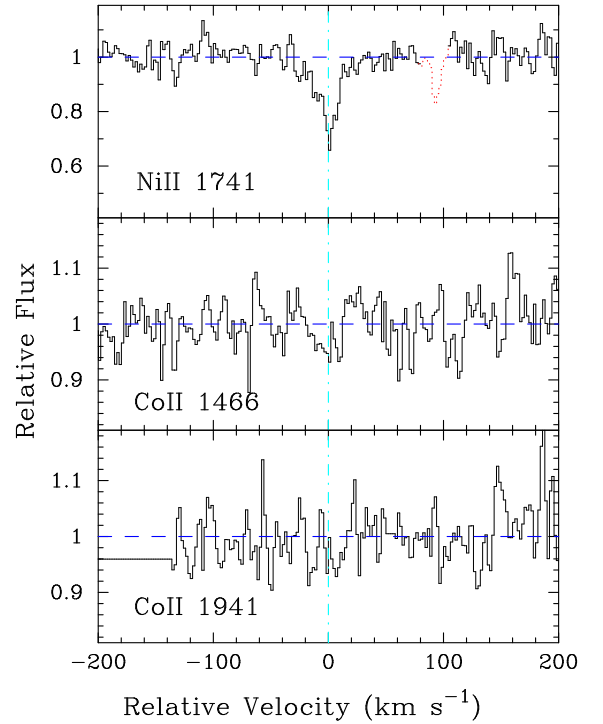


FIG. 14.— Velocity plot of two Co II profiles for the damped Ly α system at $z = 2.375$ toward Q0841+12. For comparison, we also plot the Ni II 1741 profile. The vertical line at $v = 0$ corresponds to $z = 2.374518$.

3.12. Q0841+12, $z = 2.375$ and $z = 2.476$

We augment the measurements presented in PW99 with a few additional Ni II transitions and several Co II and Ti II upper limits. These transitions are plotted in Figures 14 and 15 and tabulated in Tables 15 and 16. As

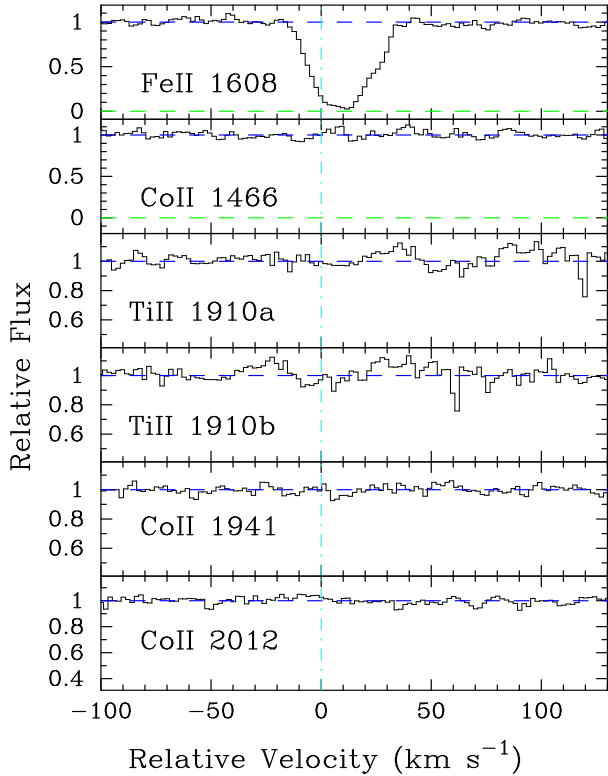


FIG. 15.— Velocity plot of the new metal-line transitions for the damped Ly α system at $z = 2.476$ toward Q0841+12. For comparison, we also plot the Fe II 1608 profile. The vertical line at $v = 0$ corresponds to $z = 2.476219$.

discussed in PW99, we based the Fe abundance for the $z = 2.476$ system on the saturated Fe II 1608 profile. We now choose to report the Fe II 1608 column density as a lower limit on $N(\text{Fe}^+)$ and adopt an Fe abundance based on averaging the lower and upper limits from Fe II 1608 and Fe II 1611 respectively: $\log N(\text{Fe}^+) = 14.53 \pm 0.05$.

TABLE 16
IONIC COLUMN DENSITIES: Q0841+12, $z = 2.476$

Ion	λ	AODM	N_{adopt}	[X/H]
HI	1215	20.780 ± 0.097		
Ti II	1910	< 12.158	< 12.158	< -1.562
Fe II	1608	> 14.517		
Fe II	1611	< 14.543		
Co II	1466	< 13.206	< 12.726	< -0.964
Co II	1941	< 12.783		
Co II	2012	< 12.726		
Ni II	1709	13.415 ± 0.060	13.355 ± 0.040	-1.675 ± 0.105
Ni II	1741	13.321 ± 0.054		
Ni II	1751	< 13.348		

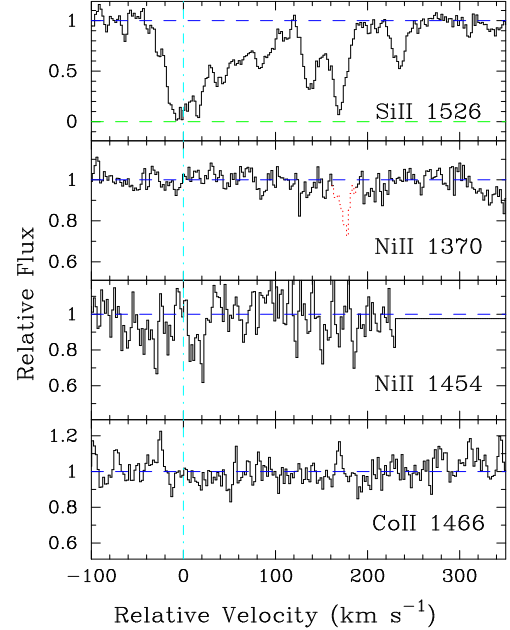


FIG. 16.— Velocity plot of the new metal-line transitions for the damped Ly α system at $z = 3.857$ toward BRI0951-04. For comparison, we also plot the Si II 1526 profile. The vertical line at $v = 0$ corresponds to $z = 3.856689$.

3.13. BRI0951-04, $z = 3.857$ and $z = 4.203$

Our combined spectrum now includes a second setup with significant coverage blueward of the Ly α peak. Unfortunately, the new data adds only a few unblended transitions to the analysis (Figures 16,17 and Tables 17,18). With respect to PW99, we now suspect that the feature at +177 km/s in the $z = 3.857$ Ni II 1370 profile is unrelated to that transition and obtain an upper limit on $N(\text{Ni}^+)$. This value is in much better agreement with the Fe and Al abundances. In terms of the system at $z = 4.203$, we still have no reliable estimate of the Fe-peak abundance. The combination of poor S/N and low HI column density have resulted in the non-detection of Fe II 1608 and our observations did not cover C II 1334 or Al II 1670. Finally, we revise the oxygen abundance to account for the saturated OI 1302 profile.

TABLE 17
IONIC COLUMN DENSITIES: BRI0951-04, $z = 3.857$

Ion	λ	AODM	N_{adopt}	[X/H]
HI	1215	20.600 ± 0.100		
Co II	1466	< 13.597	< 13.597	< 0.087
Ni II	1370	< 12.977	< 12.977	< -1.873
Ni II	1454	< 13.927		

3.14. BRI0952-01, $z = 4.024$

This damped Ly α system was identified by Storrie-Lombardi et al. (1996) and confirmed with a follow-up LRIS spectrum by Storrie-Lombardi and Wolfe (2000). We adopt

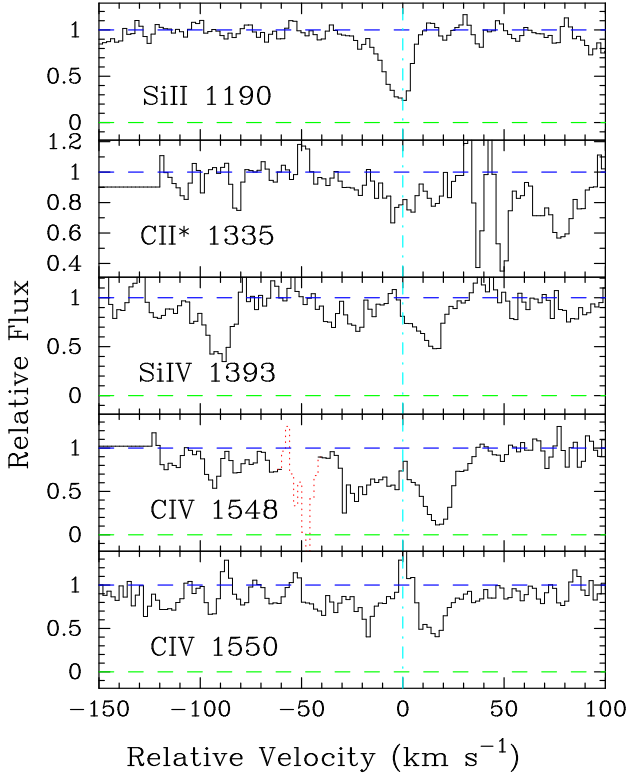


FIG. 17.— Velocity plot of the new metal-line transitions for the damped Ly α system at $z = 4.203$ toward BRI0951-04. The vertical line at $v = 0$ corresponds to $z = 4.202896$.

TABLE 18

IONIC COLUMN DENSITIES: BRI0951-04, $z = 4.203$

Ion	λ	AODM	N_{adopt}	[X/H]
HI	1215	20.400 ± 0.100		
C IV	1548			
C IV	1550	13.945 ± 0.052		
O I	1302	> 14.596	> 14.596	> -2.674
Si II	1190	13.417 ± 0.042	13.342 ± 0.030	-2.618 ± 0.104
Si II	1526	13.302 ± 0.056		
Si IV	1393	12.918 ± 0.063		

the $N(\text{HI})$ value from the latter analysis. Figure 18 presents the velocity profiles covered by our single setup. Unfortunately, a mis-estimate of the absorption redshift coupled with several line blends have limited our ionic column density measurements of this system (Table 19). As reported in Prochaska & Wolfe (2000), we estimate the Fe^+ column density by combining the unblended features observed for the Fe II 1144 and 1608 profiles. With the updated oscillator strengths, we find $N(\text{Fe}^+) = 14.187 \pm 0.07$.

3.15. *PSS0957+33*, $z=3.279$ and $z = 4.178$

The two damped Ly α systems toward this PSS quasar (Djorgovski et al. 1998) were discovered during the first night of our ongoing ESI project designed to discover and measure the metallicity of $z > 3$ damped systems (PGW01). Given the apparent brightness of this quasar we chose to obtain a HIRES spectrum. Figures 19 and 20 present the

TABLE 19

IONIC COLUMN DENSITIES: BRI0952-01, $z = 4.024$

Ion	λ	AODM	N_{adopt}	[X/H]
HI	1215	20.550 ± 0.100		
C II	1334	> 15.312	> 15.312	> -1.788
C II	1335	13.549 ± 0.024		
C IV	1550	14.796 ± 0.009		
Si IV	1393	14.134 ± 0.006		
Fe II	1144	> 13.864	14.187 ± 0.076	-1.863 ± 0.126
Fe II	1608	> 13.746		
Co II	1574	< 13.750	< 13.750	< 0.290
Ni II	1454	< 13.439	< 13.439	< -1.361

metal-line transition identified in our HIRES spectrum and Tables 20 and 21 give the ionic column densities.

TABLE 20

IONIC COLUMN DENSITIES: PSS0957+33, $z = 3.279$

Ion	λ	AODM	N_{adopt}	[X/H]
HI	1215	20.320 ± 0.080		
C IV	1548	13.979 ± 0.009		
C IV	1550	13.956 ± 0.019		
Al II	1670	> 13.322	> 13.322	> -1.488
Al III	1854	12.514 ± 0.048		
Al III	1862	12.578 ± 0.087		
Si II	1808	14.880 ± 0.053	14.880 ± 0.053	-1.000 ± 0.096
Fe II	1608	14.367 ± 0.016	14.367 ± 0.016	-1.453 ± 0.082
Co II	1941	< 13.285	< 13.285	< 0.055
Ni II	1709	13.283 ± 0.122	13.318 ± 0.070	-1.252 ± 0.106
Ni II	1741	13.339 ± 0.085		
Zn II	2026	< 12.127	< 12.127	< -0.863

TABLE 21

IONIC COLUMN DENSITIES: PSS0957+33, $z = 4.178$

Ion	λ	AODM	N_{adopt}	[X/H]
HI	1215	20.500 ± 0.100		
O I	1302	> 15.344	> 15.344	> -2.026
Al II	1670	> 13.256	> 13.256	> -1.734
Si II	1304	14.556 ± 0.012	14.556 ± 0.012	-1.504 ± 0.101
Si II	1526	> 14.488		
Si IV	1402	13.155 ± 0.049		
S II	1250	> 14.647	14.392 ± 0.060	-1.308 ± 0.117
S II	1253	14.392 ± 0.060		
Fe II	1608	14.129 ± 0.045	14.129 ± 0.045	-1.871 ± 0.110
Co II	1466	< 13.648	< 13.648	< 0.238
Co II	1574	< 13.907		
Ni II	1317	< 12.910	< 12.910	< -1.840

To test the metallicities obtained with the ESI spectrum, we can compare the HIRES values with the Fe^+ column densities adopted in PGW01 after correcting for the new oscillator strengths. For the system at $z = 3.279$, the Fe II 1608 column densities are in excellent agreement but because this transition is blended with telluric absorption it might only provide an upper limit on $N(\text{Fe}^+)$. In PGW01, we derived the Fe^+ column density from Fe II 2344 which is redward of our HIRES coverage. We now suspect this value was an underestimate of $N(\text{Fe}^+)$ as it implies $[\text{Ni}/\text{Fe}] > +0.3$ dex. For now, we adopt an Fe^+ column density based on the Fe II 1608 profile.

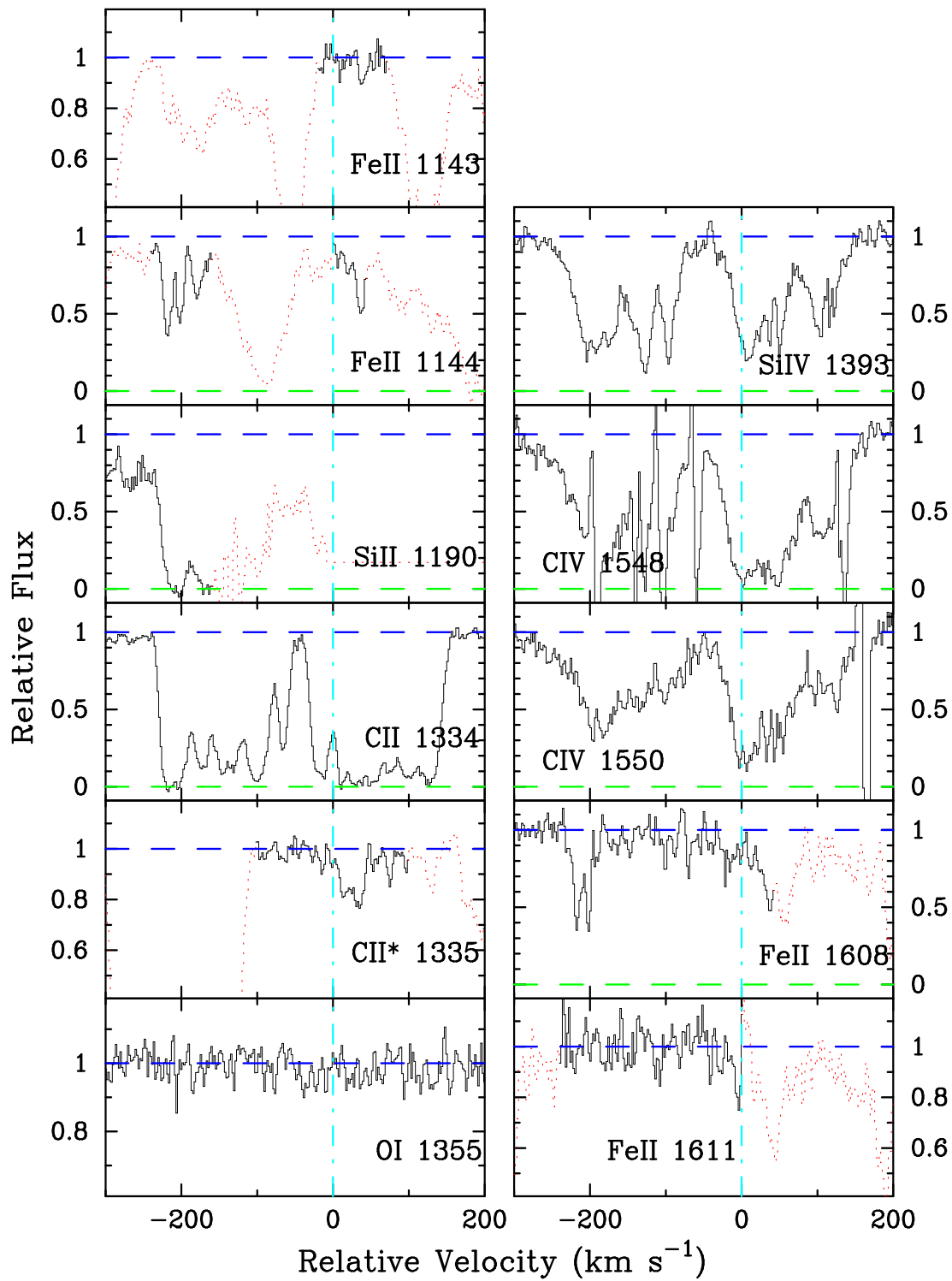


FIG. 18.— Velocity plot of the metal-line transitions for the damped Ly α system at $z = 4.024$ toward BRI0952-01. The vertical line at $v = 0$ corresponds to $z = 4.024433$.

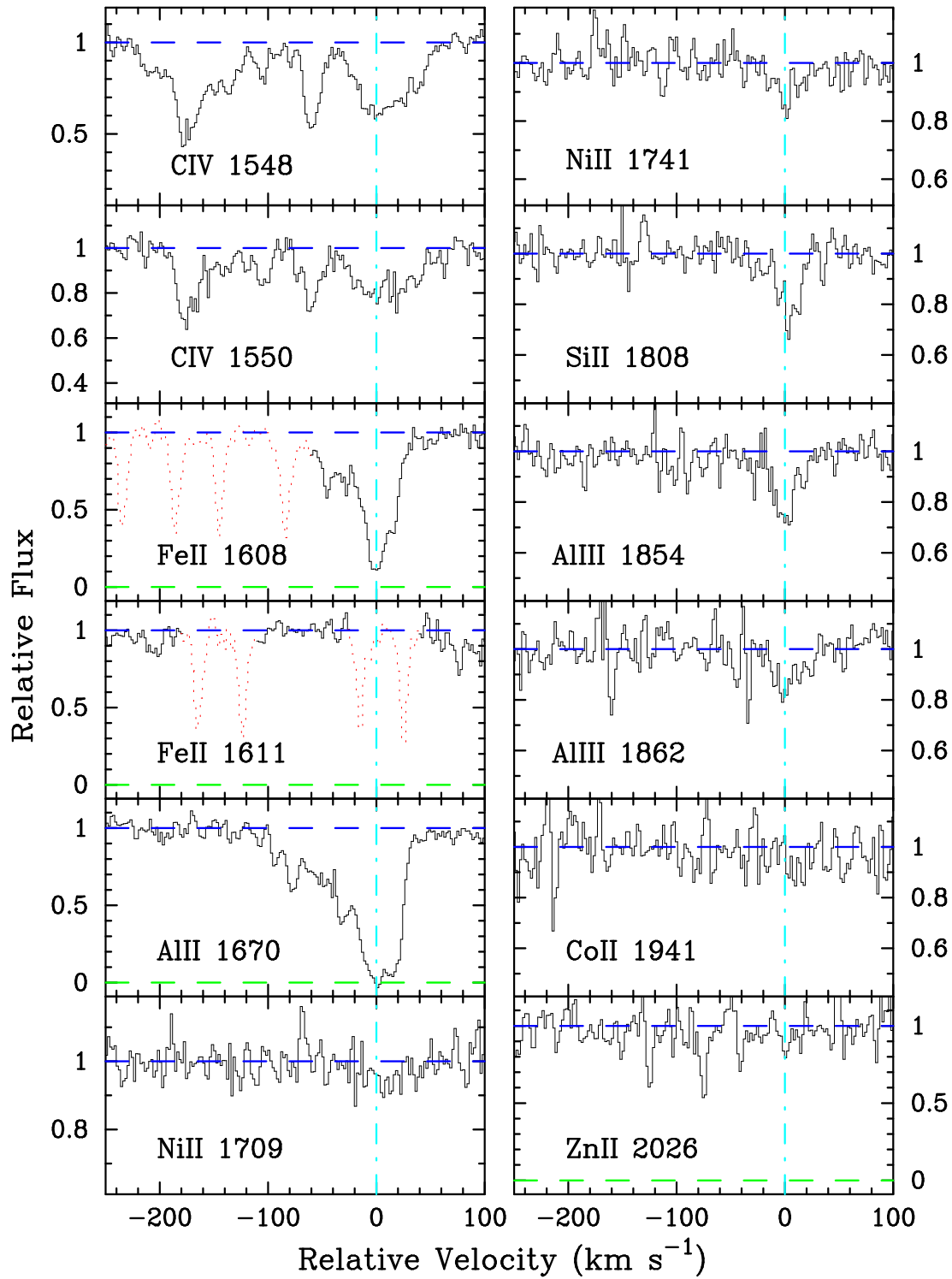


FIG. 19.— Velocity plot of the metal-line transitions for the damped Ly α system at $z = 3.279$ toward PSS0957+33. The vertical line at $v = 0$ corresponds to $z = 3.279576$.

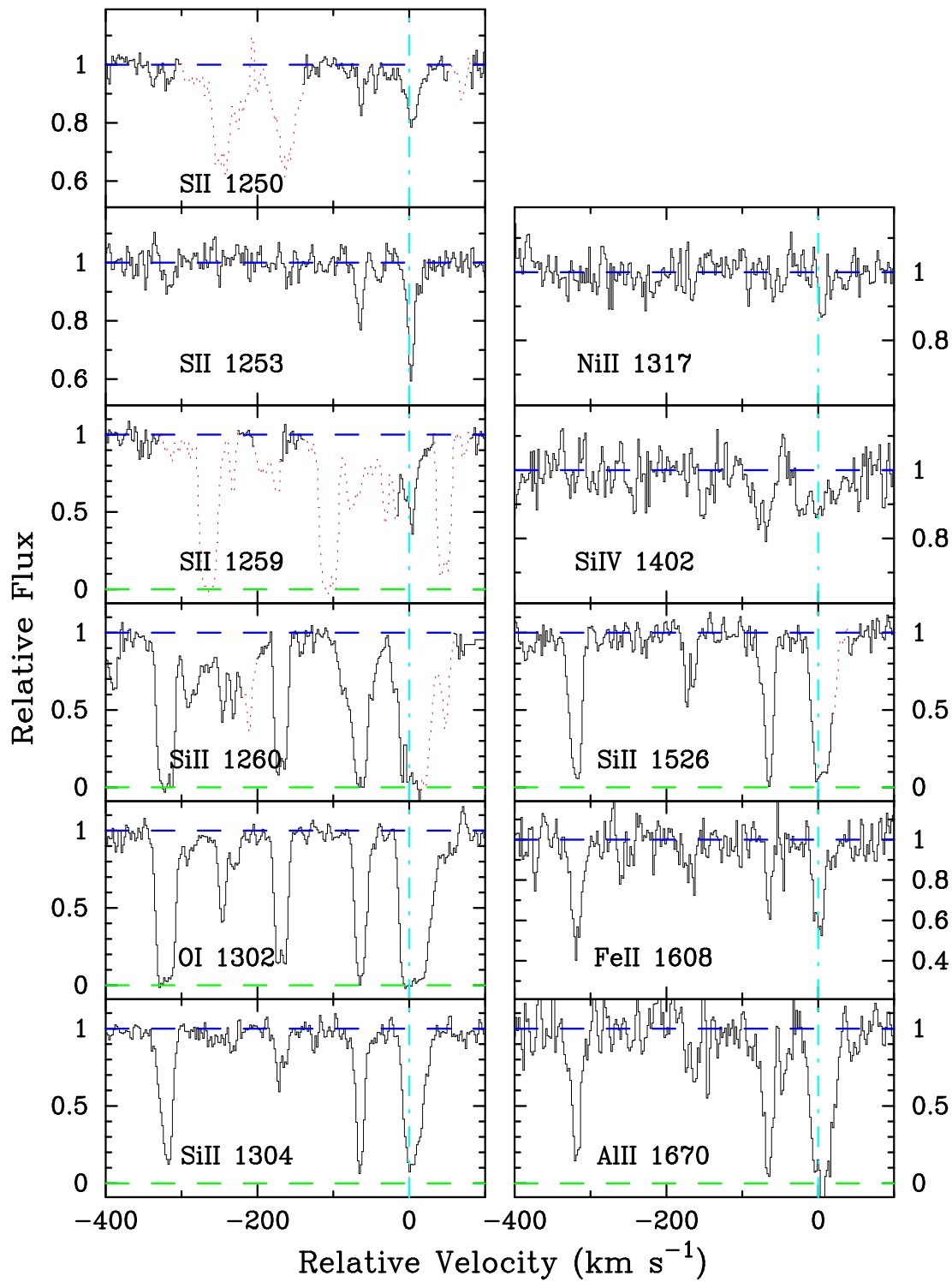


FIG. 20.— Velocity plot of the metal-line transitions for the damped Ly α system at $z = 4.178$ toward PSS0957+33. The vertical line at $v = 0$ corresponds to $z = 4.179825$.

The system at $z = 4.178$ presents a more worrisome picture regarding column densities derived from ESI echellette observations. Comparing the column densities for Fe II 1608, we find that we underestimated $N(\text{Fe}^+)$ by ≈ 0.3 dex with the ESI spectrum. It is somewhat puzzling given that the profile is not very strong (unlike the Si II profiles for example) and the quality of the ESI data is high. The strongest features are relatively narrow so the difference is probably an effect of the lower resolution. Another puzzling aspect of the $z = 4.178$ systems is the S^+ column density derived from S II 1250 and 1253. Although the S II 1250 profile is partially blended with an unrelated C IV system ($z_{\text{abs}} = 3.181$), we are confident that the absorption at $-100 \text{ km s}^{-1} < v < 20 \text{ km s}^{-1}$ is free of contamination from the C IV system. In this case, $N(\text{S II 1250})$ provides a lower limit on $\log N(\text{S}^+) > 14.65$. This lower limit, however, is well in excess of the $N(\text{S}^+)$ value derived from the unblended S II 1253 transition. The component at $v = 0 \text{ km/s}$ in the S II 1250 profile is wider than its counterpart in the S II 1253 profile, but there is no identifiable blend. Perhaps the difference suggests an extreme case of hidden saturation (Savage and Sembach 1991). If it is line saturation, this helps explain why the ESI data significantly underestimates the column densities in this case and it also raises the possibility that the abundances derived from the HIRES observations are underestimated. This would be particularly surprising given that the spectra has a resolution of $R = 47000$. Unfortunately, our HIRES spectrum did not cover any other pair of unsaturated transitions from the same ion to further test this issue. Furthermore, the difference even exists in a comparison of S II 1250 and 1253 with respect to the feature at $v \approx -75 \text{ km/s}$. Perhaps this is all the result of errors in the S II oscillator strengths, but it would have likely been identified by researchers who study the ISM (e.g. Howk, Savage, & Fabian 1999).

3.16. *BRI1108-07*, $z = 3.608$

This damped Ly α system was discovered and confirmed by Storrie-Lombardi et al. (1996). The quasar is relatively bright and we obtained a reasonably high S/N HIRES spectrum. Figure 21 presents the velocity profiles and Table 22 lists the ionic column densities. The Fe^+ and Si^+ column densities are well measured and indicate a very large Si/Fe ratio, perhaps indicative of substantial Type II SN enrichment.

3.17. *Q1210+17*, $z = 1.892$

This system is a member of the LBQS sample and we have adopted the $N(\text{HI})$ value from their analysis. We plot all of the transitions covered by our observations in Figure 22 and list the column densities in Table 23. This damped system exhibits a relatively low Zn/Fe ratio which suggests it is largely free of dust depletion. In passing, we note a remarkable similarity of the relative abundances of Si, Ni, Cr, Fe, and Zn with the same pattern observed by Molaro et al. (2000) for the damped system toward Q0000-26, albeit at a much higher metallicity.

TABLE 22
IONIC COLUMN DENSITIES: BRI1108-07, $z = 3.608$

Ion	λ	AODM	N_{adopt}	[X/H]
HI	1215	20.500 ± 0.100		
C II	1334	> 14.675	> 14.675	> -2.375
C II	1335	< 12.341		
C IV	1548	14.293 ± 0.006		
C IV	1550	14.219 ± 0.011		
O I	1302	> 14.873	> 14.873	> -2.497
Al II	1670	12.822 ± 0.015	12.822 ± 0.015	-2.168 ± 0.101
Si II	1304	14.262 ± 0.004	14.262 ± 0.004	-1.798 ± 0.100
Si II	1526	> 14.260		
Si II	1808	< 14.665		
Si IV	1402	13.685 ± 0.010		
Fe II	1608	13.884 ± 0.014	13.884 ± 0.014	-2.116 ± 0.101
Fe II	1611	< 14.269		
Ni II	1317	< 13.136	< 13.136	< -1.614
Ni II	1751	< 13.180		

TABLE 23
IONIC COLUMN DENSITIES: Q1210+17, $z = 1.892$

Ion	λ	AODM	N_{adopt}	[X/H]
HI	1215	20.600 ± 0.100		
C IV	1548	< 14.230		
C IV	1550	14.053 ± 0.017		
Al II	1670	> 13.440	> 13.440	> -1.650
Al III	1854	12.999 ± 0.017		
Al III	1862	13.005 ± 0.021		
Si II	1526	> 14.780	15.285 ± 0.018	-0.875 ± 0.102
Si II	1808	15.285 ± 0.018		
Si IV	1393	13.594 ± 0.025		
Cr II	2056	13.291 ± 0.019	13.243 ± 0.016	-1.027 ± 0.101
Cr II	2062	13.219 ± 0.030		
Cr II	2066	13.091 ± 0.058		
Fe II	1608	> 14.780	14.951 ± 0.063	-1.149 ± 0.118
Fe II	1611	14.951 ± 0.063		
Co II	1574	< 13.513	< 12.728	< -0.782
Co II	2012	< 12.728		
Ni II	1370	< 13.964	13.632 ± 0.020	-1.218 ± 0.102
Ni II	1454	< 13.832		
Ni II	1709	13.657 ± 0.031		
Ni II	1741	13.628 ± 0.029		
Ni II	1751	13.590 ± 0.049		
Zn II	2026	12.409 ± 0.032	12.370 ± 0.029	-0.900 ± 0.104
Zn II	2062	12.263 ± 0.069		

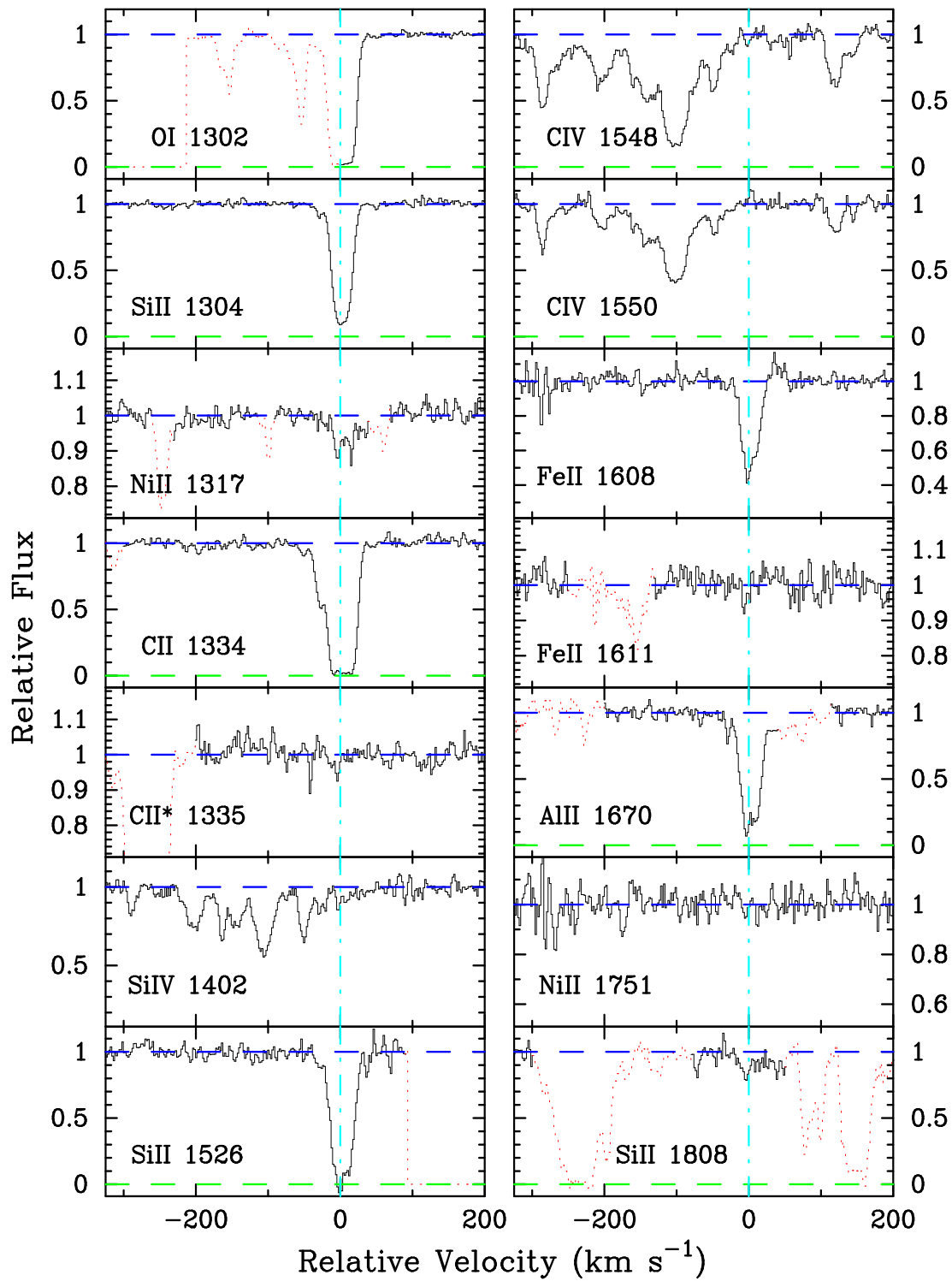


FIG. 21.— Velocity plot of the metal-line transitions for the damped Ly α system at $z = 3.608$ toward BRI1108-07. The vertical line at $v = 0$ corresponds to $z = 3.607619$.

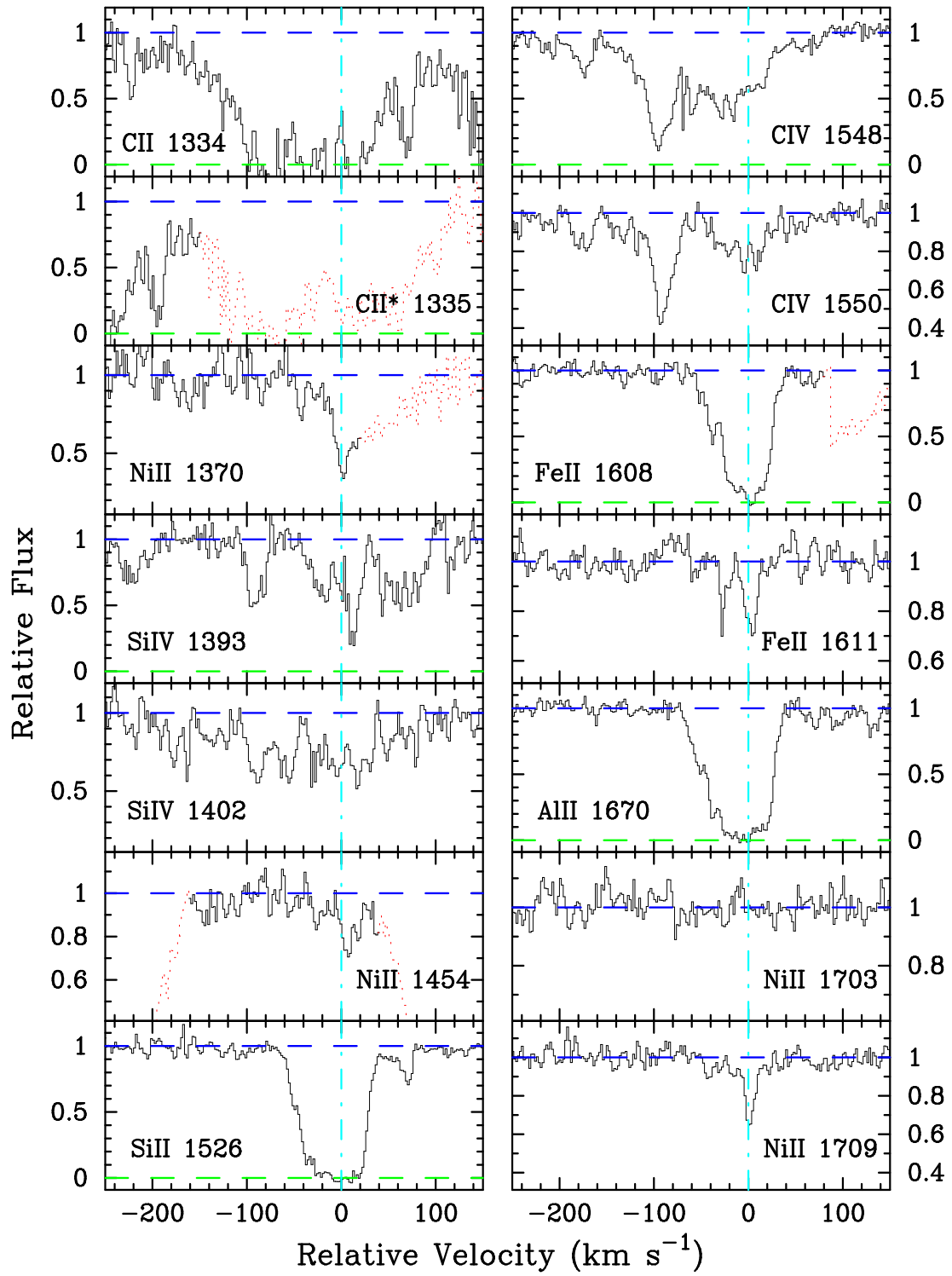
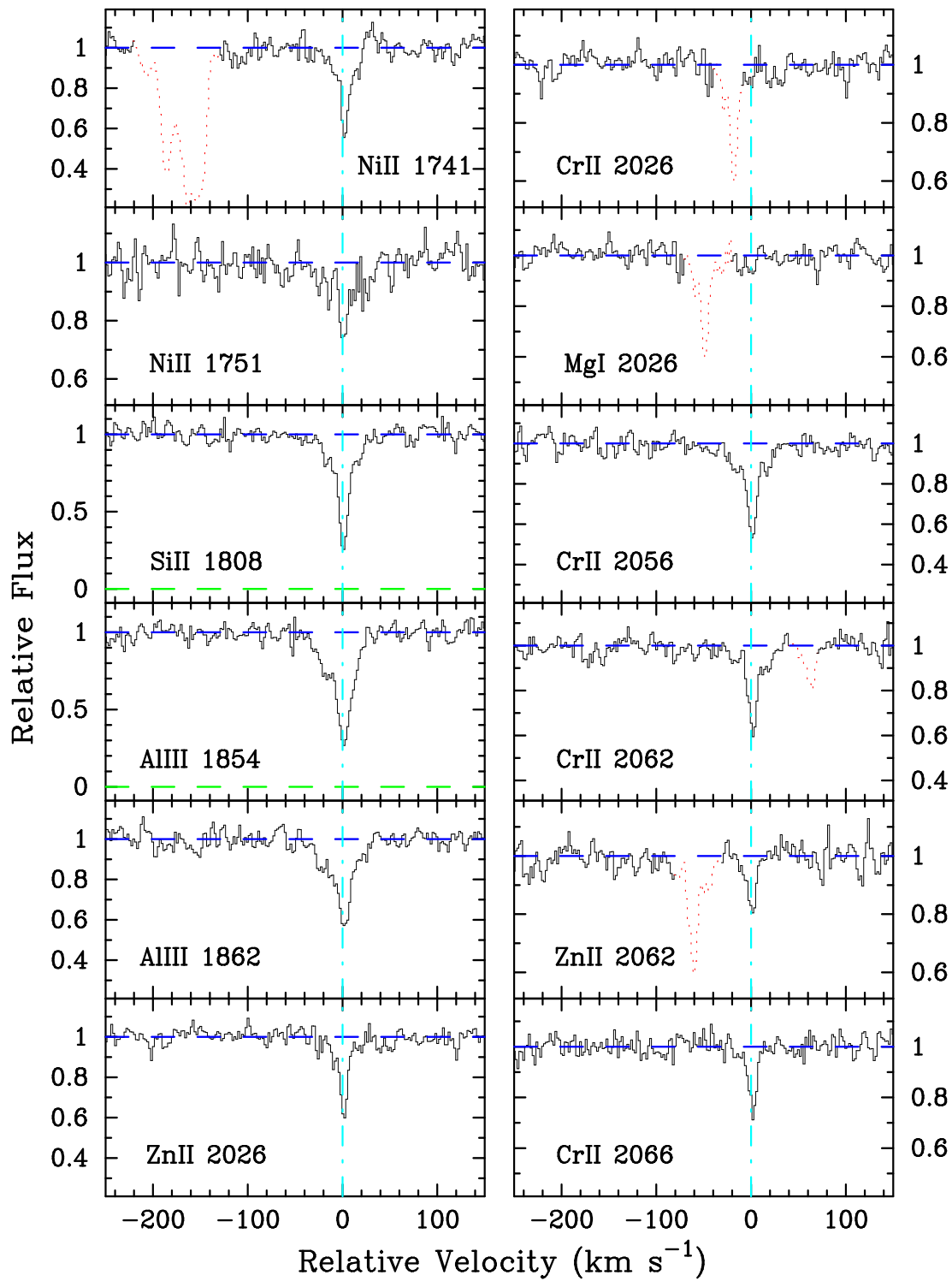


FIG. 22.— Velocity plot of the metal-line transitions for the damped Ly α system at $z = 1.892$ toward Q1210+17. The vertical line at $v = 0$ corresponds to $z = 1.891755$.



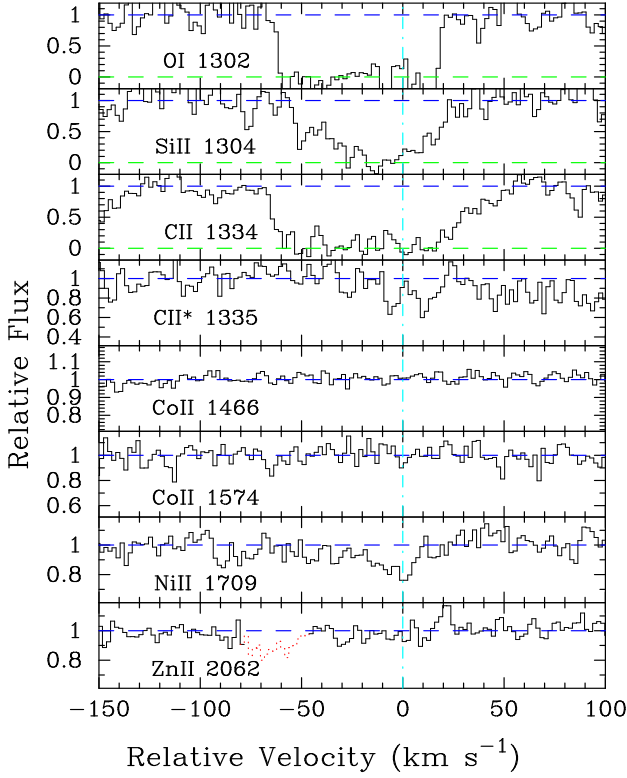


FIG. 23.— Velocity plot of the new metal-line transitions for the damped Ly α system at $z = 1.999$ toward Q1215+33. The vertical line at $v = 0$ corresponds to $z = 1.9991$.

3.18. Q1215+33, $z = 1.999$

Although we presented a full analysis of this damped system in PW99, a number of transitions were overlooked and we have revised the Fe abundance. Figure 23 plots the new transitions and Table 24 lists the ionic column densities. We now report only a limit on $N(\text{Fe}^+)$ because the Fe II 1608 profile is saturated and the Fe II 1611 transition is too weak to provide a reasonable measurement. In the subsequent analysis, we assume a value based on an average of the two limits: $N(\text{Fe}^+) = 10^{14.748 \pm 0.05} \text{ cm}^{-2}$. Finally, we also report an upper limit on $N(\text{Zn}^+)$ based on the Zn II 2062 profile. It is 0.2 dex lower than the value derived from Zn II 2026 which is difficult to understand aside from the fact that the Zn II 2026 profile is noisy and the continuum is poorly constrained in that region. For now, we continue to adopt the value from Zn II 2026.

3.19. Q1223+17, $z = 2.466$

The combination of a very large $N(\text{HI})$ value and extensive wavelength coverage allows for the analysis of a terrific number of transitions. Figure 24 and Table 25 present over 20 transitions including a large number of limits. One of the most interesting ratios is Ti/Fe whose upper limit is less than 1/2 the solar value ($[\text{Ti}/\text{Fe}] < -0.4$). In general, a subsolar Ti/Fe ratio implies significant dust depletion because Ti is more readily locked up into dust grains, but the Zn/Fe ratio is not particularly large as one would expect in a significantly dust depleted region ($[\text{Zn}/\text{Fe}] =$

TABLE 24
IONIC COLUMN DENSITIES: Q1215+33, $z = 1.999$

Ion	λ	AODM	N_{adopt}	[X/H]
HI	1215	20.950 ± 0.067		
C II	1334	> 14.630	> 14.630	> -2.870
C II	1335	< 13.173		
O I	1302	> 15.127	> 15.127	> -2.693
O I	1355	< 18.065		
Si II	1304	> 14.617	15.030 ± 0.025	-1.480 ± 0.072
Si II	1526	> 14.660		
Si II	1808	15.030 ± 0.025		
Fe II	1608	> 14.696	14.748 ± 0.053	-1.702 ± 0.085
Fe II	1611	< 14.800		
Co II	1466	< 12.860	< 12.860	< -1.000
Co II	1574	< 13.358		
Ni II	1709	13.579 ± 0.061	13.594 ± 0.027	-1.606 ± 0.072
Ni II	1741	13.602 ± 0.039		
Ni II	1751	13.592 ± 0.048		
Zn II	2026	12.330 ± 0.049	12.330 ± 0.049	-1.290 ± 0.083
Zn II	2062	< 12.138		

+0.22). Our observations also place a tight constraint on Co/Fe which is described in greater detail in Ellison et al. (2001).

TABLE 25
IONIC COLUMN DENSITIES: Q1223+17, $z = 2.466$

Ion	λ	AODM	N_{adopt}	[X/H]
HI	1215	21.500 ± 0.100		
C I	1656	< 12.426		
C II	1334	> 15.155	> 15.155	> -2.895
C II	1335	< 14.007		
C IV	1548	> 14.696		
C IV	1550	14.658 ± 0.004		
O I	1302	> 15.477	> 15.477	> -2.893
Al III	1862	12.909 ± 0.023		
Si II	1526	> 15.037	15.468 ± 0.008	-1.592 ± 0.100
Si II	1808	15.468 ± 0.008		
Si IV	1402	13.891 ± 0.004		
P II	1152	< 13.883	< 13.883	< -1.147
Ti II	1910	< 12.252	< 12.252	< -2.188
Cr II	2056	13.521 ± 0.013	13.493 ± 0.010	-1.677 ± 0.100
Cr II	2062	13.480 ± 0.018		
Cr II	2066	13.411 ± 0.032		
Fe II	1133	15.098 ± 0.059	15.157 ± 0.022	-1.843 ± 0.102
Fe II	1142	15.258 ± 0.051		
Fe II	1611	15.152 ± 0.027		
Co II	1466	< 13.174	< 12.631	< -1.779
Co II	1574	< 13.122		
Co II	1941	< 12.917		
Co II	2012	< 12.631		
Ni II	1317	13.853 ± 0.051	13.949 ± 0.011	-1.801 ± 0.101
Ni II	1703	< 13.817		
Ni II	1709	13.901 ± 0.020		
Ni II	1751	14.000 ± 0.014		
Zn II	2026	12.550 ± 0.026	12.550 ± 0.026	-1.620 ± 0.103
Zn II	2062	> 11.785		

3.20. Q1331+17, $z = 1.776$

An analysis of the damped system toward the very bright quasar Q1331+17 was given by PW99 but a number of transitions were missed (notably Ti II 1910 and Co II 2012). The new transitions are plotted in Figure 25 and the ionic column densities are given in Table 26.

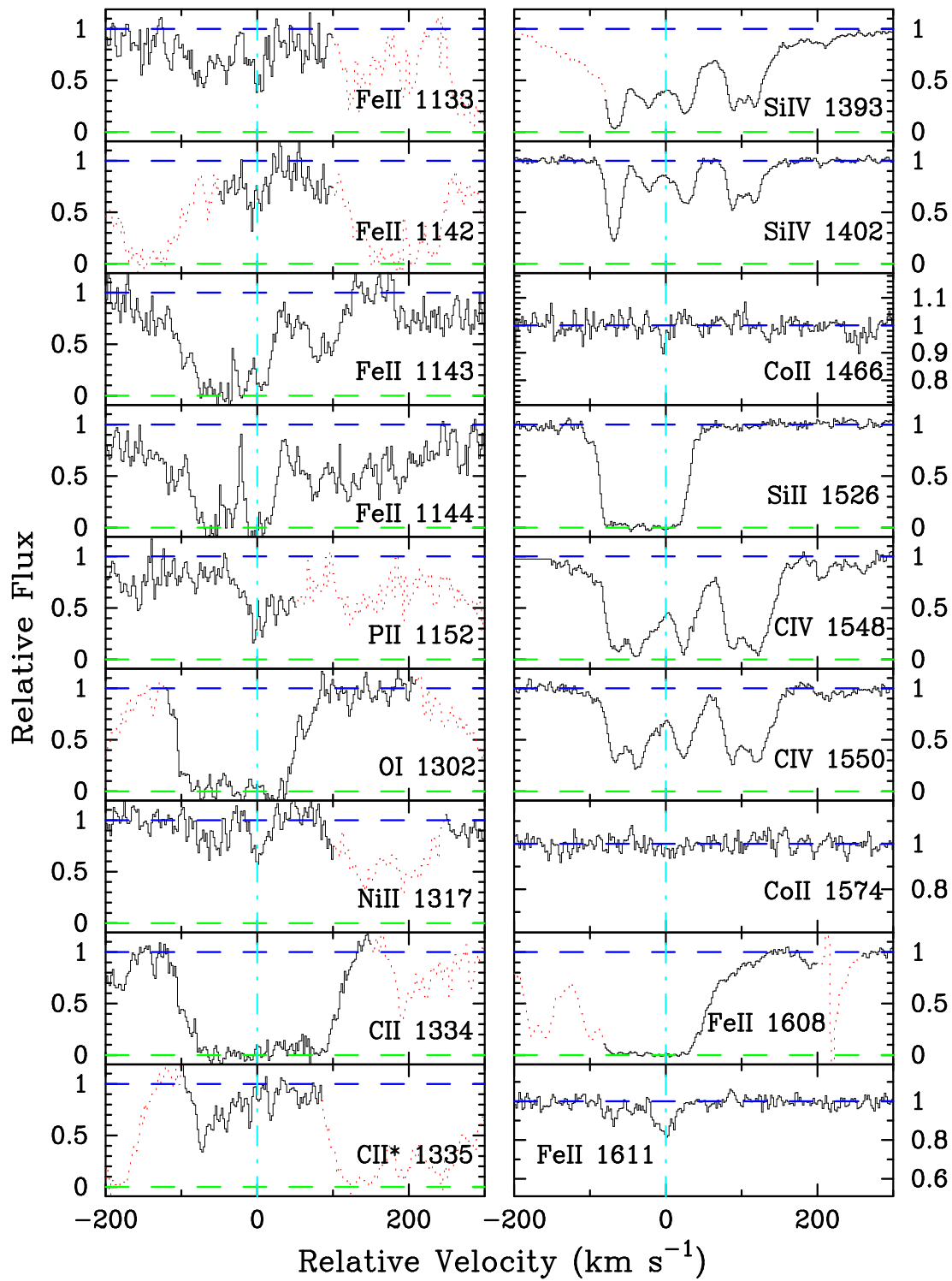
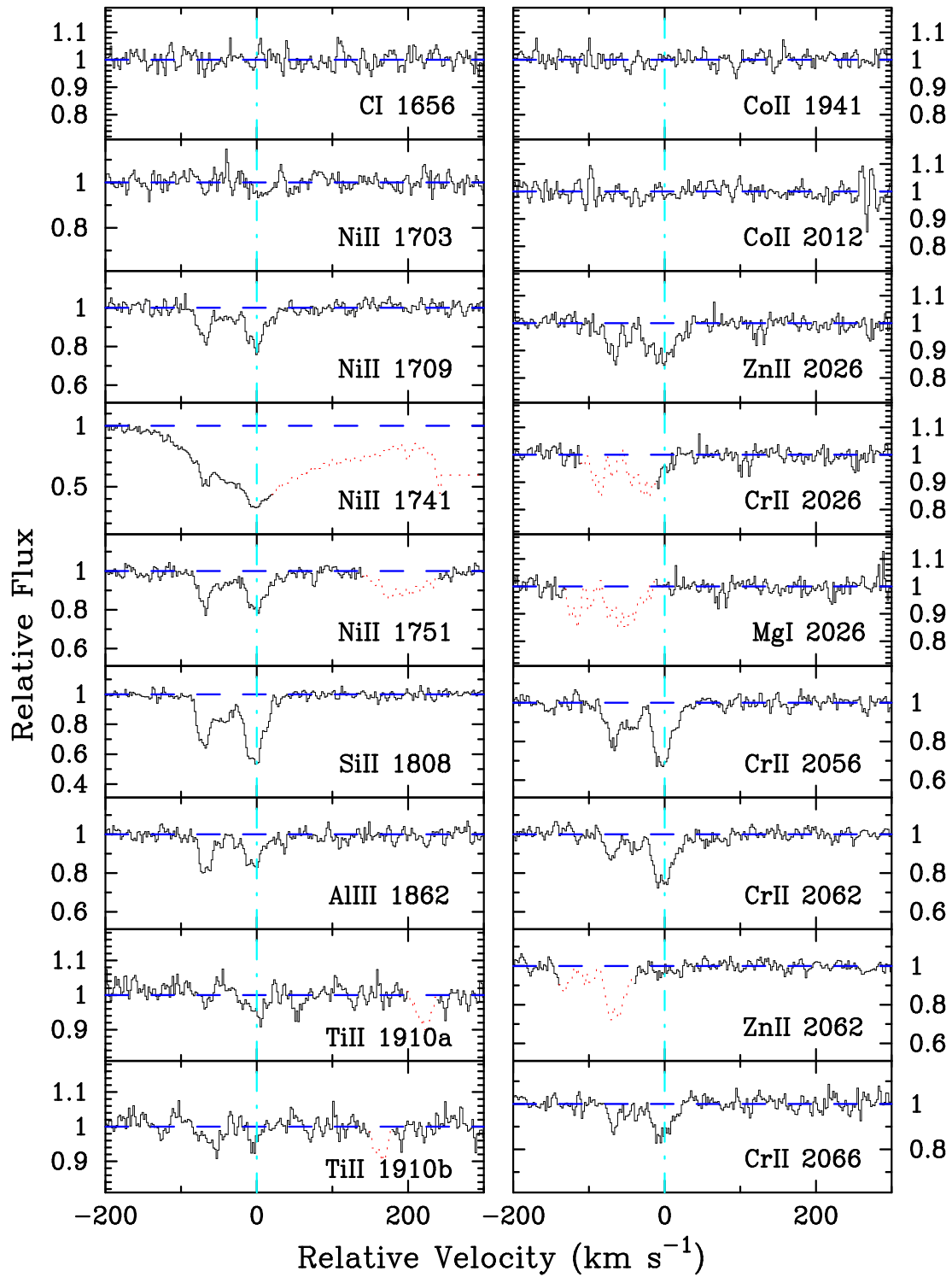


FIG. 24.— Velocity plot of the metal-line transitions for the damped Ly α system at $z = 2.466$ toward Q1223+17. The vertical line at $v = 0$ corresponds to $z = 2.466083$.



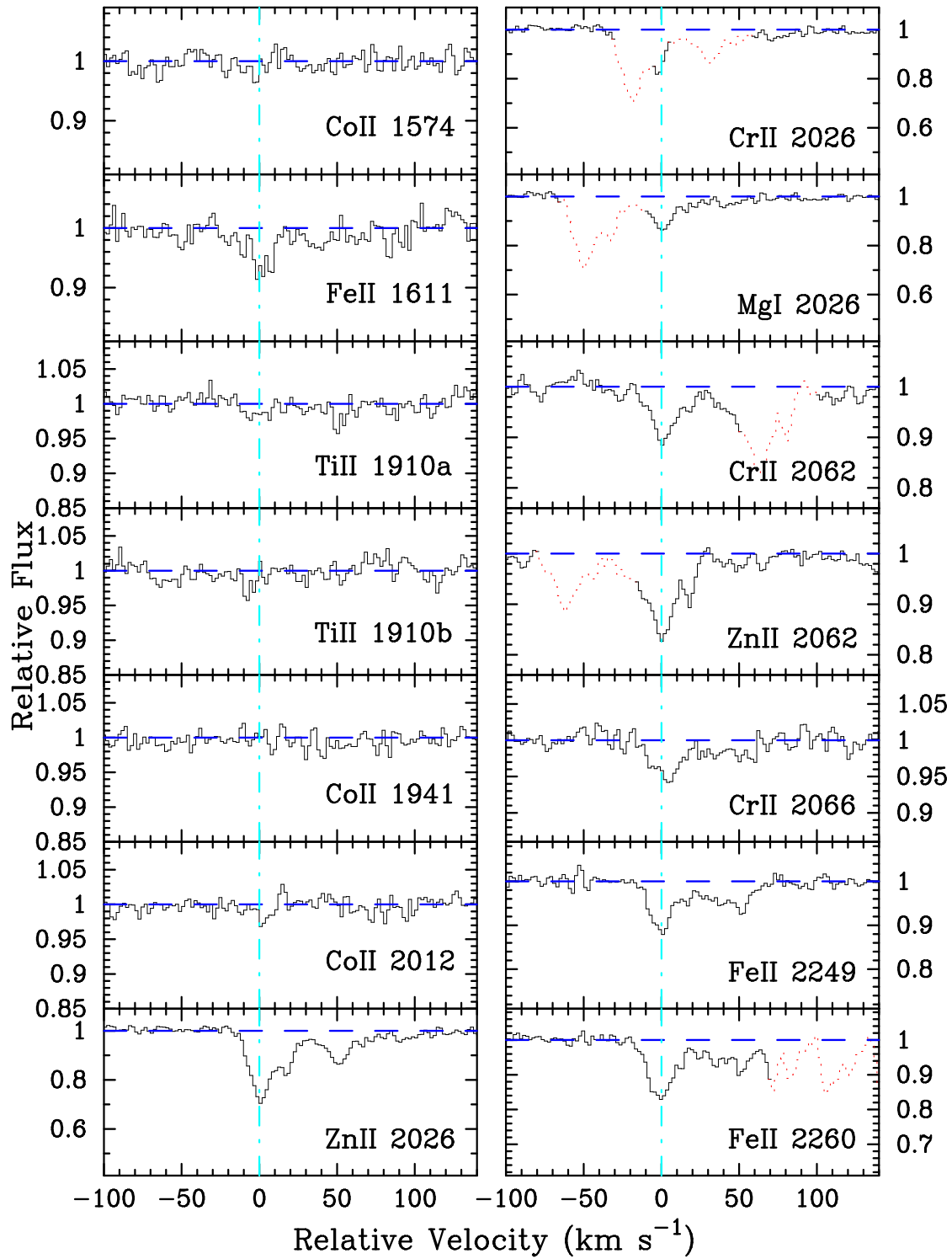


FIG. 25.— Velocity plot of the new metal-line transitions for the damped Ly α system at $z = 1.776$ toward Q1331+17. The vertical line at $v = 0$ corresponds to $z = 1.77636$.

With respect to the $N(\text{Zn}^+)$ value presented by PW99, this system exhibits one of the largest Zn/Fe ratios of any damped system. This $N(\text{Zn}^+)$ value is nearly 0.3 dex higher than the value reported in Pettini et al. (1994), however, because we did not correct for possible contamination from the Mg I 2026 transition. Although a significant feature is apparent at $v = 0 \text{ km s}^{-1}$ of the Mg I 2026 profile, this feature is perfectly aligned with an absorption feature at $v = +52 \text{ km s}^{-1}$ in the unsaturated Fe II profiles. Furthermore, the $N(\text{Zn}^+)$ value from Zn II 2062 is identical to the value derived from Zn II 2026 using the AODM method. We suspect, however, that this is a coincidence resulting from blending between the Zn II 2062 and Cr II 2062 profiles. Performing a detailed line-profile analysis of the Zn and Cr lines and including Mg I 2026, we find $\log N(\text{Zn}^+) = 12.542 \pm 0.029$ and $\log N(\text{Mg}^0) = 12.419 \pm 0.048$. We discuss this issue further and its impact on studies of Zn in Paper II, § 2.1.6.

TABLE 26

IONIC COLUMN DENSITIES: Q1331+17, $z = 1.776$

Ion	λ	AODM	N_{adopt}	[X/H]
HI	1215	21.176 ± 0.041		
C I	1560	13.573 ± 0.013		
C I	1656	13.312 ± 0.012		
Mg I	2026			
Ti II	1910	11.836 ± 0.118	11.836 ± 0.118	-2.280 ± 0.125
Cr II	2056	12.957 ± 0.017	12.874 ± 0.012	-1.972 ± 0.043
Cr II	2066	12.834 ± 0.034		
Fe II	1608	14.630 ± 0.003	14.618 ± 0.001	-2.058 ± 0.041
Fe II	1611	14.709 ± 0.046		
Fe II	2249	14.595 ± 0.015		
Fe II	2260	14.647 ± 0.010		
Fe II	2344	> 14.723		
Fe II	2374	14.616 ± 0.002		
Fe II	2382	> 14.461		
Co II	1574	< 12.659	< 12.306	< -1.780
Co II	1941	< 12.367		
Co II	2012	< 12.306		
Zn II	2026	12.542 ± 0.029	12.542 ± 0.029	-1.304 ± 0.050

In addition to the large Zn/Fe ratio, this system shows rarely observed C I absorption and a significant subsolar Ti/Fe ratio. Altogether the chemical abundances of this system represent the most compelling evidence for dust depletion in any damped Ly α system. It is particularly important to note, therefore, that it is one of the brightest (apparent magnitude) quasars observed in our sample. In Paper II, § 5 we consider the obscuration of this quasar due to this damped system and the implications for dust obscuration in general.

This damped Ly α system is one of the few cases where one can derive $N(\text{Fe}^+)$ values from both Fe II 1608 and 1611. Furthermore, our observations also cover several of the Fe II transitions longward of 2000Å, including Fe II 2249 and 2260 which are the principal diagnostics of Fe $^+$ in the Galactic ISM. Examining Table 26, one notes that nearly all of the $N(\text{Fe}^+)$ values are consistent at the 2σ level and all are in accordance at 3σ . One also notes that $N(\text{Fe II } 1611)$ exceeds all of the other measurements suggesting it is unlikely the Raassen & Uylings (1998) analysis overestimated the Fe II 1611 oscillator strength, at least relative to the other Fe II transitions.

3.21. BRI1346-03, $z = 3.736$

Our additional observations blueward of the data presented in PW99 provide coverage of a few new transitions (Figure 26, Table 27). Unfortunately, we still do not have coverage of a single unsaturated Fe II profile or any other Fe-peak metal transition. Therefore, we have adopted Al as a proxy for Fe (i.e. assume $[\text{Fe}/\text{H}] = [\text{Al}/\text{H}]$) and in this manner include the system in the metallicity and relative abundance analyses of Paper II. The implied Si/Fe ratios match typical values. If the feature at $v = 0 \text{ km s}^{-1}$ in the Ni II 1317 profile is not noise or a coincident metal line, it implies a very large Ni/Al ratio indicating we might be underestimating $N(\text{Fe}^+)$. For the moment, we consider it as an upper limit.

Our new observations also cover the C IV doublet at 1550Å. Although the spectra is particularly noisy over this region, there is no obvious C IV absorption. This marks the first DLA system with no detectable C IV absorption and we note in passing a possible trend of weaker C IV absorption at $z > 3$.

TABLE 27

IONIC COLUMN DENSITIES: BRI1346-03, $z = 3.736$

Ion	λ	AODM	N_{adopt}	[X/H]
HI	1215	20.720 ± 0.100		
C II	1335	12.550 ± 0.113	> 14.486	> -2.784
C IV	1548	< 12.717		
C IV	1550	< 13.146		
O I	1302	> 15.018	> 15.019	> -2.571
Si II	1190	13.430 ± 0.122	13.948 ± 0.009	-2.332 ± 0.100
Si II	1304	13.983 ± 0.009		
Si II	1526	13.880 ± 0.026		
Ar I	1048	< 13.114	< 13.113	< -2.127
Fe II	1125	< 14.126	< 14.126	< -2.094
Co II	1574	< 13.260	< 13.260	< -0.370
Ni II	1317	< 12.759	< 12.760	< -2.210
Ni II	1370	< 12.876		
Ni II	1709	< 13.345		
Ni II	1741	< 13.284		
Ni II	1751	< 13.428		

3.22. PSS1443+27, $z = 4.224$

This $z > 4$ damped Ly α systems was discovered by Storrie-Lombardi and Wolfe (2000) who determined the $N(\text{HI})$ value from a spectrum obtained using LRIS at Keck observatories. Its very high metallicity was first reported in Prochaska & Wolfe (2000) We have since acquired further observations of this system which confirm the $[\text{Fe}/\text{H}]$ metallicity. In particular, we observed the Ni II 1370, 1709, and 1741 transitions at reasonably high S/N and found $[\text{Ni}/\text{H}] \approx [\text{Fe}/\text{H}]$. Figure 27 presents the transitions observed for this system and the ionic column densities are presented in Table 28.

In passing, we note the remarkable C II* 1335 profile which is heavily saturated and suggests a large star formation rate for this system (Wolfe, Prochaska, & Gawiser 2001). Also, we identify possible absorption from two C I profiles which we expect is not due to coincident metal-line systems. Unfortunately our observations did not cover the stronger C II 1556 profile and strongest C I 1656 profile is located within a forest of sky lines.

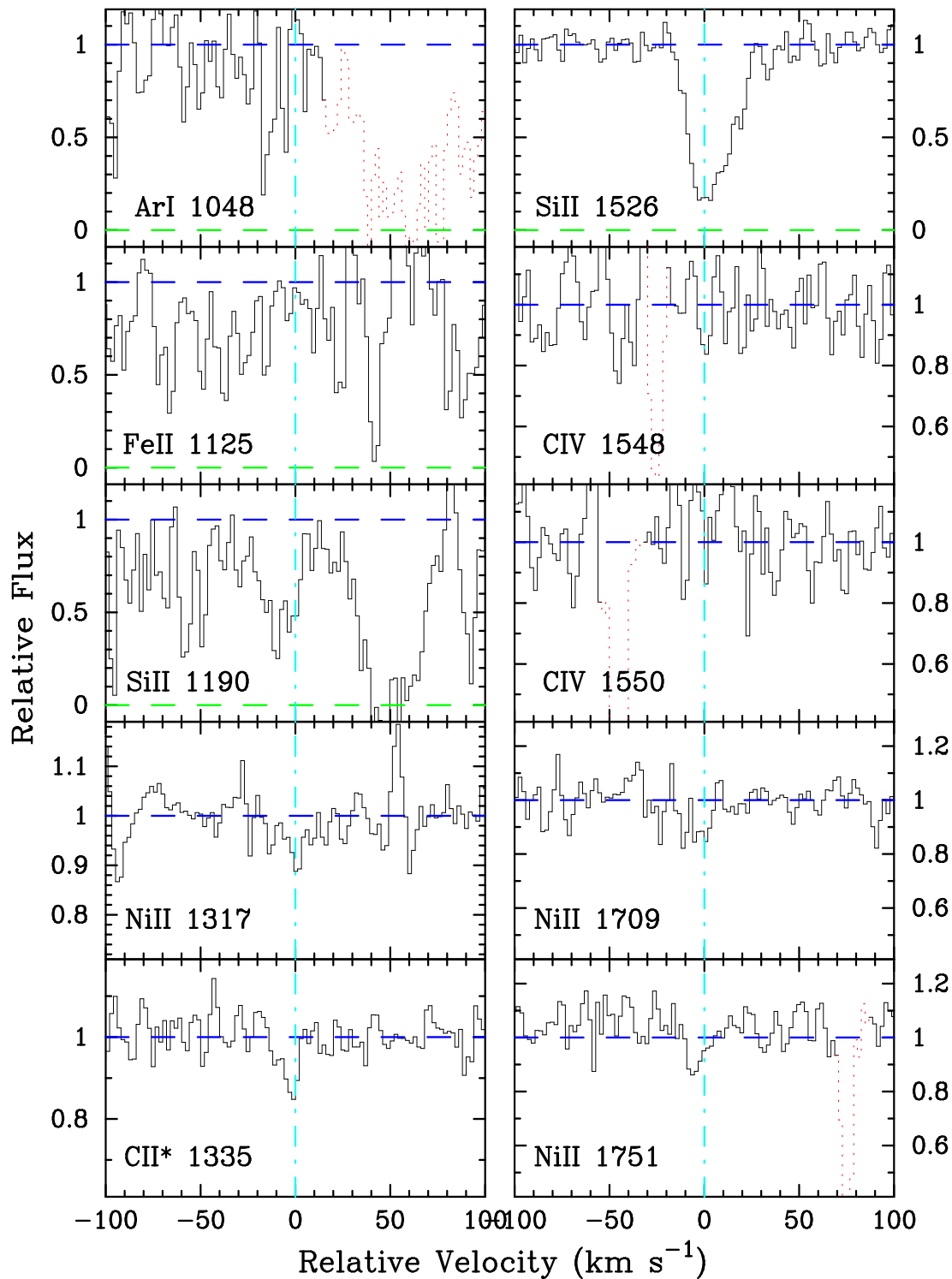


FIG. 26.— Velocity plot of the new metal-line transitions for the damped Ly α system at $z = 3.736$ toward BRI1346-03. The vertical line at $v = 0$ corresponds to $z = 3.73583$.

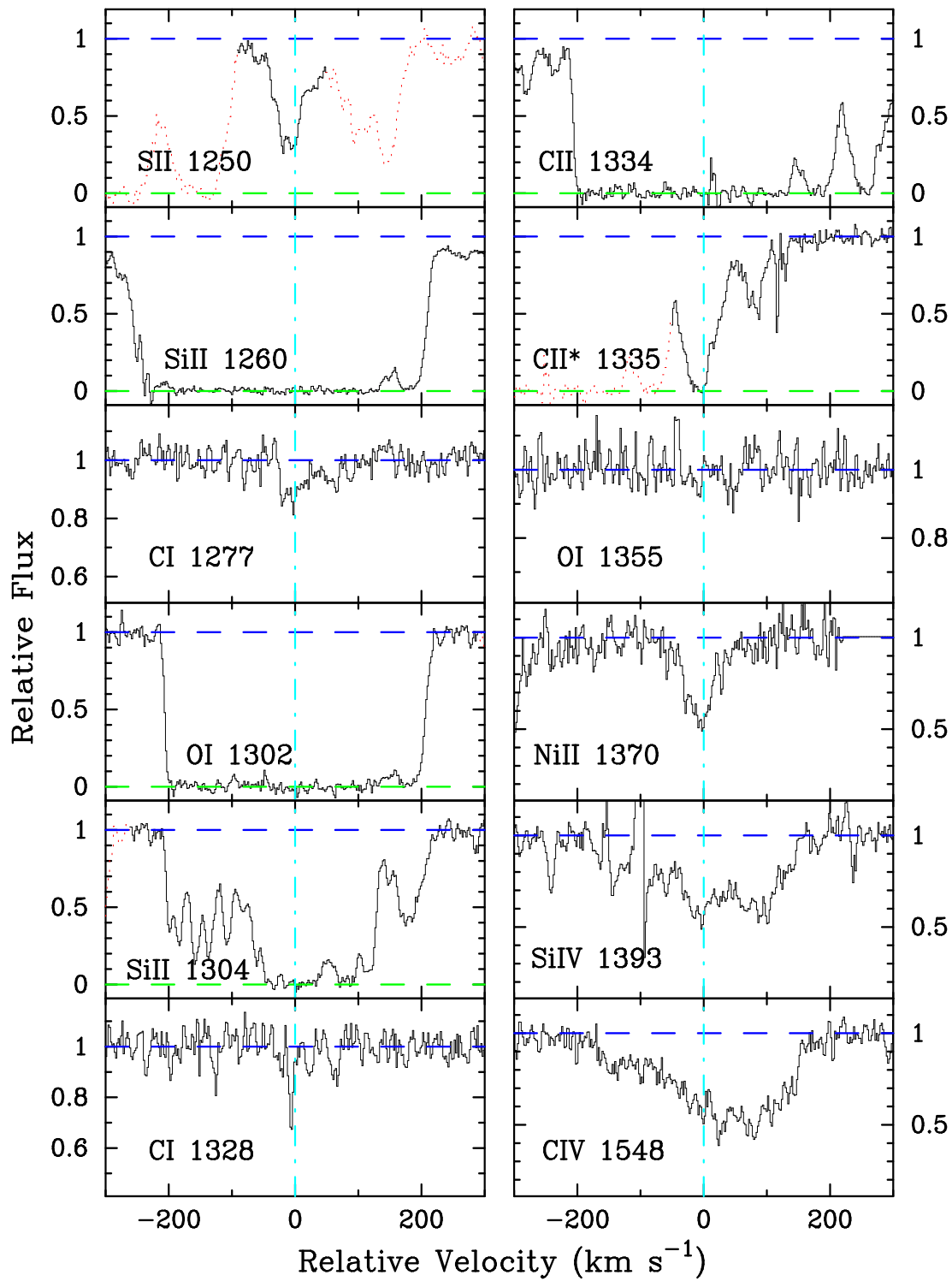


FIG. 27.— Velocity plot of the metal-line transitions for the damped Ly α system at $z = 4.224$ toward PSS1443+27. The vertical line at $v = 0$ corresponds to $z = 4.224099$.

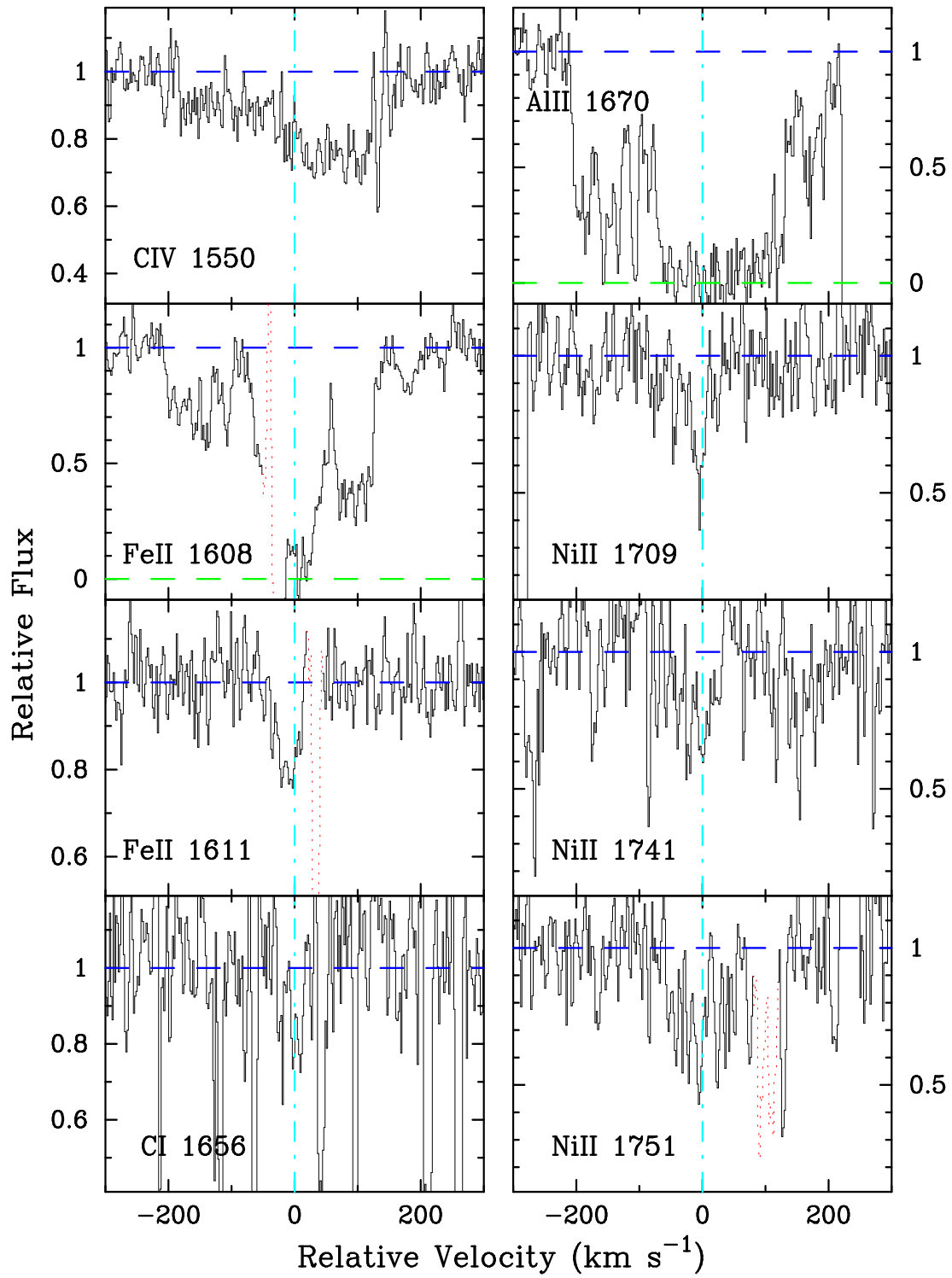


TABLE 28

IONIC COLUMN DENSITIES: PSS1443+27, $z = 4.224$

Ion	λ	AODM	N_{adopt}	[X/H]
HI	1215	20.800 ± 0.100		
C I	1277	13.446 ± 0.037		
C I	1328	13.367 ± 0.090		
C I	1656	13.041 ± 0.133		
C II	1334	> 15.613	> 15.612	> -1.738
C II	1335	> 14.709		
C IV	1548	14.245 ± 0.009		
C IV	1550	14.213 ± 0.017		
O I	1302	> 16.048	> 16.048	> -1.622
O I	1355	< 17.734		
Al II	1670	> 13.959	> 13.958	> -1.332
Si II	1304	> 15.434	> 15.434	> -0.926
Si IV	1393	13.706 ± 0.011		
S II	1253			
Fe II	1608	> 15.101	15.204 ± 0.056	-1.096 ± 0.115
Fe II	1611	15.204 ± 0.056		
Co II	1574	< 13.508	< 13.509	< -0.201
Ni II	1370	14.079 ± 0.025	14.091 ± 0.024	-0.959 ± 0.103
Ni II	1709	14.229 ± 0.069		
Ni II	1741	13.877 ± 0.074		

3.23. *Q1759+75*, $z = 2.625$

This system was presented in PW99 and has been subsequently analysed by Outram, Chaffee, & Carswell (1999). Here, we present an analysis of our spectrum blueward of Ly α emission. Figure 28 presents the transitions and Table 29 the column densities.

Our observations present measurements of a number of lines in the Ly α forest. In particular, we have excellent coverage of the FUV Fe II transitions, good measurements of the N I triplets at 1134 and 1200Å, moderate limits on Ar I and O I, and an excellent measurement of $N(\text{S}^+)$. Regarding the Fe II lines, we find very good agreement between the many transitions which confirms the f -values measured by Howk et al. (2000). The only exception is Fe II 1062 (not analysed by Howk et al.) whose f -value appears to be systematically high. We recommend using a value ≈ 0.2 dex below the value reported by Morton (1991). Finally, we point out significant absorption at $v \approx -300$ km/s in the Si II 1190 and 1193 transitions which coincide with a strong feature in C IV and a weaker feature in Al II 1670 (PW99). We suspect this metal-line system corresponds to a nearby Lyman limit system although there is no significant evidence for asymmetry in the Ly α profile.

3.24. *Q1946+76*, $z = 2.844$

Kirkman & Tytler (1997) analysed this very high S/N spectrum of Q1946+76 to describe the Ly α forest at $z \sim 2.8$. Here, we analyse the metal-line transitions for the system at $z = 2.844$, ignoring the probably damped Ly α system at $z = 1.73$ because we have no measure of its HI column density. Figure 29 presents the metal-line profiles for the $z = 2.844$ system and Table 30 summarizes the column density measurements. For the HI column density we adopt the value presented in L96. This systems is notable for providing one of the few cases where one can accurately determine $N(\text{O}^0)$. The observed O/Fe ratio is enhanced relative to solar, but at a lower level than metal-poor halo stars with comparable metallicity. Interestingly,

TABLE 29

IONIC COLUMN DENSITIES: Q1759+75, $z = 2.625$

Ion	λ	AODM	N_{adopt}	[X/H]
HI	1215	20.800 ± 0.100		
C I	1656	< 12.336		
C II	1334	> 15.300	> 15.300	> -2.050
C II	1335	13.138 ± 0.032		
O I	1039	> 16.261	> 16.261	> -1.409
O I	1302	> 15.759		
Si II	1190	> 14.928	15.536 ± 0.008	-0.824 ± 0.100
Si II	1193	> 14.614		
Si II	1260	> 14.396		
Si II	1304	> 15.198		
Si II	1808	15.536 ± 0.008		
P II	1152	> 13.046	> 13.047	> -1.283
S II	1250	15.243 ± 0.009	15.243 ± 0.010	-0.757 ± 0.100
S II	1253	< 15.486		
S II	1259	< 15.335		
Ar I	1048	< 13.714	< 13.714	< -1.606
Ar I	1066	< 14.053		
Fe II	1062	14.860 ± 0.037	15.091 ± 0.004	-1.209 ± 0.100
Fe II	1063	> 15.002		
Fe II	1063	15.287 ± 0.020		
Fe II	1081	15.182 ± 0.007		
Fe II	1096	15.059 ± 0.007		
Fe II	1112	< 15.389		
Fe II	1121	< 15.260		
Fe II	1142	< 15.565		
Fe II	1143	15.079 ± 0.005		
Fe II	1144	> 15.051		
Fe II	1608	> 15.077		
Fe II	1611	14.923 ± 0.034		
Co II	1466	< 13.066	< 13.019	< -0.691
Co II	1466	< 13.019		
Co II	1574	< 13.108		
Ni II	1317	< 14.248	13.802 ± 0.007	-1.248 ± 0.100
Ni II	1370	13.766 ± 0.010		
Ni II	1454	13.791 ± 0.039		
Ni II	1703	< 13.908		
Ni II	1709	13.929 ± 0.020		
Ni II	1741	13.841 ± 0.017		
Ni II	1751	13.868 ± 0.021		

the implied O/Si ratio is sub-solar which is almost never observed in metal-poor stars. Nevertheless, we believe the $N(\text{O}^0)$ value is accurate. In a separate paper, we examine the N/O ratio of this system.

TABLE 30

IONIC COLUMN DENSITIES: Q1946+7658, $z = 2.844$

Ion	λ	AODM	N_{adopt}	[X/H]
HI	1215	20.270 ± 0.060		
O I	936	15.036 ± 0.030	14.819 ± 0.007	-2.321 ± 0.060
O I	948	14.835 ± 0.025		
O I	971	< 14.725		
O I	988	< 15.244		
O I	988	< 14.862		
O I	988	> 14.627		
O I	1039	14.811 ± 0.008		
O I	1302	> 14.587		
Si II	1190	< 13.579	13.602 ± 0.005	-2.228 ± 0.060
Si II	1304	13.602 ± 0.005		
S II	1250	< 13.491	< 13.491	< -1.979
Fe II	1121	13.241 ± 0.057	13.238 ± 0.009	-2.532 ± 0.061
Fe II	1144	13.238 ± 0.009		

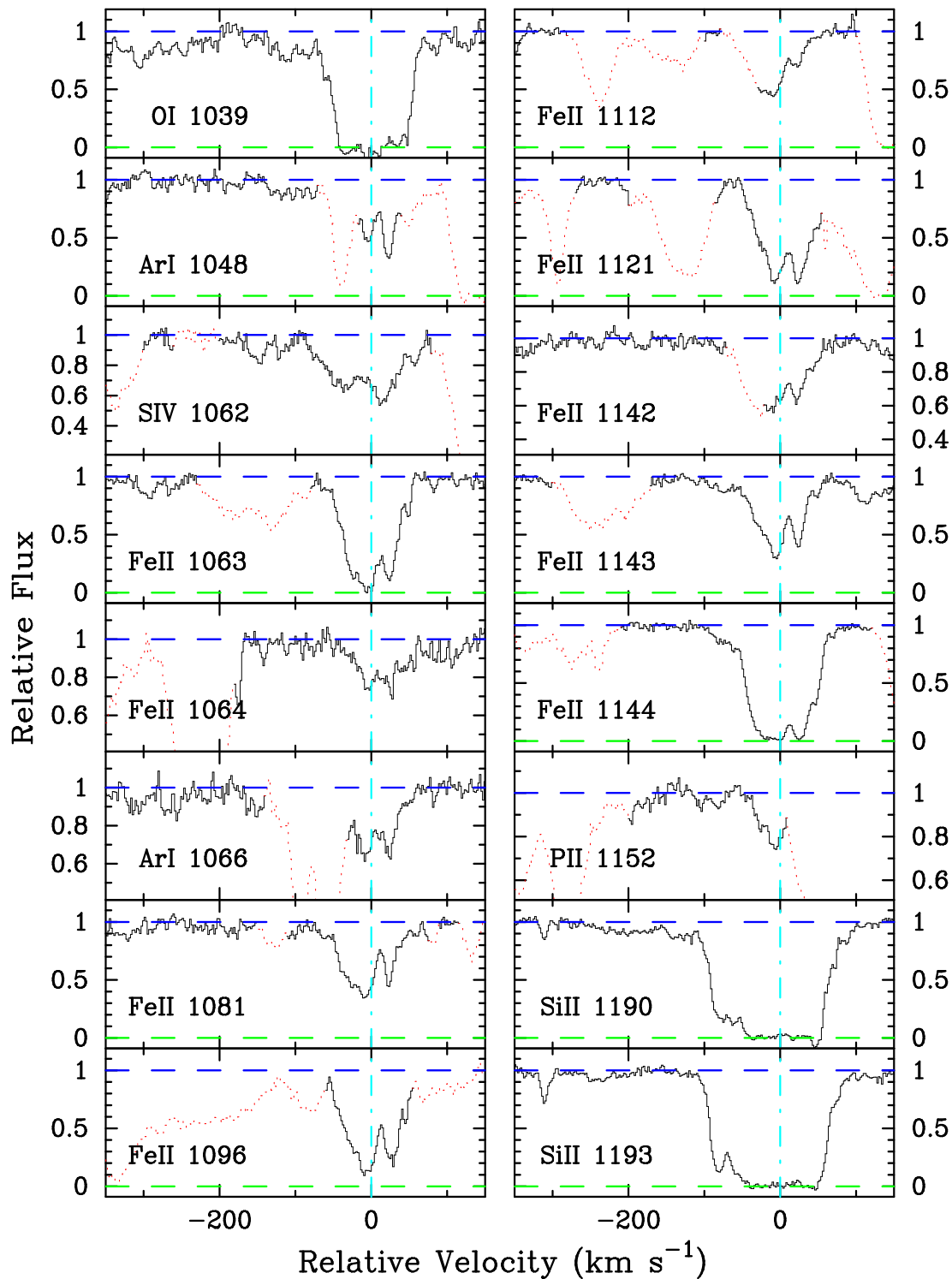
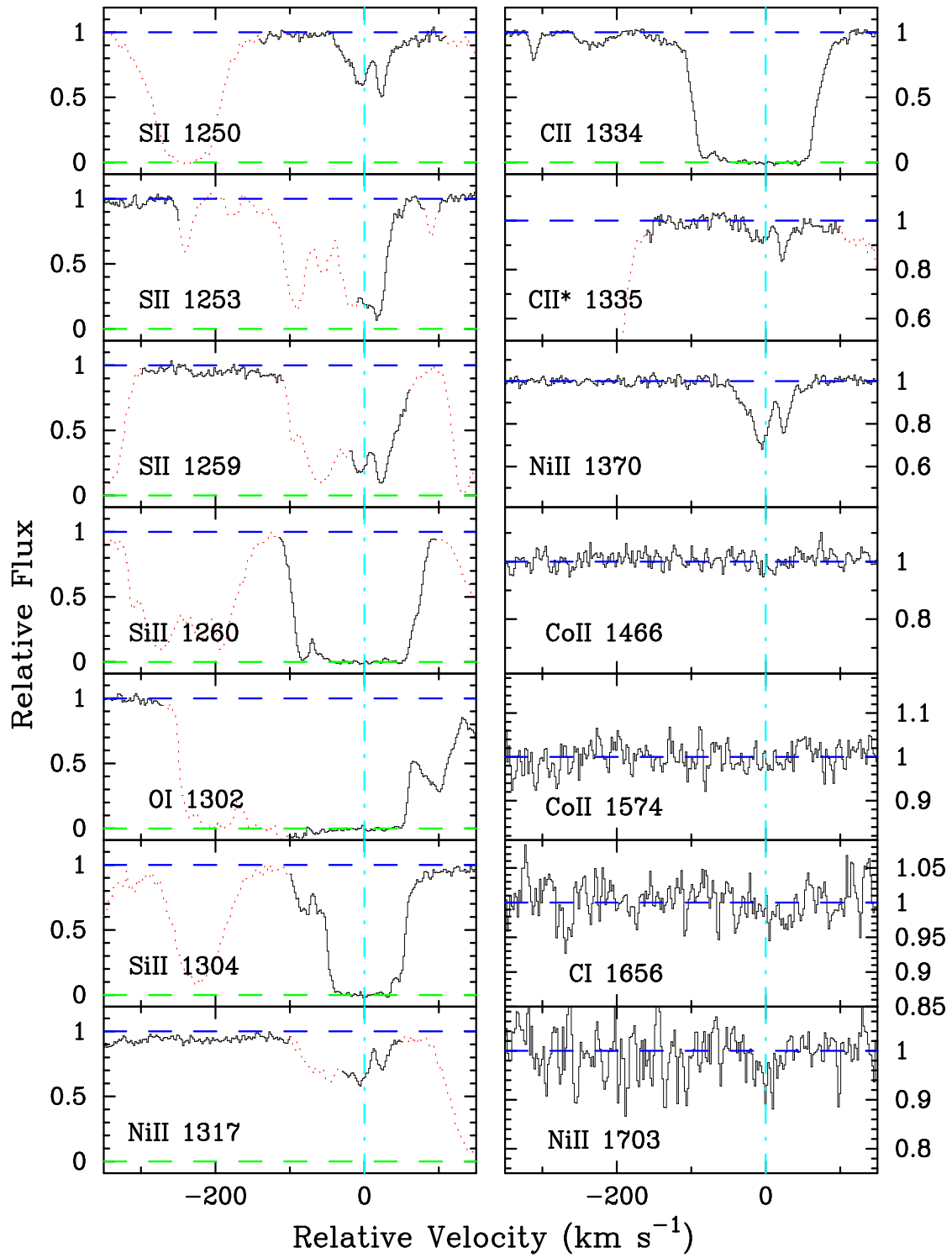


FIG. 28.— Velocity plot of the new metal-line transitions for the damped Ly α system at $z = 2.625$ toward Q1759+75. The vertical line at $v = 0$ corresponds to $z = 2.62530$.



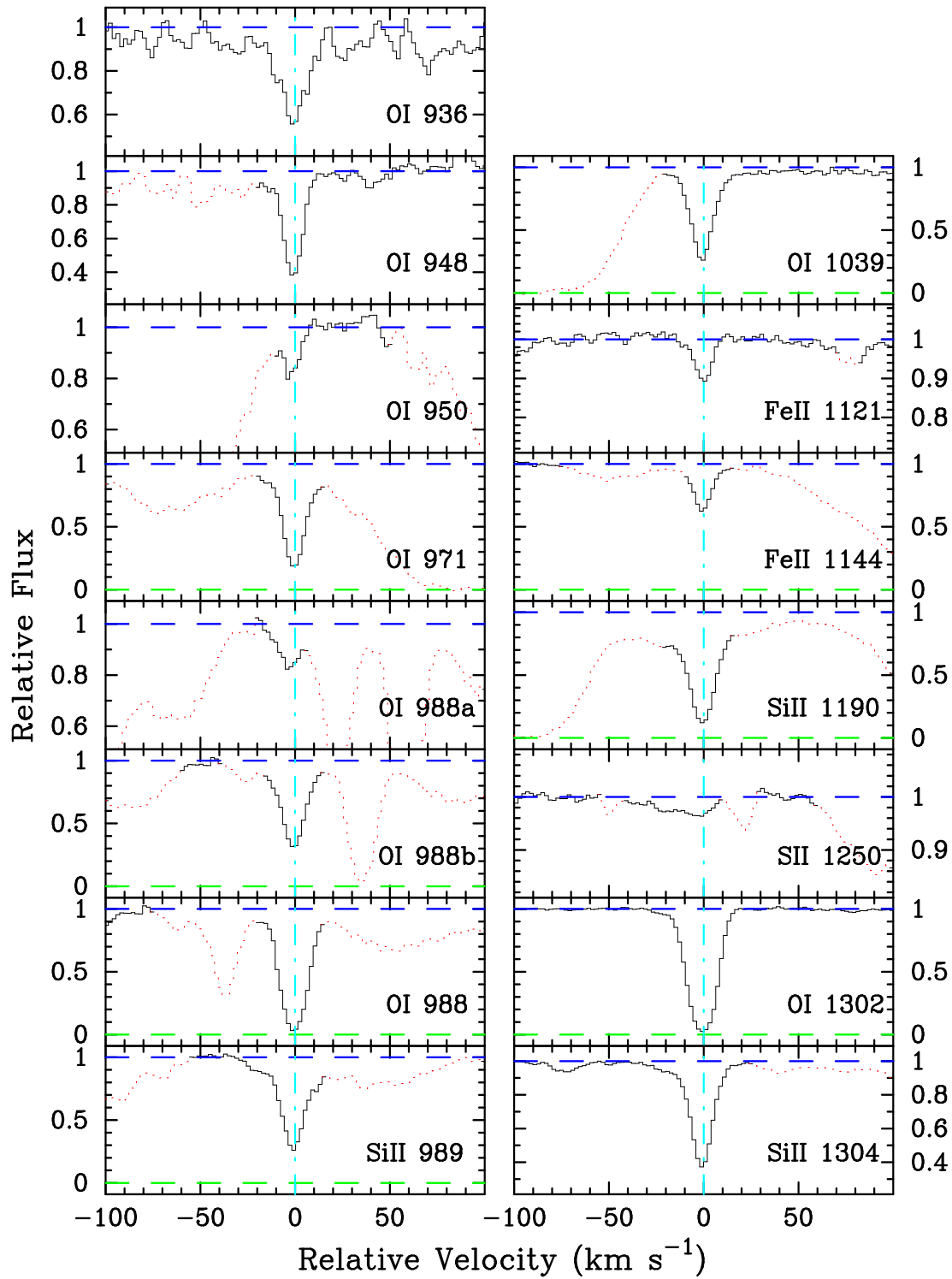


FIG. 29.— Velocity plot of the metal-line transitions for the damped Ly α system at $z = 2.844$ toward Q1946+76. The vertical line at $v = 0$ corresponds to $z = 2.8443$.

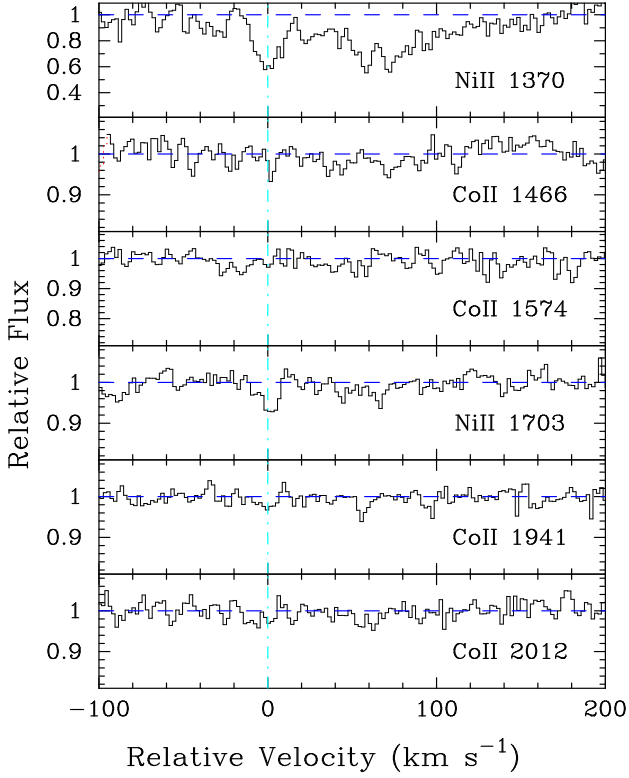


FIG. 30.— Velocity plot of the new metal-line transitions for the damped Ly α system at $z = 1.920$ toward Q2206-19. The vertical line at $v = 0$ corresponds to $z = 1.920$.

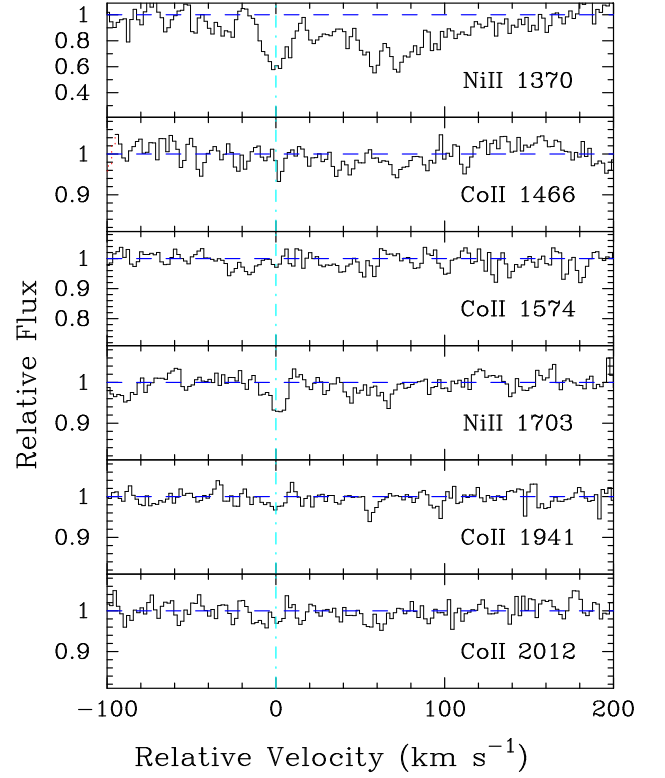


FIG. 31.— Velocity plot of the new metal-line transitions for the damped Ly α system at $z = 2.076$ toward Q2206-19. The vertical line at $v = 0$ corresponds to $z = 2.07623$.

TABLE 31

IONIC COLUMN DENSITIES: Q2206-19, $z = 1.920$

Ion	λ	AODM	N_{adopt}	$[X/H]$
HI	1215	20.653 ± 0.071		
Al II	1670	> 14.070	> 14.070	> -1.073
Si II	1526	> 15.275	15.796 ± 0.005	-0.417 ± 0.071
Si II	1808	15.796 ± 0.005		
Ti II	1910	12.768 ± 0.040	12.768 ± 0.040	-0.825 ± 0.081
Cr II	2056	13.627 ± 0.009	13.638 ± 0.007	-0.685 ± 0.071
Cr II	2066	13.665 ± 0.013		
Fe II	1608	> 15.376	15.296 ± 0.018	-0.857 ± 0.073
Fe II	1611	15.296 ± 0.018		
Co II	1574	12.960 ± 0.139	12.960 ± 0.140	-0.603 ± 0.157
Co II	1941	< 12.814		
Co II	2012	< 12.832		
Ni II	1370	14.154 ± 0.022	14.232 ± 0.005	-0.671 ± 0.071
Ni II	1703	13.807 ± 0.116		
Ni II	1709	14.221 ± 0.009		
Ni II	1741	14.239 ± 0.006		
Ni II	1751	14.266 ± 0.010		
Zn II	2026	12.914 ± 0.009	12.914 ± 0.009	-0.409 ± 0.072

3.25. *Q2206-19, $z = 1.920$ and $z = 2.076$*

In Figures 30 and 31 we show a number of transitions left unanalysed by Prochaska & Wolfe (1997) and PW99 for the two damped Ly α systems toward Q2206-19. Furthermore, we now consider only ionic column densities measured with the apparent optical depth method in order

TABLE 32

IONIC COLUMN DENSITIES: Q2206-19, $z = 2.076$

Ion	λ	AODM	N_{adopt}	$[X/H]$
HI	1215	20.431 ± 0.060		
C II	1334	> 14.207	> 14.207	> -2.774
C II	1335	< 13.157		
C IV	1548	13.707 ± 0.005		
C IV	1550	13.739 ± 0.008		
O I	1302	> 14.540	> 14.540	> -2.761
Al II	1670	12.158 ± 0.012	12.158 ± 0.012	-2.763 ± 0.061
Al III	1854	11.515 ± 0.098		
Al III	1862	11.719 ± 0.103		
Si II	1304	13.682 ± 0.035	13.682 ± 0.035	-2.309 ± 0.069
Si IV	1402	12.845 ± 0.016		
Cr II	2056	< 11.911	< 11.911	< -2.190
Cr II	2062	< 12.158		
Fe II	1608	13.325 ± 0.017	13.325 ± 0.017	-2.606 ± 0.062
Fe II	1611	< 13.948		
Ni II	1709	< 12.585	< 12.585	< -2.096
Ni II	1751	< 12.591		
Zn II	2026	< 11.199	< 11.199	< -1.902

to coincide with the rest of the database. As we showed in Prochaska & Wolfe (1997), there is very little difference between the abundances derived from a Voigt profile analysis and the AODM. All of the values are listed in Tables 31 and 32.

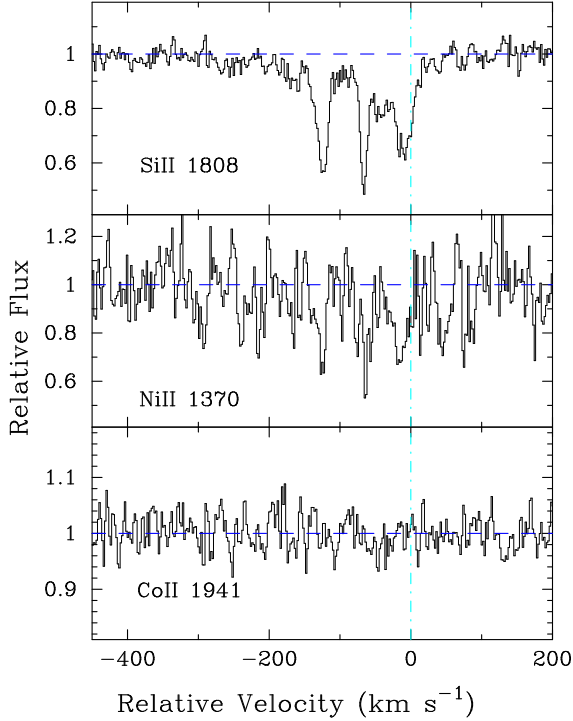


FIG. 32.— Velocity plot of CII* 1335 transition for the damped Ly α system at $z = 1.864$ toward Q2230+02. For comparison, we plot the Si II 1304 and C II 1334 profiles. The vertical line at $v = 0$ corresponds to $z = 1.864388$.

3.26. Q2230+02, $z = 1.864$

This system was extensively analysed in PW99. We simply add a limit on $N(\text{Co}^+)$ from the Co II 1941 transition and a measurement for Ni II 1370 (Figure 32). We also include the new values for $N(\text{Fe}^+)$ as the extensive wavelength coverage provides a comparison between the Fe II 1611, 2249, and 2260 transitions. All three values are in good agreement which indicates the relative f -values are reasonably accurate.

TABLE 33

IONIC COLUMN DENSITIES: Q2230+02, $z = 1.864$

Ion	λ	AODM	N_{adopt}	[X/H]
HI	1215	20.850 ± 0.084		
Fe II	1608	> 15.160	15.184 ± 0.016	-1.166 ± 0.086
Fe II	1611	15.148 ± 0.084		
Fe II	2249	15.119 ± 0.036		
Fe II	2260	15.210 ± 0.019		
Fe II	2344	> 15.039		
Fe II	2374	> 15.213		
Fe II	2382	> 14.744		
Co II	1941	< 13.118	< 13.118	< -0.642
Ni II	1370	14.161 ± 0.052	14.128 ± 0.011	-0.972 ± 0.085
Ni II	1709	14.171 ± 0.014		
Ni II	1741	14.097 ± 0.023		
Ni II	1751	14.049 ± 0.028		

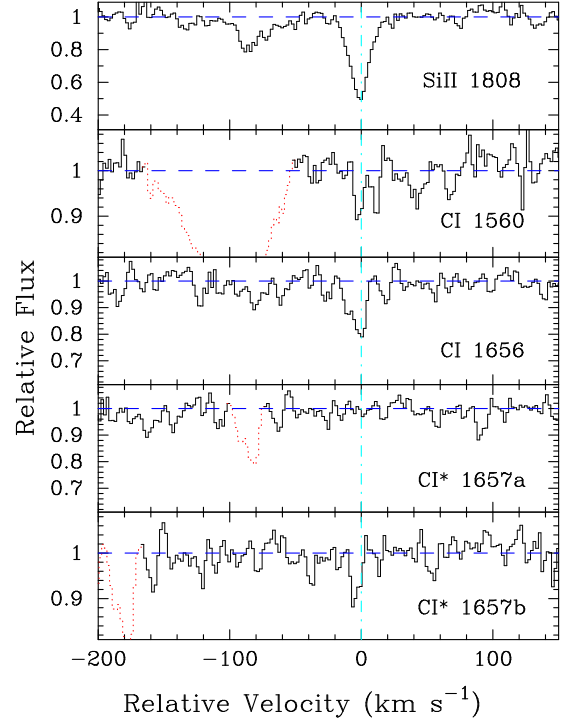


FIG. 33.— Velocity plot of the new metal-line transitions for the damped Ly α system at $z = 2.066$ toward Q2231-00. For comparison, we also plot the Si II 1808 profile. The vertical line at $v = 0$ corresponds to $z = 2.066150$.

3.27. Q2231-00, $z = 2.066$

This damped system was analysed in PW99. At the time we considered possible absorption from the C I 1656 and C I* 1657 transitions but were unconvinced that the profiles were associated with the damped Ly α system. Figure 33 presents the two transitions and the Si II 1808 profile for comparison. We are now reasonably confident that these profiles arise in the damped Ly α system and their relative strengths place constraints on the temperature of the CMB at this redshift (Prochaska, O’Meara, & Wolfe 2001c).

TABLE 34

IONIC COLUMN DENSITIES: Q2231-002, $z = 2.066$

Ion	λ	AODM	N_{adopt}	[X/H]
HI	1215	20.560 ± 0.100		
C I	1656	12.701 ± 0.035		
C I	1657	12.662 ± 0.108		
Co II	1941	< 12.816	< 12.816	< -0.654

3.28. Q2344+12, $z = 2.538$

This system has been observed previously by Lu, Sargent, & Barlow (1999) and they presented an [Fe/H] metallicity and $N(\text{HI})$ value. We adopt their measurement of the HI column density and have an independent measurement of $N(\text{Fe}^+)$ from several FUV Fe II transitions.

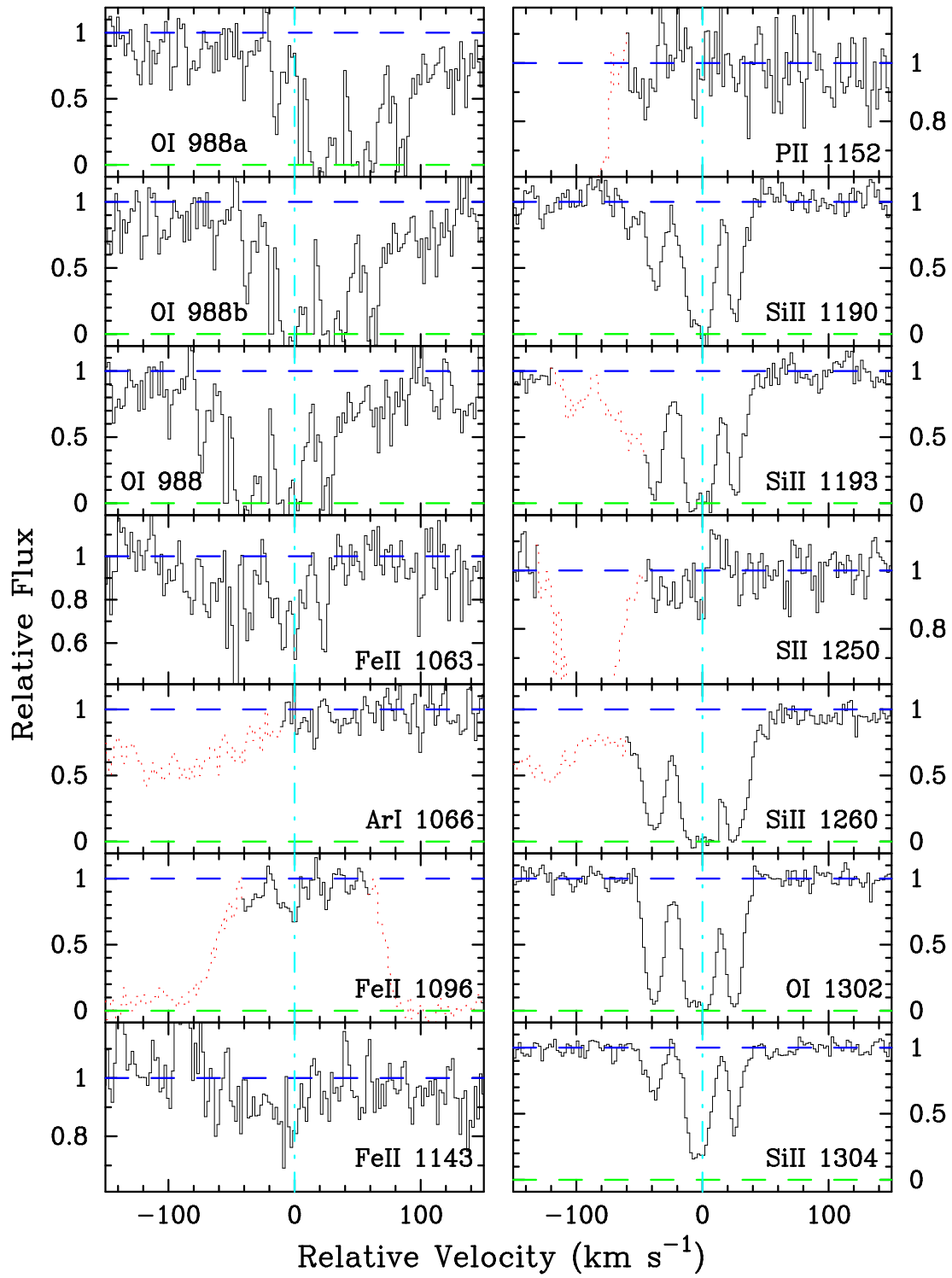


FIG. 34.— Velocity plot of the metal-line transitions for the damped Ly α system at $z = 2.538$ toward Q2344+12. The vertical line at $v = 0$ corresponds to $z = 2.53790$.

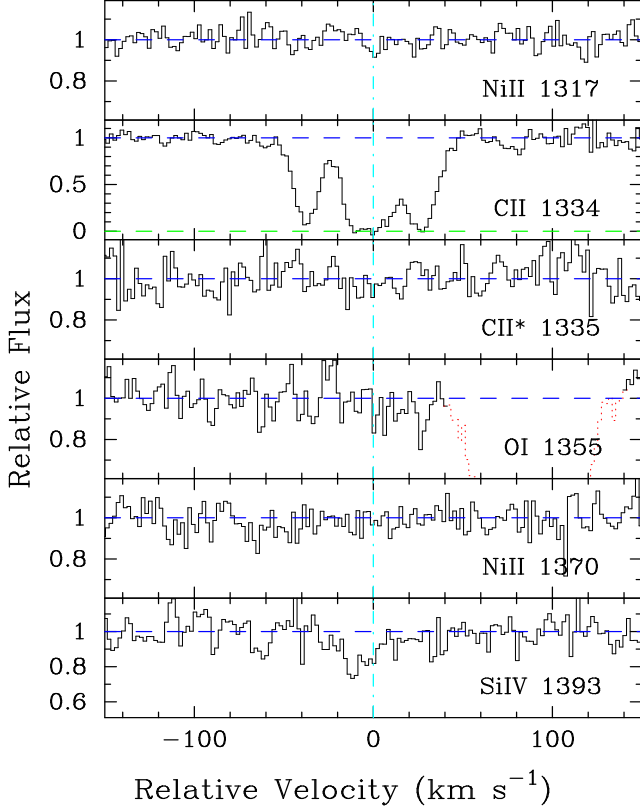


Figure 34 – cont

In addition, our blue spectra cover a number of transitions in the Ly α forest (Figure 34, Table 35).

TABLE 35
IONIC COLUMN DENSITIES: Q2344+12, $z = 2.538$

Ion	λ	AODM	N_{adopt}	[X/H]
HI	1215	20.360 ± 0.100		
C II	1334	> 14.646	> 14.645	> -2.265
C II	1335	< 12.831		
O I	988	> 15.031	> 15.031	> -2.199
O I	1302	> 15.020		
O I	1355	< 17.814		
Si II	1190	> 14.131	14.179 ± 0.012	-1.741 ± 0.101
Si II	1193	> 14.007		
Si II	1260	> 13.838		
Si II	1304	14.179 ± 0.012		
Si IV	1393	12.569 ± 0.087		
P II	1152	< 12.744	< 12.744	< -1.146
S II	1250	< 14.201	< 14.201	< -1.359
Ar I	1066	< 13.262	< 13.262	< -1.618
Fe II	1063	14.021 ± 0.046	14.030 ± 0.032	-1.830 ± 0.105
Fe II	1096	14.007 ± 0.053		
Fe II	1143	14.147 ± 0.077		
Ni II	1317	< 12.814	< 12.814	< -1.796
Ni II	1370	< 12.999		

3.29. Q2348–01, $z = 2.426$ and $z = 2.615$

The two damped systems along this sightline were first identified by Turnshek et al. (1989) and are both part

of the LBQS statistical sample. This quasar is very faint and the S/N of our 4.5hr spectrum is relatively poor. Figures 35,36 and Tables 36,37 present the transitions and column densities for the two systems. With respect to the system at $z = 2.426$, the Fe II 1608 profile is blended at $v > 40$ km/s and we estimate the $N(\text{Fe}^+)$ value by integrating this profile at $v < 40$ km/s. Therefore the value is strictly a lower limit, although the Fe II 1611 indicates that the column density at $v > 40$ km/s is less than $10^{14.46} \text{ cm}^{-2}$. The system at $z = 2.426$ is special for showing absorption from C I and C I*. In a companion paper, we analyse these transitions to place a limit on the temperature of the cosmic microwave background radiation at $z = 2.4$ (Prochaska, O’Meara, & Wolfe 2001c). The system at $z = 2.615$ is notable for exhibiting a very low metallicity ($[\text{Fe}/\text{H}] \sim -2.2$, $[\text{Ni}/\text{H}] \sim -2.5$). In fact, this is the only system with $N(\text{HI}) > 10^{21} \text{ cm}^{-2}$ which also has a metallicity less than 1/100 solar. For the Fe^+ column density, we have averaged the lower and upper limits established by Fe II 1608 and 1611 respectively.

TABLE 36
IONIC COLUMN DENSITIES: Q2348-01, $z = 2.426$

Ion	λ	AODM	N_{adopt}	[X/H]
HI	1215	20.500 ± 0.100		
C IV	1548	> 14.705		
C IV	1550	14.767 ± 0.008		
Al II	1670	> 13.939	> 13.939	> -1.051
Al III	1854	13.379 ± 0.011		
Al III	1862	13.515 ± 0.021		
Si II	1526	> 15.160	15.365 ± 0.022	-0.695 ± 0.102
Si II	1808	15.365 ± 0.022		
Cr II	2056	< 12.713	< 12.713	< -1.457
Fe II	1608	14.614 ± 0.012	14.614 ± 0.012	-1.386 ± 0.101
Ni II	1709	13.434 ± 0.109	13.350 ± 0.104	-1.400 ± 0.144
Ni II	1741	13.350 ± 0.104		

TABLE 37
IONIC COLUMN DENSITIES: Q2348-01, $z = 2.615$

Ion	λ	AODM	N_{adopt}	[X/H]
HI	1215	21.300 ± 0.100		
C IV	1548	13.291 ± 0.024		
C IV	1550	13.336 ± 0.046		
Al II	1670	> 13.139	> 13.139	> -2.651
Al III	1854	< 12.203		
Si II	1526	> 14.562	14.892 ± 0.072	-1.968 ± 0.123
Si II	1808	14.892 ± 0.072		
Si IV	1402	12.899 ± 0.051		
Cr II	2056	12.619 ± 0.100	12.674 ± 0.060	-2.296 ± 0.117
Cr II	2062	12.718 ± 0.075		
Fe II	1608	> 14.483	14.573 ± 0.088	-2.227 ± 0.133
Fe II	1611	< 14.663		
Ni II	1454	13.121 ± 0.110	13.193 ± 0.074	-2.357 ± 0.124
Ni II	1709	13.296 ± 0.097		
Ni II	1741	< 13.100		
Zn II	2026	< 11.871	< 11.871	< -2.099

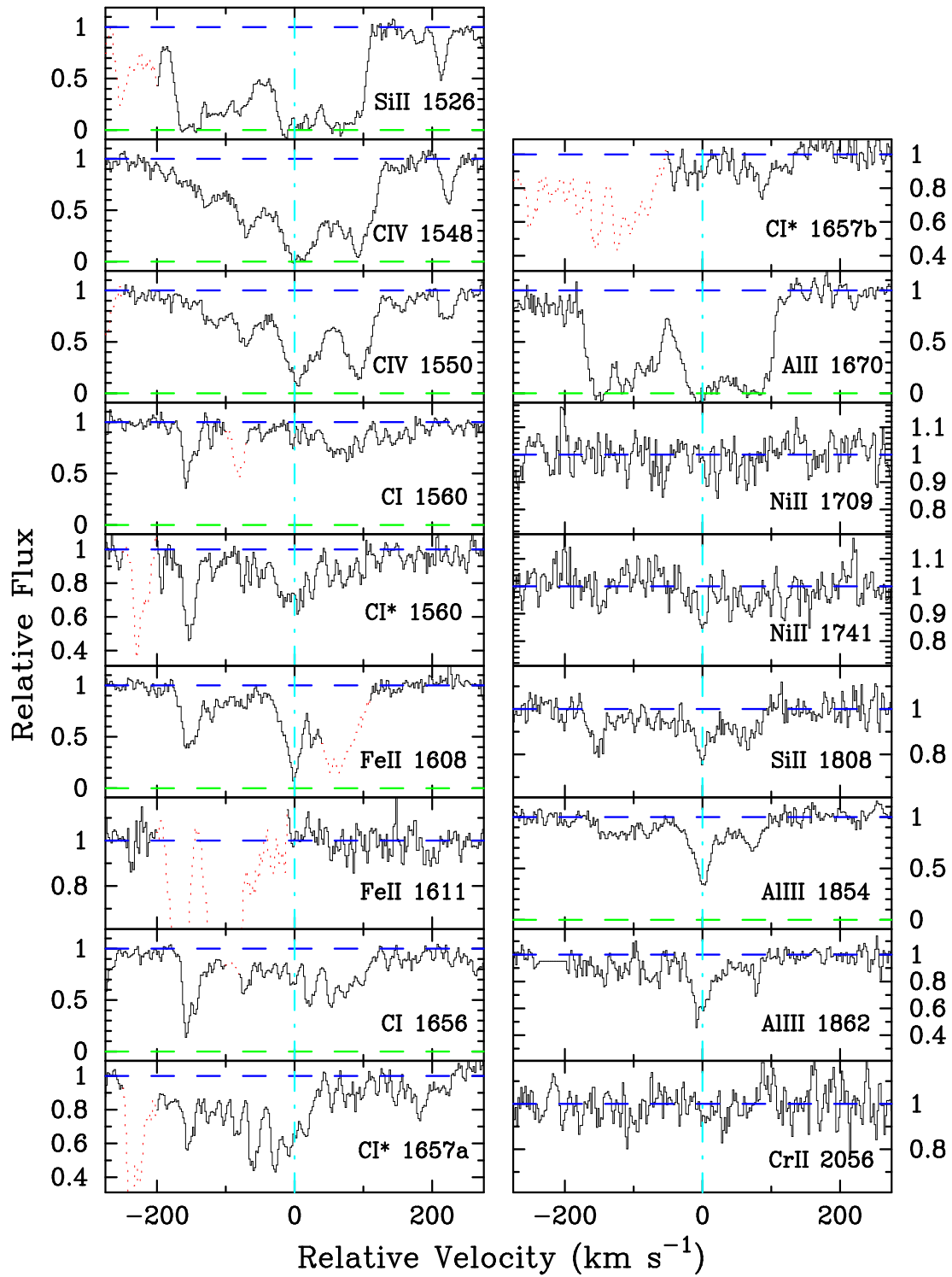


FIG. 35.— Velocity plot of the metal-line transitions for the damped Ly α system at $z = 2.426$ toward Q2348–01. The vertical line at $v = 0$ corresponds to $z = 2.426301$.

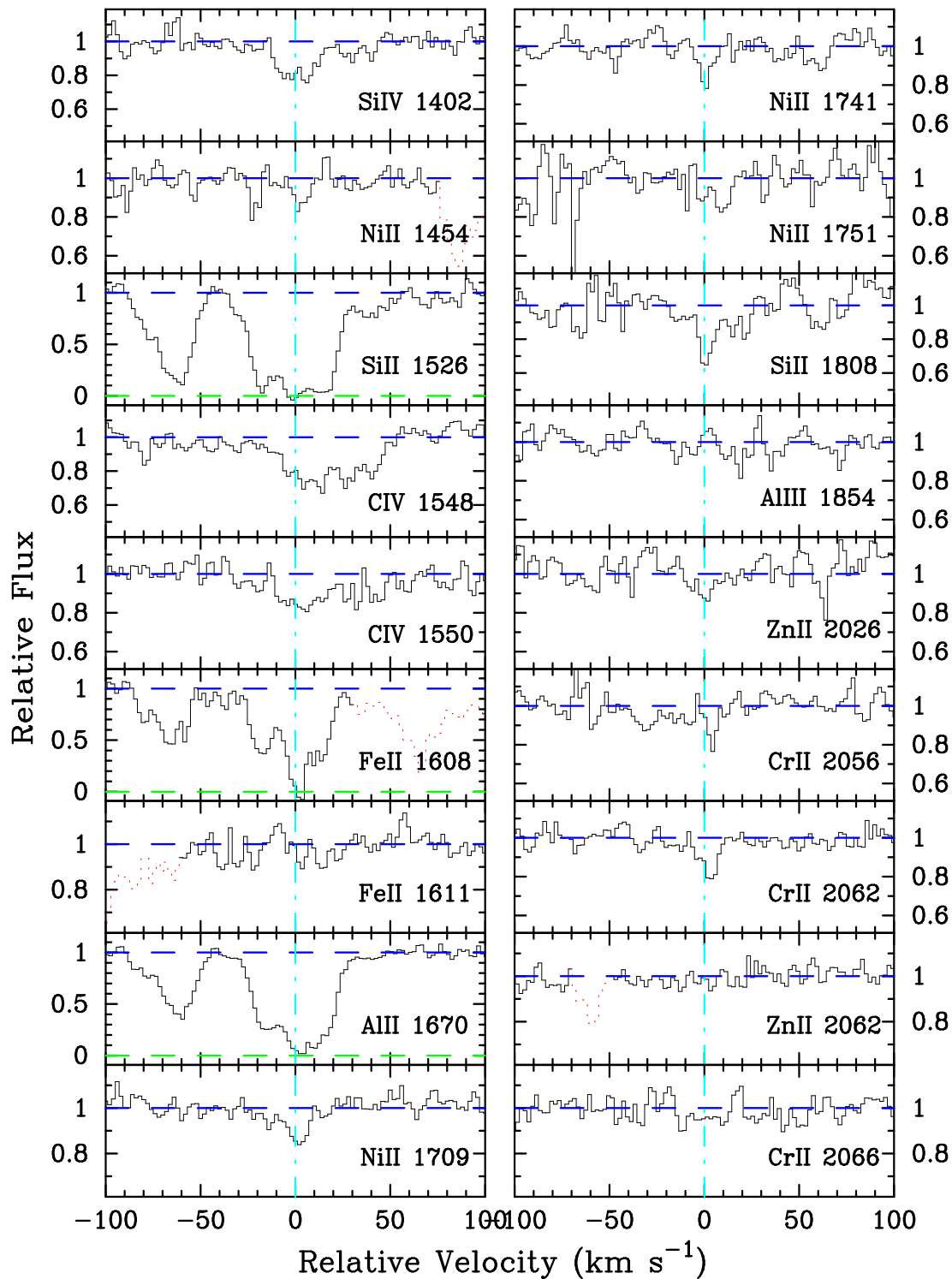


FIG. 36.— Velocity plot of the metal-line transitions for the damped Ly α system at $z = 2.615$ toward Q2348-01. The vertical line at $v = 0$ corresponds to $z = 2.614714$.

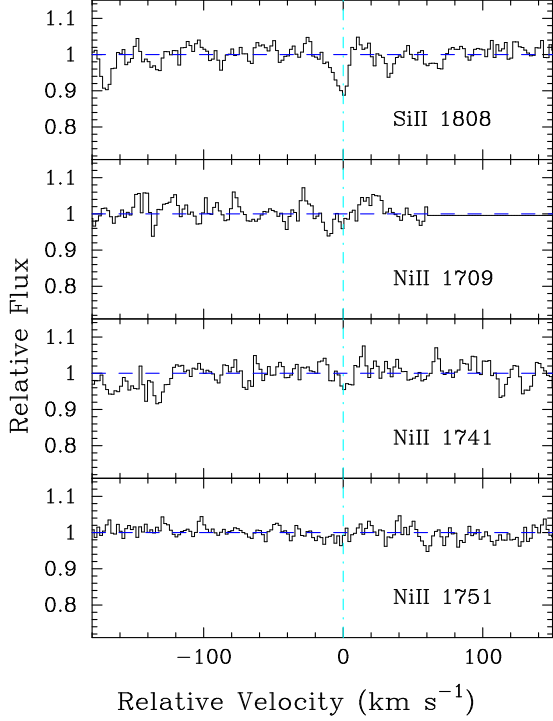


FIG. 37.— Velocity plot of the new metal-line transitions for the damped Ly α system at $z = 2.066$ toward Q2348–14. For comparison, we also plot the Si II 1808 profile. The vertical line at $v = 0$ corresponds to $z = 2.066150$.

3.30. *Q2348–14*, $z = 2.279$

The abundances for this damped system were first measured by Pettini et al. (1995) and subsequently by PW99. We now include a limit on $N(\text{Ni}^+)$ from the non-detection of two Ni II transitions (Figure 37, Table 38).

TABLE 38

IONIC COLUMN DENSITIES: Q2348-14, $z = 2.279$

Ion	λ	AODM	N_{adopt}	[X/H]
HI	1215	20.560 ± 0.075		
Ni II	1709	< 12.752	< 12.583	< -2.227
Ni II	1741	< 12.583		
Ni II	1751	< 12.704		

3.31. *Q2359–02*, $z=2.095$ & $z=2.154$

Although these two systems were analysed in PW99, we have now identified several new profiles including measurements for C II* 1335 for the two systems. The C II* column density for the $z = 2.154$ is very high and as we discuss in Wolfe, Prochaska, & Gawiser (2001) may indicate a high star formation rate in this damped Ly α system. The C II* profile is within the Ly α forest, however, and may be significantly blended with a Ly α forest cloud. We also report a tentative measurement of Ti II 1910 for the system at $z = 2.095$. Given the very large Zn/Fe ratio

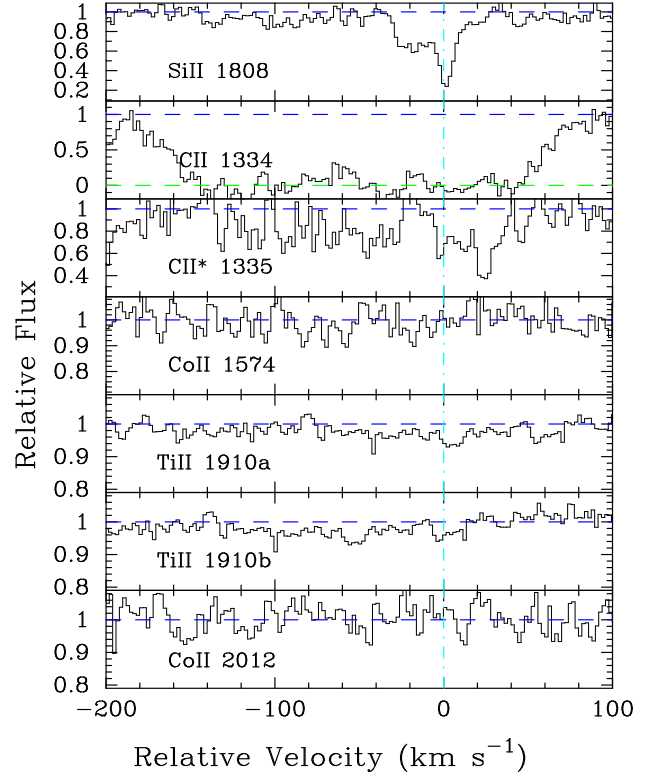


FIG. 38.— Velocity plot of the new metal-line transitions for the damped Ly α system at $z = 2.095$ toward Q2359–02. For comparison, we also plot the Si II 1808 profile. The vertical line at $v = 0$ corresponds to $z = 2.095067$.

for this system, the enhanced Ti/Fe ratio is strongly suggestive of Type II SN enrichment. Figures 38,39 present all of the new transitions and Tables 39,40 list the column densities.

TABLE 39

IONIC COLUMN DENSITIES: Q2359-02, $z = 2.095$

Ion	λ	AODM	N_{adopt}	[X/H]
HI	1215	20.700 ± 0.100		
C II	1334	> 15.147	> 15.147	> -2.103
C II	1335	13.704 ± 0.061		
Ti II	1910	12.330 ± 0.055	12.330 ± 0.055	-1.310 ± 0.114
Co II	1574	< 13.398	< 12.828	< -0.782
Co II	2012	< 12.828		

TABLE 40

IONIC COLUMN DENSITIES: Q2359-02, $z = 2.154$

Ion	λ	AODM	N_{adopt}	[X/H]
HI	1215	20.300 ± 0.100		
C II	1334	> 14.991	> 14.991	> -1.859
C II	1335	14.475 ± 0.020		
Si II	1304	> 15.098	14.277 ± 0.015	-1.583 ± 0.101
Ni II	1703	< 14.171	< 13.208	< -1.342

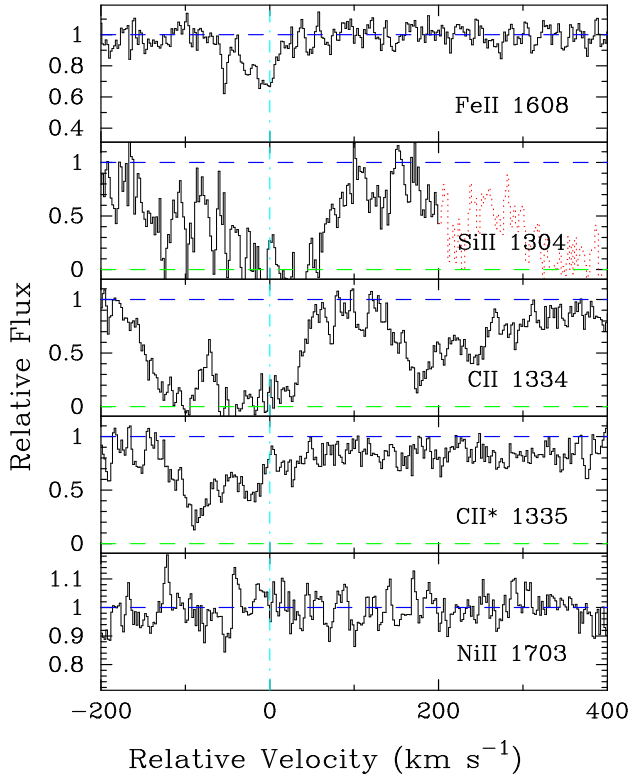


FIG. 39.— Velocity plot of the new metal-line transitions for the damped Ly α system at $z = 2.154$ toward Q2359-02. For comparison, we also plot the Fe II 1608 profile. The vertical line at $v = 0$ corresponds to $z = 2.153934$.

4. SUMMARY

Tables 41 and 42 present a summary of the absolute and relative abundances of the 38 damped Ly α systems in our complete database. Regarding Table 42 where we present abundances relative to Fe, in a few cases we have considered Ni, Cr, or Al as a proxy for Fe, as noted.

We have presented ionic column density measurements for our complete sample of damped Ly α systems. With the exception of a few important transitions which exhibit blends with other profiles, we have measured each column density with the apparent optical depth method. In general, therefore, all of the data has been reduced and analysed with an identical approach. We have used the most up to date atomic data and will continue to update the database as new information becomes available. Visit <http://kingpin.ucsd.edu/~hiresdla> for tables, figures and updated measurements. A series of companion papers, in particular Paper II present new scientific results based on this database.

The authors wish to extend special thanks to those of Hawaiian ancestry on whose sacred mountain we are privileged to be guests. Without their generous hospitality, none of the observations presented herein would have been possible. We thank T. Barlow for providing the HIRES reduction package. We also thank Jim Lawler and Chris Howk for helpful discussions. We acknowledge the Keck

support staff for their efforts in performing these observations. We thank R. Carswell and J. Webb for providing the VPFIT software package. J.X.P. acknowledges support from a Carnegie postdoctoral fellowship. AMW was partially supported by NASA grant NAGW-2119 and NSF grant AST 86-9420443.

TABLE 41
ABUNDANCE SUMMARY

Name	z_{abs}	$N(\text{HI})$	[C/H]	[O/H]	[Al/H]	[Si/H]	[P/H]	[S/H]	[Ar/H]	[Ti/H]	[Cr/H]	[Fe/H]	[Co/H]	[Ni/H]	[Zn/H]
Q0000-2619	3.390	21.41				-1.884						-2.160		-2.295	
BR0019-15	3.439	20.92				-1.057						> -1.631		-1.487	
PH957	2.309	21.40		< -0.596		> -2.241				< -2.133	-1.686	-1.929	< -1.146	-1.778	-1.623
Q0149+33	2.141	20.50	> -2.406	< 0.428	> -2.017	-1.488				< -1.271	-1.450	-1.770		-1.581	-1.674
Q0201+36	2.463	20.38			> -0.737	-0.406				< -1.124	-0.802	-0.870	< -0.333	-0.608	-0.286
J0255+00	3.253	20.70			> -1.311	-0.937				< -0.835		-1.436	< -0.352	-1.342	
J0255+00	3.915	21.30	> -3.118	> -3.003		> -2.667		-1.779				-2.050	< -0.998	-2.279	
Q0336-01	3.062	21.20	> -2.792	> -1.130		> -1.619	-1.597	-1.406	-1.374			-1.795		-1.981	
Q0347-38	3.025	20.80	> -2.285	> -1.717	> -1.882	-1.343		< -1.240	-1.038			-1.797	< -0.514	-1.667	
Q0458-02	2.040	21.65		> -3.110	> -2.377	> -1.167				< -2.095	-1.501	-1.767	< -1.467	-1.719	-1.186
HS0741+4741	3.017	20.48	> -2.166	> -1.639	-2.146	-1.686	< -1.930	-1.680	-1.834			-1.928	< -0.432	-1.972	
Q0836+11	2.465	20.58	> -2.104	> -1.965		-1.153		< -1.120		< -0.982	< -1.352	-1.403	< -0.107	-1.442	< -1.131
Q0841+12	2.375	20.95			> -2.105	-1.271						-1.548	< -0.870	-1.677	-1.507
Q0841+12	2.476	20.78			> -2.054	> -1.845				< -1.562	-1.608	-1.750	< -0.964	-1.675	-1.401
BRI0951-04	3.857	20.60			-1.814	> -1.535						-1.997	< 0.087	< -1.873	
BRI0951-04	4.203	20.40		> -2.674		-2.618						< -2.591		-1.730	
BRI0952-01	4.024	20.55	> -1.788									-1.863	< 0.290	< -1.361	
PSS0957+33	3.279	20.32			> -1.488	-1.000						-1.453	< 0.055	-1.252	< -0.863
PSS0957+33	4.178	20.50		> -2.026	> -1.734	-1.504		-1.308				-1.871	< 0.238	< -1.840	
BRI1108-07	3.608	20.50	> -2.375	> -2.497	> -2.168	-1.798						-2.116		< -1.614	
Q1210+17	1.892	20.60			> -1.650	-0.875					-1.027	-1.149	< -0.782	-1.218	-0.900
Q1215+33	1.999	20.95	> -2.870	> -2.693	> -2.039	-1.480					-1.516	-1.702	< -1.000	-1.606	-1.290
Q1223+17	2.466	21.50	> -2.895	> -2.893		-1.592	< -1.147					-1.677	< -1.779	-1.801	-1.620
Q1331+17	1.776	21.18			> -1.927	-1.451					-2.280	-1.972	< -1.780	-1.890	-1.304
BRI1346-03	3.736	20.72	> -2.784	> -2.571	-2.634	-2.332			< -2.127			< -2.094	< -0.370	< -2.210	
PSS1443+27	4.224	20.80	> -1.738	> -1.622	> -1.332	> -0.926						-1.096	< -0.201	-0.959	
Q1759+75	2.625	20.80	> -2.050	> -1.409		-0.824	> -1.283	-0.757	< -1.606			-1.259	-1.209	< -0.691	-1.248
Q1946+7658	2.844	20.27		-2.321		-2.228		< -1.979				-2.532			> -1.782
Q2206-19	1.920	20.65			> -1.073	-0.417				-0.825	-0.685	-0.857	-0.603	-0.671	-0.409
Q2206-19	2.076	20.43	> -2.774	> -2.761	-2.763	-2.309					< -2.190	-2.606		< -2.096	< -1.902
Q2230+02	1.864	20.85				-0.754				-1.175	-1.117	-1.166	< -0.642	-0.972	-0.720
Q2231-002	2.066	20.56		> -1.877		-0.873				-1.022	-1.065	-1.402	< -0.654	-1.206	-0.882
Q2344+12	2.538	20.36	> -2.265	> -2.199		-1.741	< -1.146	< -1.359	< -1.618			-1.830		< -1.796	
Q2348-01	2.426	20.50			> -1.051	-0.695					< -1.457	-1.386		-1.400	
Q2348-01	2.615	21.30			> -2.651	-1.968					-2.296	-2.227		-2.357	< -2.099
Q2348-14	2.279	20.56	> -2.459	> -2.581	-2.393	-1.917		-2.035				-2.238		< -2.227	
Q2359-02	2.095	20.70	> -2.103		> -1.476	-0.777				-1.310	-1.550	-1.655	< -0.782	-1.526	-0.775
Q2359-02	2.154	20.30	> -1.859		-1.625	-1.583						-1.368		< -1.342	< -1.069

TABLE 42
RELATIVE ABUNDANCE SUMMARY

Name	z_{abs}	$N(\text{HI})$	[C/Fe]	[O/Fe]	[Al/Fe]	[Si/Fe]	[P/Fe]	[S/Fe]	[Ar/Fe]	[Ti/Fe]	[Cr/Fe]	[Co/Fe]	[Ni/Fe]	[Zn/Fe]	
Q0000-2619 ^a	3.390	21.41				+0.411									
BR0019-15 ^a	3.439	20.92				+0.430									
PH957	2.309	21.40		< +1.333		> -0.312				< -0.204	+0.243	< +0.783	+0.151	+0.306	
Q0149+33	2.141	20.50	> -0.636	< +2.198	> -0.247	+0.282				< +0.499	+0.320		+0.189	+0.096	
Q0201+36	2.463	20.38			> +0.133	+0.464				< -0.254	+0.068	< +0.537	+0.262	+0.584	
J0255+00	3.253	20.70			> +0.125	+0.499				< +0.601		< +1.084	+0.094		
J0255+00	3.915	21.30	> -1.068	> -0.953		> -0.617		+0.271				< +1.052	-0.229		
Q0336-01	3.062	21.20	> -0.997	> +0.665		> +0.176	+0.198	+0.389	+0.421				-0.186		
Q0347-38	3.025	20.80	> -0.488	> +0.080	> -0.085	+0.454		< +0.557	+0.759			< +1.283	+0.130		
Q0458-02	2.040	21.65		> -1.343	> -0.610	> +0.600				< -0.328	+0.266	< +0.300	+0.048	+0.581	
HS0741+4741	3.017	20.48	> -0.238	> +0.289	-0.218	+0.242	< -0.002	+0.248	+0.094			< +1.496	-0.044		
Q0836+11	2.465	20.58	> -0.701	> -0.562		+0.250		< +0.283		< +0.421	< +0.051	< +1.296	-0.039	< +0.272	
Q0841+12 ^a	2.375	20.95			> -0.428	+0.406					+0.129	< +0.807		+0.170	
Q0841+12	2.476	20.78			> -0.304	> -0.095				< +0.188	+0.142	< +0.786	+0.075	+0.349	
BRI0951-04	3.857	20.60			+0.183	> +0.462						< +2.084	< +0.124		
BRI0951-04	4.203	20.40													
BRI0952-01	4.024	20.55	> +0.075									< +2.153	< +0.502		
PSS0957+33	3.279	20.32			> -0.035	+0.453						< +1.508	+0.201	< +0.590	
PSS0957+33	4.178	20.50		> -0.155	> +0.137	+0.367		+0.563				< +2.109	< +0.031		
BRI1108-07	3.608	20.50	> -0.259	> -0.381	-0.052	+0.318							< +0.502		
Q1210+17	1.892	20.60			> -0.501	+0.274					+0.122	< +0.367	-0.069	+0.249	
Q1215+33	1.999	20.95	> -1.168	> -0.991	> -0.337	+0.222					+0.186	< +0.702	+0.096	+0.412	
Q1223+17	2.466	21.50	> -1.052	> -1.050		+0.251	< +0.696			< -0.345	+0.166	< +0.064	+0.042	+0.223	
Q1331+17	1.776	21.18			> +0.131	+0.607					-0.222	+0.086	< +0.278	+0.168	+0.754
BRI1346-03 ^c	3.736	20.72	> -0.150	> +0.063		+0.302			< +0.507			< +2.264	< +0.424		
PSS1443+27	4.224	20.80	> -0.642	> -0.526	> -0.236	> +0.170						< +0.895	+0.137		
Q1759+75	2.625	20.80	> -0.841	> -0.200		+0.385	> -0.074	+0.452	< -0.397		-0.050	< +0.518	-0.039	> -0.573	
Q1946+7658	2.844	20.27		+0.211		+0.304		< +0.553							
Q2206-19	1.920	20.65			> -0.216	+0.440				+0.032	+0.172	+0.254	+0.186	+0.448	
Q2206-19	2.076	20.43	> -0.168	> -0.155	-0.157	+0.297					< +0.416		< +0.510	< +0.704	
Q2230+02	1.864	20.85				+0.412				-0.009	+0.049	< +0.524	+0.194	+0.446	
Q2231-002	2.066	20.56		> -0.475		+0.529				+0.380	+0.337	< +0.748	+0.196	+0.520	
Q2344+12	2.538	20.36	> -0.435	> -0.369		+0.089	< +0.684	< +0.471	< +0.212				< +0.034		
Q2348-01	2.426	20.50			> +0.335	+0.691					< -0.071		-0.014		
Q2348-01 ^a	2.615	21.30			> -0.294	+0.389					+0.061			< +0.258	
Q2348-14	2.279	20.56	> -0.221	> -0.343	-0.155	+0.321		+0.203					< +0.011		
Q2359-02	2.095	20.70	> -0.448		> +0.179	+0.878				+0.345	+0.105	< +0.873	+0.129	+0.880	
Q2359-02	2.154	20.30	> +0.018		+0.252	+0.294					+0.509		< +0.535	< +0.808	

^aNi is serving as a proxy for Fe^bCr is serving as a proxy for Fe^cAl is serving as a proxy for Fe

REFERENCES

- Bergeson, S.D. & Lawler, J.E. 1993, ApJ, 408, 382
 Bergeson, S.D. & Lawler, J.E. 1993, ApJ, 414, L137
 Bergeson, S.D., Mullman, K.L., & Lawler, J.E. 1993, ApJ, 435, L157
 Bergeson, S.D., Mullman, K.L., Wickliffe, M.W., Lawler, J.E., Litzen, U., and Johansson, S. 1996, ApJ464, 1044
 Djorgovski, S.G., Gal, R.R., Odewahn, S.C., de Carvalho, R.R., Brunner, R., Longo, G., & Scaramella, R. 1998, in "Wide Field Surveys in Cosmology", eds. S. Colombi & Y. Mellier, (astro-ph/9809187)
 Ellison, S.L., Ryan, S., & Prochaska, J.X. 2001, MNRAS, in press
 Fan, X., SDSS collaboration, 1999, AJ, 118, 1 (SDSS Collaboration)
 Fedchak, J. A. & Lawler, J. E. 1999, ApJ, 523, 734
 Fedchak, J. A., Wiese, L. M., & Lawler, J. E. 2000, ApJ, 538, 773
 Grevesse, N., Noels, A., & Sauval, A.J. 1996, In: Cosmic Abundances, S. Holt and G. Sonneborn (eds.), ASPCS, V. 99, (BookCrafters: San Fransisco), p. 117
 Hagen, H.J., Engels, D., & Reimers, D. 1999, A&AS, 134, 483
 Howk, J.C., Savage, B.D., & Fabian, D. 1999, ApJ, 525, 253
 Howk, J.C., Sembach, K.R., Roth, K.C., & Kruk, J.W. 2000, ApJ, 544, 867
 Kirkman, D. & Tytler, D. 1997, ApJ, 484, 672
 Lanzetta, K. M., Wolfe, A. M., & Turnshek 1995, ApJ, 440, 435
 Lu, L., Sargent, W.L.W., Barlow, T.A., Churchill, C.W., & Vogt, S. 1996, ApJS, 107, 475 (L96)
 Lu, L., Sargent, W.L.W., & Barlow, T.A. 1999, *ASP Conference Series: Highly Redshifted Radio Lines*, ed. C. Carilli, S. Radford, K. Menten, & G. Langston (San Fransisco: ASP), p. XXX, (astro-ph/9711298)
 Molaro, P., Bonifacio, P., Centuri n, M., D'Odorico, S., Vladilo, G., Santin, P., & Di Marcantonio, P. 2000, ApJ, 541, 54
 Molaro, P. et al. 2001, ApJ, in press
 Morton, D.C. 1991, ApJS, 77, 119
 Morton, D. 2001, in prep
 Mullman, K. L., Lawler, J. E., Zsargo, J., & Federman, S. R. 1998, ApJ, 500, 1064
 Outram, P.J., Chaffee, F.H., & Carswell, R.F. 1999, MNRAS, 310, 289
 Pettini, M., Smith, L. J., Hunstead, R. W., and King, D. L. 1994, ApJ, 426, 79
 Pettini, M., Lipman, K., & Hunstead, R.W. 1995, ApJ, 451, 100
 Pettini, M., Smith, L.J., King, D.L., & Hunstead, R.W. 1997, ApJ, 486, 665
 Pettini, M., Ellison, S.L., Steidel, C.C., Shapley, A.E., & Bowen, D.V. 2000, ApJ, 532, 65
 Prochaska, J. X. & Wolfe, A. M. 1996, ApJ, 470, 403
 Prochaska, J. X. & Wolfe, A. M. 1997, ApJ, 474, 140
 Prochaska, J. X. & Wolfe, A. M. 1999, ApJS, 121, 369 (PW99)
 Prochaska, J.X. & Wolfe, A.M., 2000, ApJ, 533, L5
 Prochaska, J. X., Naumov, S.O., Carney, B.W., McWilliam, A., & Wolfe, A.M. 2000, AJ, 120, 2513
 Prochaska, J.X., Gawiser, E., & Wolfe, A.M. 2001, ApJ, in press (PGW01)
 Prochaska, J.X. & Wolfe, A.M. 2001, ApJ, in press, (Paper II)
 Prochaska, J.X. & Wolfe, A.M. 2001, ApJ, in prep
 Prochaska, J.X., O'Meara, J.M., & Wolfe, A.M. 2001, in prep
 Raassen, A.J.J. & Uylings, P.H.M. 1998, A&A, 340, 300
 Savage, B. D. and Sembach, K. R. 1991, ApJ, 379, 245
 Schectman, R.M., Povolny, H.S., & Curtis, L.J. 1998, ApJ, 504, 921
 Storrie-Lombardi, L.J., Irwin, M.J. 1996, & McMahon, R.G. MNRAS, 282, 1330
 Storrie-Lombardi, L.J. & Wolfe, A.M. 2000, ApJ, 543, 552
 Tripp, T. M., Lu L., & Savage B.D. 1996, ApJS, 102, 239
 Turnshek, D.A., Wolfe, A.M., Lanzetta, K.M., Briggs, F.H., Cohen, R.D., Foltz, C.B., Smith, H.E., & Wilkes, B.J. 1989, ApJ, 344, 567
 Verner, D. A., Barthel, P. D., Tytler, D. 1994, A&AS, 108, 287
 Verner, D. A. 1996, Atomic Data, Nuc. Data Tables, 64, 1
 Vogt, S.S., Allen, S.L., Bigelow, B.C., Bresee, L., Brown, B., et al. 1994, SPIE, 2198, 362
 Wiese, L.M., Fedchak, J. A., & Lawler, J. E. 2001, ApJ, 547, 1178
 Wolfe, A.M., Turnshek, D.A., Smith, H.E., & Cohen, R.D. 1986, ApJS, 61, 249
 Wolfe, A. M., Fan, X-M., Tytler, D., Vogt, S. S., Keane, M. J., & Lanzetta, K. M. 1994, ApJ, 435, L101
 Wolfe, A. M., Lanzetta, K. M., Foltz, C. B., and Chaffee, F. H. 1995, ApJ, 454, 698
 Wolfe, A.M. et al. 2001, in prep
 Wolfe, A. M. & Prochaska, J.X. 2000a, ApJ, 545, 591
 Wolfe, A. M., Prochaska, J.X., & Gawiser, E. 2001, in preparation